THE ASTROPHYSICAL JOURNAL, 508:791–830, 1998 December 1

SONIC-POINT MODEL OF KILOHERTZ QUASI-PERIODIC BRIGHTNESS OSCILLATIONS IN LOW-MASS X-RAY BINARIES

M. COLEMAN MILLER[1]
Department of Astronomy and Astrophysics, University of Chicago, 5640 South Ellis Avenue, Chicago, IL 60637; miller@bayes.uchicago.edu

AND

FREDERICK K. LAMB AND DIMITRIOS PSALTIS[2]
Department of Physics and Department of Astronomy, University of Illinois at Urbana-Champaign, 1110 West Green Street, Urbana, IL 61801-3080; f-lamb@uiuc.edu

Received 1996 September 24; accepted 1998 June 26

ABSTRACT

Quasi-periodic brightness oscillations (QPOs) with frequencies ranging from ~ 300 to ~ 1200 Hz have been discovered in the X-ray emission from 14 neutron stars in low-mass binary systems and from another neutron star in the direction of the Galactic center. These kilohertz QPOs are very strong, with rms relative amplitudes ranging up to $\sim 15\%$ of the total X-ray count rate, and are remarkably coherent, with frequency-to-FWHM ratios as large as ~ 200. Two simultaneous kilohertz QPOs differing in frequency by ~ 250–350 Hz have been detected in 12 of the 15 sources. Here we propose a model for these QPOs. In this model, the X-ray source is a neutron star with a surface magnetic field $\sim 10^7$–10^{10} G and a spin frequency of a few hundred hertz, accreting gas via a Keplerian disk. Some of the accreting gas is channeled by the stellar magnetic field but some remains in a Keplerian disk flow that penetrates to within a few kilometers of the stellar surface. The frequency of the higher frequency QPO in a kilohertz QPO pair is the Keplerian frequency at a radius near the sonic point at the inner edge of the Keplerian flow, whereas the frequency of the lower frequency QPO is the difference between the Keplerian frequency at a radius near the sonic point and the fundamental or first overtone of the stellar spin frequency. The difference between the frequencies of the pair of QPOs is therefore close to (but not necessarily equal to) the stellar spin frequency. The amplitudes of the QPOs at the sonic-point Keplerian frequency and at the beat frequency depend on the strength of the neutron star's magnetic field and the accretion rate, and hence one or both of these QPOs may sometimes be undetectable. Oscillations at the stellar spin frequency and its overtones are expected to be weak but may sometimes be detectable. This model is consistent with the magnetic field strengths, accretion rates, and scattering optical depths inferred from previous modeling of the X-ray spectra and rapid X-ray variability of the atoll and Z sources. It explains naturally the frequencies of the kilohertz QPOs and the similarity of these frequencies in sources with different accretion rates and magnetic fields. The model also explains the high coherence and large amplitudes of the kilohertz QPOs and the steep increase of QPO amplitude with photon energy. The increase in QPO frequency with inferred accretion rate seen in many sources is also understandable in this model. We show that if the frequency of the higher frequency QPO in a pair is an orbital frequency, as in the sonic-point model, the frequencies of these QPOs place interesting upper bounds on the masses and radii of the neutron stars in the kilohertz QPO sources and provide new constraints on the equation of state of matter at high densities. Further observations of these QPOs may provide compelling evidence for the existence of a marginally stable orbit, confirming a key prediction of general relativity in the strong-field regime.

Subject headings: accretion, accretion disks — shock waves — stars: neutron — stars: oscillations — stars: rotation — X-rays: stars

1. INTRODUCTION

Observations of accreting neutron stars in low-mass X-ray binaries (LMXBs) with the *Rossi X-Ray Timing Explorer* (*RXTE*) have revealed that the persistent X-ray emission of at least 15 show remarkably coherent quasi-periodic brightness oscillations (QPOs), with frequencies $\nu_{\rm QPO}$ ranging from ~ 300 to ~ 1200 Hz. These kilohertz QPOs are the highest frequency oscillations ever seen in any astrophysical object.

Eight of the 14 identified sources in which kilohertz QPOs have been detected are "atoll" sources (4U 0614+091, 4U 1608−52, 4U 1636−536, 4U 1728−34, KS 1731−260, 4U 1735−444, 4U 1820−30, and Aql X-1). Kilohertz QPOs have also been detected in all six of the originally identified "Z" sources (Sco X-1, GX 5−1, GX 17+2, GX 340+0, GX 349+2, and Cyg X-2). (For the definitions of atoll and Z sources, see Hasinger & van der Klis 1989.) Highly coherent brightness oscillations with frequencies ranging from ~ 360 to ~ 580 Hz have been detected during type I (thermonuclear) X-ray bursts from four kilohertz QPO sources. Another neutron star in the direction of the Galactic center shows burst oscillations with a frequency of 589 Hz, but this source has not yet been positively identified. The frequency ranges and rms amplitudes of the currently known kilohertz QPOs and burst oscillations are listed in Table 1, with references.

Two simultaneous kilohertz QPOs have so far been seen in six of the eight atoll sources in which kilohertz QPOs have been detected (all except 4U 1735−444 and Aql X-1)

[1] *Compton Gamma-Ray Observatory* Fellow.

[2] Present address: Harvard-Smithsonian Center for Astrophysics, 60 Garden Street, Cambridge, MA 02138; dpsaltis@cfa.harvard.edu.

TABLE 1

KNOWN HIGH-FREQUENCY QPOs AND BURST OSCILLATIONS[a]

Source	Type	Frequencies (Hz)	RMS Amplitude (percent)	References
4U 0614+091	Atoll	400–600	6–15	Ford et al. 1996, 1997a, 1997b
		500–1145		van der Klis et al. 1996c
		327		Méndez et al. 1997
		630, 727	16.5, 15.8	
4U 1608−52	Atoll	650–890	5–14	Berger et al. 1996
		940–1125		Méndez et al. 1998
		570–800		Yu et al. 1997
4U 1636−536	Atoll	840–920	6.0	Zhang et al. 1996, 1997a
		1150–1220	6.6, 6.1	van der Klis et al. 1996c
		580[b]		Wijnands et al. 1997c
4U 1728−34	Atoll	637–716	5.2–6.9	Strohmayer et al. 1996b, 1996c, 1996d, 1997a
		500–1100	5.5–8.1	
		363[b]	1.5–5	
KS 1731−260.....	Atoll	524[b]	12	Morgan & Smith 1996
		900, 1170–1207	4–5	Smith et al. 1997; Wijnands & van der Klis 1997
4U 1735−444	Atoll	1149	3.1	Wijnands et al. 1996
4U 1820−30	Atoll	546–796	3.2–5.0	Smale et al. 1996, 1997
		1066		
Aql X−1	Atoll	750–830	–	Zhang et al. 1998a
		549[b]		
Cyg X-2.....	Z	730–1020	3–5	Wijnands et al. 1998
		490–530		
GX 5−1	Z	567–895	2.0–6.7	van der Klis et al. 1996e
		325–448		
GX 17+2	Z	470–780	3–5	van der Klis et al. 1997b
		645–1087		Wijnands et al. 1997a
GX 340+02	Z	247–625	2.5	Jonker et al. 1998
		625–820	2-5	
GX 349+2	Z	712	1.2	Zhang, Strohmayer, & Swank 1998b
		978	1.3	
Sco X-1	Z	570–830	0.9–1.2	van der Klis et al. 1996a, 1996b, 1996d, 1997a
		870–1130	0.6–0.9	
Unknown.....	Unknown	589[b]	2–4	Strohmayer et al. 1996a

[a] Complete as of 1998 May 31.
[b] Burst oscillation.

and in all six of the Z sources. The differences $\Delta\nu$ between the frequencies of the two QPOs seen in these sources all fall in the range $\sim$250–350 Hz. In the atoll sources 4U 0614+091 (Ford et al. 1996, 1997a), 4U 1636−536 (Wijnands et al. 1997c), and 4U 1728−34 (Strohmayer et al. 1996b, 1996c, 1996d) and in the Z sources GX 5−1 (van der Klis et al. 1996e), GX 17+2 (Wijnands et al. 1997a), and Cyg X-2 (Wijnands et al. 1998), $\Delta\nu$ is constant in time, within the errors. In the Z source Sco X-1, $\Delta\nu$ changed from $\sim$250 Hz when the accretion rate was probably near and sometimes even slightly greater than the Eddington critical rate to $\sim$300 Hz when the accretion rate was significantly lower (van der Klis et al. 1997a).

In 4U 0614+091, a brightness oscillation with a frequency consistent with the difference $\Delta\nu = 328$ Hz between the frequencies of the two kilohertz QPOs seen simultaneously in this source was detected with marginal significance during one 30 minute interval (Ford et al. 1996, 1997a). In 4U 1728−34, a strong, relatively coherent brightness oscillation was detected in six of the 12 X-ray bursts so far observed from this source, with a frequency that has remained constant, within the errors, for more than a year and is consistent with the difference $\Delta\nu = 363$ Hz between the frequencies of the two kilohertz QPOs seen simultaneously in this source (Strohmayer et al. 1996b, 1996d; Strohmayer, Zhang, & Swank 1997b; T. Strohmayer 1997, private communication). Burst oscillations have also been seen in 4U 1636−536, with a frequency $\sim$580 Hz (Zhang et al. 1996, 1997a), and in KS 1731−260, with a frequency $\sim$520 Hz (Morgan & Smith 1996; Smith, Morgan, & Bradt 1997). In both cases the frequency of the burst oscillation is approximately *twice* the difference between the frequencies of the two kilohertz QPOs observed simultaneously in these sources.

The peaks in power density spectra associated with these kilohertz QPOs are relatively narrow, with FWHM $\delta\nu_{\rm QPO}$ as small as $0.005\nu_{\rm QPO}$. When integrated over all photon energies, the rms relative amplitudes of the kilohertz QPOs seen in the atoll sources range up to $\sim$15% of the total 2–60 keV X-ray count rate and are typically much greater than the $\lesssim$1% amplitudes of the kilohertz QPOs observed in the Z sources. The amplitudes of the kilohertz QPOs increase steeply with photon energy, up to at least 15 keV, in all the atoll and Z sources where the photon-energy dependence of the kilohertz QPOs has been studied (4U 1608−52: Berger et al. 1996; 4U 1636−536: Zhang et al. 1996; 4U 1728−34: Strohmayer et al. 1996d; KS 1731−260: Wijnands & van der Klis 1997; GX 5−1: van der Klis et al. 1996e; GX 17+2: Wijnands et al. 1997a; Cyg X-2: Wijnands et al. 1998).

The frequencies of the kilohertz QPOs have been seen to vary by as much as a factor $\sim$2. The frequencies of the two kilohertz QPOs observed in the persistent X-ray emission between type I X-ray bursts of the atoll sources 4U 0614+091 (Ford et al. 1996, 1997a), 4U 1728−34 (Strohmayer et al. 1996b, 1996c, 1996d), KS 1731−260 (Wijnands & van der Klis 1997), and 4U 1820−30 (Smale, Zhang, & White 1996, 1997) increase steeply with increasing

count rate ($d \log \nu / d \log CR \gtrsim 1$). The frequencies of the pair of kilohertz QPOs seen during two different observations of 4U 0614+091 (Ford et al. 1997a) correlated tightly and positively with the energy of the peak in the keV X-ray spectrum (Ford et al. 1997b), even though the tracks in the frequency–count rate plane made by the source during the two observations differed significantly. The frequencies of the pair of high-frequency QPOs observed in the Z sources Sco X-1, GX 5−1, GX 17+2, and Cyg X-2 increase steeply with the inferred accretion rate in these sources (van der Klis et al. 1996a, 1996b, 1996d, 1996e, 1997b; Wijnands et al. 1997a, 1998; as discussed by van der Klis 1989 and Lamb 1989, 1991, there is no simple relation between count rate and accretion rate in the Z sources).

Two simultaneous kilohertz QPOs are so common that attention has focused on models that might be able to explain the occurrence of such kilohertz QPO pairs. Strohmayer et al. (1996d) and Ford et al. (1997a) have suggested adapting the magnetospheric beat-frequency model to explain these QPOs. This model was originally proposed by Alpar & Shaham (1985) and Lamb et al. (1985) and developed further by Shibazaki & Lamb (1987) to explain the *single* 15–60 Hz horizontal-branch oscillation (HBO) discovered earlier in the Z sources (see van der Klis 1989). As we discuss in § 2, it is very difficult to understand several key features of the kilohertz QPOs, including the simultaneous occurrence of two kilohertz QPOs, in terms of the magnetospheric beat-frequency model.

Here we propose a model for the kilohertz QPOs that is fundamentally different from the magnetospheric beat-frequency model. In the model presented here, the X-ray source is a neutron star with a surface magnetic field of $\sim 10^7$–10^{10} G and a spin frequency of a few hundred Hertz, accreting gas via a Keplerian disk. In this model the key characteristics of the kilohertz QPOs are explained as follows (details are presented in § 3).

Accretion flow.—Magnetoturbulence, differential cooling, and radiation forces create density inhomogeneities ("clumps") in the gas in the nearly Keplerian disk flow. These clumps are dissipated by the shear in the azimuthal velocity combined with gas pressure forces and turbulence. If the neutron star has a magnetic field $\gtrsim 10^7$ G, some of the accreting gas is channeled out of the disk flow by the stellar magnetic field. Channeling occurs at several stellar radii if the stellar magnetic field is $\sim 10^9$–10^{10} G, but only very close to the stellar surface if the field is $\sim 10^7$–10^8 G. Even if the field is as strong as $\sim 10^9$–10^{10} G, some of the accreting gas continues to drift inward in a nearly Keplerian disk flow until either radiation drag forces become important, the gas reaches the innermost stable circular orbit, or the gas begins to interact viscously with the stellar surface. The fraction of the accreting gas that remains in the Keplerian flow close to the star depends primarily on the strength of the stellar magnetic field and the accretion rate.

Role of radiation drag and general relativity.—For the accretion rates typical of the Z and atoll sources, the nearly Keplerian flow ends and the inward radial velocity of the gas in the disk increases sharply as the gas nears the star, either because of the azimuthal drag force exerted on the gas in the disk by the radiation coming from near the stellar surface or—if the drag force is weak and the radius of the neutron star is less than the radius of the innermost stable circular orbit—because of the general relativistic corrections to Newtonian gravity that produce an innermost stable orbit. In either case, the inward radial velocity of the gas becomes supersonic within a very short radial distance from the radius at which it begins to increase.

Effect of inhomogeneities in the flow.—Roughly speaking, clumps that form outside the radius where the radial inflow becomes supersonic are dissipated before gas from them reaches the stellar surface, whereas gas from clumps that form near the radius where the flow becomes supersonic falls inward and collides with the stellar surface before the clumps are destroyed. Where the streams of denser gas from the clumps orbiting near the sonic point collide with the stellar surface, the streams create arc-shaped areas of brighter X-ray emission that move around the star's equator with a frequency equal to the orbital frequency of the clumps, which is approximately the Keplerian frequency at the sonic point.

Higher frequency kilohertz QPO.—The frequency $\nu_{\rm QPO2}$ of the higher frequency of the two kilohertz QPOs is approximately equal to the Keplerian frequency at the sonic point. A detectable quasi-periodic oscillation of the X-ray flux and energy spectrum may be produced at this frequency by the periodically changing aspect (and, for most viewing directions, by the neutron star's periodic eclipse) of the arc-shaped areas of brighter X-ray emission, as they move around the star with a frequency equal to the orbital frequency of clumps in the Keplerian disk flow near the sonic point. The oscillation appears quasi-periodic because the clumps have finite lifetimes and slightly different orbital frequencies. We find that $\nu/\delta\nu$ can be as large as ~ 100 for these oscillations, consistent with the observed coherence of the kilohertz QPOs. The frequency of the sonic-point Keplerian QPO is almost independent of the spin rate of the neutron star (frame dragging causes the Keplerian frequency at the sonic point, and hence the QPO frequency, to depend weakly on the star's spin rate).

Lower frequency kilohertz QPO.—The frequency $\nu_{\rm QPO1}$ of the lower frequency of the two kilohertz QPOs is equal to 1 (or possibly 2) times the difference between the Keplerian frequency at a radius near the sonic point and the stellar spin frequency. A QPO may be produced at this beat frequency if the magnetic field of the neutron star is weak enough that a Keplerian disk flow penetrates close to the star but strong enough to channel some of the accreting gas before it collides with the stellar surface. For the accretion rates of the Z and atoll sources, this requires surface magnetic fields B_s in the range $\sim 10^7$–10^{10} G.

Channeling of gas out of the disk generates a QPO at the beat frequency because it creates slightly brighter regions that *rotate with the star* (these slightly brighter regions are distinct from the brighter spots that move around the star at the sonic-point Keplerian frequency). The slightly brighter regions that rotate with the star produce a weakly beamed radiation pattern that rotates at the stellar spin frequency. The radiation in this pattern produces a slight increase of the azimuthal drag force on the gas in the clumps orbiting near the sonic point, once or twice each beat period (depending on the symmetry of the slightly brighter region).

This oscillation of the drag force in turn creates an oscillation of the inward flux of gas from a given clump at the sonic point once or twice each beat period. This modulation of the mass flux in the gas streams flowing inward from all clumps orbiting near the sonic point generates a quasi-periodic oscillation of the luminosity and spectrum of the

X-ray emission from the stellar surface, with a frequency equal to 1 (or possibly 2) times the difference between the Keplerian frequency at a radius near the sonic point and the fundamental or first overtone of the stellar spin frequency. The difference between the frequencies of the two QPOs in a pair is therefore close to (but not necessarily *exactly* equal to) the stellar spin frequency.

Oscillation amplitudes.—The amplitudes of the QPOs at the sonic-point Keplerian frequency and at the beat frequency depend on the strength of the neutron star's magnetic field and the mass accretion rate, and hence one or both of these QPOs may sometimes be undetectable. Oscillations at the stellar spin frequency and its overtones are expected to be weak but may sometimes be detectable.

Similarity of kilohertz QPO frequency behavior in different sources.—The similar frequency ranges and the similarity of the frequency–accretion rate correlations of the kilohertz QPOs observed in the Z and atoll sources—which have accretion rates and magnetic fields that differ by factors of 10 or more—is explained by the crucial role of radiation drag, which is effective only within 1 or 2 stellar radii, the approximate proportionality of the angular momentum carried by the accreting matter and the radiation drag force, the fact that the stellar magnetic fields as well as the accretion rates are larger in the Z sources, and the tendency for the vertical thickness of the disk to increase with increasing mass flux.

The radius where the radiation drag or general relativistic corrections to Newtonian gravity cause the radial velocity to increase abruptly plays a key role in the model of the kilohertz QPOs proposed here. Once the radial velocity begins to increase, the flow becomes supersonic within a very short radial distance (the inward radial velocity increases so abruptly that the location of the sonic point is insensitive to the precise definition used), so the sonic point is a useful indicator of the point in the disk flow where the radial velocity begins to increase steeply. Hence, for convenience we shall call the point where the radial velocity increases sharply the "sonic point" and refer to this model for the kilohertz QPOs as the "sonic-point model."

We show that if the frequency of the higher frequency QPO in a pair of kilohertz QPOs is the orbital frequency of gas in a stable Keplerian orbit around the neutron star, as in the sonic-point model proposed here, the frequencies of these QPOs provide interesting new upper bounds on the masses and radii of the neutron stars in the Z and atoll sources and new constraints on the equation of state of matter at high densities.

Any model of how the kilohertz QPOs are produced must be consistent with the known properties of the atoll and Z sources. Hence, before analyzing the sonic-point QPO model of the kilohertz QPOs in more detail, we first summarize in § 2 the previously known X-ray spectral and lower frequency X-ray variability properties of the atoll and Z sources and the physical picture of these sources that has been developed based on these properties. In § 3 we analyze the physics of the sonic-point model and show that it is consistent with the basic properties of the kilohertz QPOs. In § 4 we demonstrate that the sonic-point model is also consistent with the existing physical picture of the Z and atoll sources and with many of the more detailed properties of the kilohertz QPOs. In § 5 we show how to derive upper bounds on the masses and radii of the neutron stars in the kilohertz QPO sources from the frequencies of stable Keplerian orbits in the kilohertz range and discuss the constraints on the properties of neutron-star matter that follow from these bounds; the bounds we derive include the effects of frame dragging. Finally, in § 6 we discuss several specific predictions of the sonic-point model.

2. PROPERTIES OF THE NEUTRON STARS IN LMXBs

2.1. *Observed Properties of the Atoll and Z Sources*

The atoll sources are LMXBs that, over time, trace atoll-shaped patterns in X-ray color-color diagrams (Hasinger & van der Klis 1989). They have luminosities $L \sim 10^{36}$–10^{37} ergs s^{-1}, i.e., $\sim$1%–10% of the Eddington critical luminosity L_E of a neutron star. Power-density spectra of their brightness variations show broad, band-limited noise components at frequencies below $\sim$100 Hz. No QPOs with frequencies $\lesssim$100 Hz have so far been detected in any of the atoll sources with the exception of Cir X-1, which has a QPO that increases in frequency from 1 to 30 Hz as the count rate increases, when the source is very bright (Oosterbroek et al. 1995; Shirey et al. 1996; Bradt, Shirey, & Levine 1998).

Recent comparisons of models of the X-ray emission of neutron stars in LMXBs with the X-ray spectra of atoll sources observed with *EXOSAT* (Psaltis & Lamb 1998a, 1998b, 1998c) suggest that these sources can be subdivided into two groups, the "4U" atoll sources (such as 4U 1636−53, 4U 1705−44, 4U 1820−30, 4U 1608−52, and 4U 1728−34) and the "GX" atoll sources (such as GX 9+1, GX 9+9, GX 3+1, and GX 13+1), based on the strengths of their inferred magnetic fields; one atoll source, 4U 1735−44, has intermediate spectral properties and therefore probably has a magnetic field of intermediate strength.

The Z sources are LMXBs that produce a characteristic Z-shaped track in X-ray color-color diagrams (Hasinger & van der Klis 1989). They have luminosities $L \sim 10^{38}$ ergs s^{-1}, i.e., comparable to L_E. The three branches of the Z are called the horizontal, normal, and flaring branches. When a Z source is on the horizontal branch, a QPO with a frequency in the range 15–60 Hz is observed (van der Klis et al. 1985; van der Klis 1989). This "horizontal branch oscillation" (HBO) is also detectable in some Z sources when they are on the upper part of the normal branch. The relative width $\delta\nu/\nu$ of the HBO peak in power density spectra is typically $\sim$0.1–0.3, and its centroid frequency typically increases with increasing count rate. As a Z source moves down the normal branch, the HBO becomes weaker and eventually disappears into the noise continuum.

Near the middle of the normal branch, a different QPO appears. The peaks in power density spectra produced by this QPO have relative widths $\delta\nu/\nu \sim 0.3$ and centroid frequencies in the range 4–8 Hz (Middleditch & Priedhorsky 1986; van der Klis 1989). The properties of this QPO do not vary appreciably on the lower normal branch. As a Z source moves from the lower normal branch to the flaring branch, the frequency of this second QPO increases abruptly to $\sim$15–20 Hz and the QPO becomes weaker and less coherent, eventually disappearing into the noise (van der Klis 1995; Dieters & van der Klis 1998). This QPO is the "normal/flaring branch oscillation" (N/FBO).

In addition to these two types of quasi-periodic oscillations, power spectra of the brightness variations of the Z sources also show three distinct band-limited noise com-

ponents at frequencies below ~ 200 Hz (Hasinger & van der Klis 1989). The properties of the QPO and noise components vary systematically with the position of a source on its Z track (Hasinger & van der Klis 1989; for detailed studies of this behavior and possible exceptions, see Kuulkers 1995; Dieters & van der Klis 1998; Wijnands et al. 1997b).

Recent analyses of archival *EXOSAT* data (Kuulkers 1995; Kuulkers et al. 1995; Kuulkers, van der Klis, & Vaughn 1996) suggest that the Z sources can be subdivided into two groups, based on the morphology of their Z tracks and power spectra: the "Cyg-like" Z sources (Cyg X-2, GX 5−1, and GX 340+0) and the "Sco-like" Z sources (Sco X-1, GX 17+2, and GX 349+2). At a more detailed level, GX 17+2 shares some of the characteristics of the "Cyg-like" sources and therefore probably has intermediate properties (Hasinger & van der Klis 1989; Wijnands et al. 1997b).

2.2. *Current Physical Picture of the Atoll and Z Sources*

The atoll and Z sources are neutron stars accreting gas from a Keplerian disk fed by a low-mass companion star (see van der Klis 1989). The magnetic fields and the accretion rates of these neutron stars are thought to be the most important parameters that determine their X-ray spectral and temporal characteristics. According to the most complete and self-consistent current model of these sources, the so-called "unified model" (Lamb 1989, 1991), the atoll sources have dipole magnetic fields $\lesssim 5 \times 10^9$ G and luminosities $\sim 1\%$–10% of the Eddington critical luminosity, whereas the Z sources have dipole fields $\sim 10^9$–10^{10} G and luminosities very close to (and sometimes slightly above) the Eddington critical luminosity.

X-ray spectra.—The X-ray spectra of the Z and atoll sources and the low upper limits on the amplitudes of any periodic variations of their persistent X-ray brightness (less than 1% in some cases; see, e.g., Vaughan et al. 1994) constrain the properties of these neutron stars. The low upper limits on brightness variations at their spin frequencies can be understood if the magnetic fields of these neutron stars are $\lesssim 10^{10}$ G and the magnetospheres and inner disks are surrounded by central coronae with electron scattering optical depths ~ 3–5, even at low accretion rates (Lamb et al. 1985; Lamb 1989, 1991), because such a corona strongly suppresses the X-ray flux oscillations produced by any radiation pattern that rotates with the star (Brainerd & Lamb 1987). This effect is discussed further in § 3.6.

When, as in the Z sources, the total luminosity of the neutron star, inner disk, and central corona becomes comparable to $L_{\rm E}$, the vertical radiation force drives gas upward, out of the disk, and radiation drag removes its angular momentum in less than 1 orbit, creating a region of approximately radial inflow that extends out to ~ 300 km (Lamb 1989, 1991). Oscillations in this radial flow are thought to be responsible for the N/FBO (Lamb 1989; Fortner, Lamb, & Miller 1989; Fortner 1992; Miller & Lamb 1992).

Detailed physical modeling of the X-ray spectra of the atoll and Z sources indicates that soft (~ 0.5–1 keV) photons are produced by optically thick bremsstrahlung and other processes at the surface of the star and by self-absorbed, high-harmonic cyclotron emission in the inner magnetosphere (Psaltis, Lamb, & Miller 1995; Psaltis & Lamb 1998a, 1998b, 1998c). As we discuss below, the accretion rate and the strength of the stellar magnetic field determine whether emission from the stellar surface or cyclotron emission in the magnetosphere is the dominant source of soft photons. These soft photons are upscattered by electrons in the magnetosphere and the central corona that surrounds the neutron star to produce the X-ray spectrum that emerges from the corona. In the Z sources, scattering by cooler electrons in the region of approximately radial inflow that surrounds the inner disk and corona further deforms the X-ray spectrum.

Cyclotron emission is the dominant source of soft photons if upscattered cyclotron photons are able to supply the full accretion luminosity (see Psaltis et al. 1995). The range of stellar magnetic fields for which cyclotron emission is dominant can be estimated as follows. Within the magnetosphere, the spectrum of self-absorbed cyclotron photons can be approximated by a blackbody spectrum truncated at the energy at which cyclotron emission becomes optically thin. Comptonization within the magnetosphere and central corona increases the energy of a typical photon by a factor $\sim e^y$, where $y \equiv (4k_{\rm B}T_e/m_e c^2) \max\{\tau, \tau^2\}$ is the Compton y parameter, T_e and m_e are the electron temperature and rest mass, τ is the electron scattering optical depth, and $k_{\rm B}$ is the Boltzmann constant (see Rybicki & Lightman 1979, pp. 195–223). Hence cyclotron emission is the dominant source of soft photons if $e^y L_{\rm cyc} \approx GM\dot{M}/R$ or, equivalently,

$$\mu_{\rm cyc,27} \gtrsim 16 e^{-y/3} \left(\frac{\dot{M}_{\rm ns}}{\dot{M}_{\rm E}}\right)^{1/3} \left(\frac{T_e}{5\ {\rm keV}}\right)^{-1/3} \left(\frac{R_{\rm cyc}}{10^6\ {\rm cm}}\right)^{-2/3} \times \left(\frac{n}{15}\right)^{-1} \left(\frac{M}{1.4\ M_\odot}\right)^{1/3} \left(\frac{R}{10^6\ {\rm cm}}\right)^{-1/3}, \quad (2)$$

where $\dot{M}_{\rm ns}$ is the mass accretion rate onto the neutron star surface, $R_{\rm cyc}$ is the effective radius of the cyclotron photosphere, n is the harmonic number at which the transition from optically thick to optically thin emission occurs, and R is the radius of the neutron star. Figure 2 shows how $\mu_{\rm cyc,27}$ depends on $\dot{M}$ for the range of electron temperatures expected in the magnetospheres and central coronae of the atoll and Z sources.

As Figure 2 shows, if the star's magnetic field is $\lesssim 5 \times 10^8$ G and the accretion rate is ~ 0.01–$0.03\dot{M}_{\rm E}$, the dominant source of photons is the thermal emission from the surface of the neutron star. These photons are then upscattered by the electrons in the magnetosphere and the central corona. Numerical calculations of the X-ray spectra produced by stars with these field strengths and accretion rates agree well with *EXOSAT* observations of the spectra of the "4U" atoll sources when they are in the so-called "banana" spectral state (Psaltis & Lamb 1998c).

If instead the star's magnetic field is $\sim 5 \times 10^8$–5×10^9 G and the accretion rate is $\lesssim 0.1\dot{M}_{\rm E}$, cyclotron emission is the dominant source of photons. These photons are then upscattered by the electrons in the magnetosphere and the central corona. Numerical calculations of the X-ray spectra produced by stars with these field strengths and accretion rates agree well with *EXOSAT* observations of the spectra of the "GX" atoll sources (Psaltis & Lamb 1998a, 1998b, 1998c).

If the stellar magnetic field is $\sim 10^9$–10^{10} G and the mass accretion rate is $> 0.5\dot{M}_{\rm E}$, electron cyclotron emission in the magnetosphere is very efficient in producing soft photons. At these accretion rates, soft photons are Comptonized not

only by the hot electrons in the magnetosphere and central corona but also by the cool electrons in the approximately radial inflow. Numerical computations of the X-ray spectra and color tracks predicted by this physical model agree well with *EXOSAT* and *Ginga* measurements of the X-ray spectra and color tracks of the Z sources (Psaltis et al. 1995; Psaltis & Lamb 1998a, 1998b, 1998c).

Accretion flows.—If the magnetic field of the neutron star is $\lesssim 10^6$ G and the accretion rate is $\gtrsim 0.01 L_{\rm E}$, the Keplerian disk flow may extend inward all the way to the surface of the neutron star without being channeled by the stellar magnetic field. (Here and below we refer to accretion flows confined near the orbital plane as "disk flows," whether or not the azimuthal velocity field is nearly Keplerian, and as "Keplerian disk flows" if the azimuthal velocity field is nearly Keplerian, that is, if the flow is nearly circular.) If instead the stellar magnetic field is $\gtrsim 10^{11}$ G, most of the gas in the disk will couple to the stellar field and be funneled out of the disk plane toward the magnetic poles of the star at a characteristic cylindrical radius ϖ_0 (Ghosh & Lamb 1979a, 1979b, 1992) that is much larger than the radius of the star. Hence, the disk flow around such a star ends far above the stellar surface.

For stellar magnetic fields of intermediate strength, some of the accreting gas is likely to couple to the stellar magnetic field beginning at ϖ_0, which will then channel it toward the star's magnetic poles, but some is also likely to continue as a disk flow inside ϖ_0, as a result of Rayleigh-Taylor instability and incomplete coupling of the flow in the inner disk to the stellar magnetic field (see, e.g., Scharlemann 1978; Ghosh & Lamb 1979a, 1991; Lamb 1984; Spruit & Taam 1990). In this case we expect some of the gas in the disk flow to be channeled out of the disk by the magnetic field over a range of radii inside ϖ_0, with the rest of the gas remaining in a geometrically thin Keplerian flow that penetrates close to the stellar surface, as shown in Figure 1. This last case is the one that we expect to be relevant to the Z sources and most of the atoll sources.

Ghosh & Lamb (1992) derived expressions for the characteristic cylindrical radius ϖ_0 at which gas in the disk couples strongly to the stellar magnetic field and begins to be channeled out of the disk flow, as a function of the stellar dipole magnetic moment μ, the mass accretion rate $\dot{M}_i$ through the inner disk, and the neutron star gravitational mass M, both for gas-pressure–dominated (GPD) and for radiation-pressure–dominated (RPD) inner disks, assuming ϖ_0 is much larger than the radius R of the star. The GPD model is expected to be valid for the atoll sources. The disks around the Z sources are expected to be RPD. The scaling of ϖ_0 with μ, $\dot{M}_i$, and M given by the analytical RPD model is expected to be valid for the Z sources, but the vertical thickness of the boundary layer given by the model is not expected to be reliable. We have therefore reduced the vertical thickness of the boundary layer in the model so that the Keplerian frequency at the radius where the gas couples strongly to the magnetic field agrees quantitatively with the Keplerian frequency inferred from the spin frequency of Cyg X-2, based on the frequencies of its kilohertz QPOs (Wijnands et al. 1998; Psaltis et al. 1998) and the magnetospheric beat-frequency interpretation of its HBO (Psaltis et al. 1998), for a magnetic moment equal to the moment inferred from its X-ray spectrum (Psaltis & Lamb 1998c). Specifically, the Keplerian frequency at the coupling radius was assumed to be 380 Hz, as indicated by the sum of the spin and HBO frequencies when Cyg X-2 is on the normal branch, for a magnetic moment of 3.5×10^{27} G cm^3 and a mass flux through the inner disk equal to the mass accretion rate $\dot{M}_{\rm E}$ onto the neutron star that produces the Eddington critical luminosity.

The resulting two expressions for $\varpi_0(\mu, \dot{M}_i, M)$ can be solved for the dipole moment μ_0 that gives a Keplerian frequency $\nu_{\rm K0}$ at the coupling radius; this characteristic dipole moment is

$$\mu_{0,27} = \begin{cases} 1.5(\nu_{\rm K0}/1100\ {\rm Hz})^{-1.1}(\dot{M}_i/\dot{M}_{\rm E})^{0.43} \\ \quad \times (M/1.4\ M_\odot)^{0.94}\ , \quad \text{for GPD disks}\ ; \\ 0.88(\nu_{\rm K0}/1100\ {\rm Hz})^{-1.3}(\dot{M}_i/\dot{M}_{\rm E})^{0.29} \\ \quad \times (M/1.4\ M_\odot)^{0.91}\ , \quad \text{for RPD disks}\ . \end{cases} \tag{1}$$

Here $\mu_{0,27} \equiv \mu_0/10^{27}$ G cm^3. If the star's dipole moment exceeds μ_0, most of the gas in the disk flow will couple to the magnetic field and be channeled out of the disk at a radius where the Keplerian frequency is less than $\nu_{\rm K0}$. Figure 2 shows the dipole moment that gives Keplerian frequencies of 500 and 1100 Hz at the main coupling radius, as a function of the mass accretion rate. These two curves show that for the neutron star magnetic fields inferred from X-ray spectral modeling, the Keplerian frequency at the gas coupling radius cannot be made simultaneously consistent with the 500–1100 Hz ranges of the kilohertz QPOs in the 4U and Z sources.

Accreting gas that is not channeled out of the disk plane at ϖ_0 is expected to continue to drift slowly inward in a Keplerian disk flow until (1) it is channeled out of the disk at smaller radii, (2) it begins to flow rapidly inward, either because it loses angular momentum to the radiation drag force or because it crosses the radius of the marginally stable orbit, or (3) it collides with the stellar surface. Gas that is flowing rapidly inward remains in a (non-Keplerian) disk flow unless it is channeled out of the disk by the stellar magnetic field. We emphasize that *the accretion disk ends above the stellar surface only if all the gas in the disk is channeled out of the disk flow before it reaches the star.*

In the magnetospheric beat-frequency model of the 15–60 Hz HBO observed in the Z sources (Alpar & Shaham 1985; Lamb et al. 1985; Shibazaki & Lamb 1987), a substantial fraction of the gas in the Keplerian disk flow is channeled out of the disk at $\sim$2–3 stellar radii and flows toward the star's magnetic poles. This model therefore requires that the Z sources have magnetic fields $\sim 10^9$–10^{10} G. The atoll sources have not previously shown any direct indications that they have dynamically important magnetic fields (e.g., no HBO-like QPOs have so far been observed in an atoll source), and hence their magnetic fields are thought to be $\lesssim 5 \times 10^9$ G. However, the existence of kilohertz QPOs at the difference between an orbital frequency and the spin frequency of the neutron star indicates that most if not all of the atoll sources have magnetic fields $\gtrsim 10^7$ G. This is consistent with detailed modeling of their X-ray spectra (described above), which indicates that some atoll sources have magnetic fields as strong as 5×10^9 G. These sources may produce weak HBOs, which may be detected in the future.

2.3. *Magnetospheric Beat-Frequency Model and the Kilohertz QPOs*

As noted in § 1, Strohmayer et al. (1996d) and Ford et al. (1997a) have suggested adapting the magnetospheric beat-

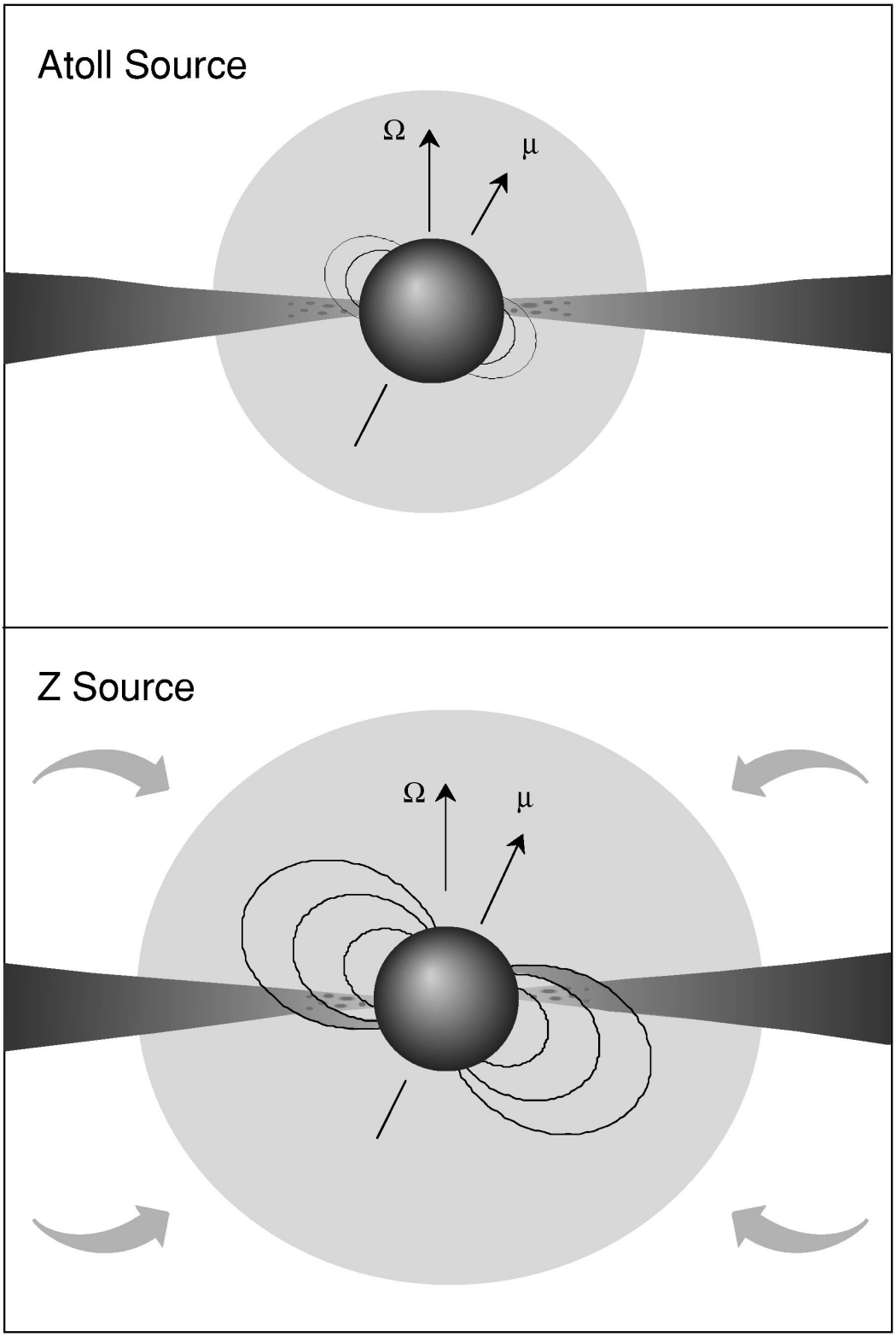

FIG. 1.—Schematic drawings of the accretion flows expected around atoll and Z sources. *Top panel*: Side view of an atoll source with a dipole magnetic field $\sim 10^8$ G and a mass accretion rate $\sim 0.01 \dot{M}_{\rm E}$. The star's spin axis and the direction of its magnetic moment are indicated by the arrows labeled "Ω" and "μ." Gas in the inner part of the Keplerian disk is clumpy and penetrates very close to the stellar surface before some of it is channeled by the star's magnetic field. Collision of the channeled gas with the stellar surface produces slightly brighter spots that rotate with the star. The light shading indicates the hot gas in the magnetosphere and the central corona that surrounds the neutron star. *Bottom panel*: Side view of a Z source with a magnetic field ~ 1–5×10^9 G and a mass accretion rate $\sim \dot{M}_{\rm E}$, showing how some of the gas in the disk is channeled out of the disk by the star's magnetic field at ~ 2–3 stellar radii but some continues to flow inward in a Keplerian disk flow that penetrates close to the stellar surface. Collision of the channeled gas with the stellar surface produces brighter spots that rotate with the star. The light shading again indicates the hot gas in the magnetosphere and the central corona that surrounds the neutron star. The arrows indicate the cooler, approximately radial inflow outside the central corona that is present in the Z sources.

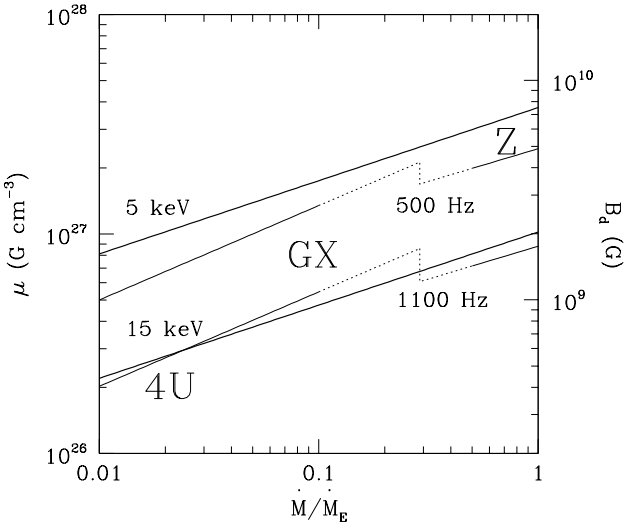

FIG. 2.—Parameter space of dipole magnetic moment μ and mass accretion rate (in units of the Eddington mass accretion rate $\dot{M}_E$ that produces an Eddington luminosity) for neutron star LMXBs. The axis on the right shows the equivalent surface magnetic field at the pole for a neutron star with a radius of 10 km. The thin solid lines, plotted using equation (1), indicate the magnetic moment for which, at the given accretion rate, the Keplerian frequency is 500 Hz (*top line*) and 1100 Hz (*bottom line*) at the radius where a substantial fraction of the gas in the disk first couples to the stellar field and is channeled out of the disk. The break at $\dot{M} = 0.3\dot{M}_E$ illustrates the effect of the expected transition from gas-pressure–dominated flow at low accretion rates to radiation-pressure–dominated flow at high accretion rates. The lines in this $\dot{M}$ range are dotted to indicate that they are not accurate. The solid lines, plotted using equation (2) for electron temperatures $kT_e = 5$ keV (*top line*) and $kT_e = 15$ keV (*bottom line*), divide the $\dot{M}$-B_d plane into the regions where the dominant source of soft photons is cyclotron emission in the neutron star magnetosphere (above the line) or blackbody emission from the neutron star surface (below the line). The labels "4U," "GX," and "Z" indicate the approximate regions in the $\dot{M}$-B_d plane occupied, respectively, by 4U atoll sources, GX atoll sources, and Z sources. These curves were calculated assuming a neutron star mass $M = 1.4\ M_\odot$, an effective cyclotron photosphere of radius $R_{cyc} = 1.5 \times 10^6$ cm, a neutron star radius of 10^6 cm, and a spectrum truncated at cyclotron harmonic number n = 15, appropriate for a scattering optical depth $\tau = 6$. For masses, radii, or optical depths different from these values, the curves can shift by as much as 50% in magnetic field at a given accretion rate.

frequency QPO model to explain the two simultaneous kilohertz QPOs. As described in § 2.2, the magnetospheric beat-frequency model was originally proposed by Alpar & Shaham (1985) and Lamb et al. (1985) and developed further by Shibazaki & Lamb (1987) to explain the *single*, variable frequency, 15–60 Hz HBO seen in the Z sources. Strohmayer et al. and Ford et al. have suggested that the frequency of the higher frequency QPO in a kilohertz QPO pair might be the Keplerian orbital frequency at the radius where gas in the accretion disk begins to couple to the stellar magnetic field and that the frequency of the lower frequency QPO is the beat between this frequency and the stellar spin frequency. There are several difficulties with this application of the magnetospheric beat-frequency model.

Widespread occurrence of two simultaneous, highly coherent kilohertz QPOs.—The occurrence of two simultaneous, strong (amplitudes up to ~15% rms), and highly coherent ($\nu/\delta\nu \sim 50$–100) kilohertz QPOs appears inconsistent with the magnetospheric beat frequency model, because a strong, highly coherent oscillation with a frequency equal to the orbital frequency at which gas first couples to the stellar magnetic field is not expected, nor is it observed in other types of sources where the magnetospheric beat frequency mechanism is thought to be operating.

The magnetospheric beat-frequency mechanism is expected to produce a single, strong, moderately coherent oscillation with a frequency equal to the beat frequency (power is of course also expected at overtones of this frequency), but it is not expected to produce a strong, highly coherent oscillation with a frequency equal to the orbital frequency at the initial gas coupling radius, for two reasons. First, no effect is known that would select a sufficiently narrow range of radii near this radius. Second, even if a narrow range of radii were selected, no mechanism is known that would make the orbital frequencies at these radii visible.

Gas is expected to leave the disk along field lines that thread a very narrow annulus where the gas couples strongly to the magnetic field of the star (Ghosh & Lamb 1979a). The range of orbital frequencies in this annulus is likely to be very small, consistent with the ~5–10 Hz observed width of the HBO (Lamb et al. 1985). The magnetic field is expected to couple more weakly to the gas in the disk over a wider annulus (Ghosh & Lamb 1979a). However, in both annuli, the gas–magnetic field interaction repeats each beat period, not each orbital period (Lamb et al. 1985), so there is no obvious way that this interaction would make the orbital period visible in X-rays. No other mechanism is known that would single out a narrow range of radii in the inner disk.

Even if a narrow range of radii were singled out, little luminosity is expected to be generated in such a narrow annulus, as was explained in the context of the HBOs by Lamb (1988). Generation of a QPO by beaming of radiation via periodic occultation of the emission from the neutron star by clumps orbiting at the initial coupling radius would require us to be viewing *all* the kilohertz QPO sources from within a small range of special inclinations and would also require the height of the disk at its inner edge to vary with accretion rate in just the right way (again see Lamb 1988). Moreover, such beaming would be strongly suppressed by scattering in the ionized gas that surrounds the neutron star (see Lamb et al. 1985; Brainerd & Lamb 1987; Kylafis & Phinney 1989; Lamb 1988, 1989; Psaltis et al. 1995).

A QPO that appears to be the magnetospheric beat frequency QPO has been observed in several accretion-powered pulsars (see, e.g., Angelini, Stella, & Parmar 1989; Lamb 1989, 1991; Shibazaki 1989; Shinoda et al. 1990; Finger, Wilson, & Harmon 1996; Ghosh 1996). In these pulsars, only a single, fairly coherent oscillation has been seen, with properties that indicate that it is the magnetospheric beat-frequency QPO; no QPO is observed at what would be the Keplerian frequency at the coupling radius.

To summarize this point, the theory of the magnetospheric beat-frequency QPO mechanism predicts, and observations of accretion-powered pulsars confirm, that this mechanism produces only a *single* strong, moderately coherent oscillation, with a frequency equal to the beat frequency. In order to explain the two simultaneous kilohertz QPOs, the magnetospheric beat-frequency mechanism would have to generate two strong, highly coherent oscillations, at the beat frequency *and* at the Keplerian frequency at the radius where gas in the disk first strongly couples to the magnetic field. This is the most important reason that

the magnetospheric beat-frequency mechanism appears unpromising as an explanation of the two kilohertz QPOs.

Simultaneous occurrence of two kilohertz QPOs and the HBO in the Z sources.—Identification of the 15–60 Hz HBO in the Z sources as the magnetospheric beat-frequency oscillation is supported by the fact that (1) the magnetic field strengths required are in agreement with those inferred from the spin-down rates of the millisecond recycled rotation-powered pulsars and detailed modeling of the X-ray spectra of the Z sources (see Alpar & Shaham 1985; Lamb et al. 1985; Ghosh & Lamb 1992; and § 2.2); (2) the $\sim$200–350 Hz neutron star spin frequencies predicted by the magnetospheric beat-frequency model (Lamb et al. 1985; Ghosh & Lamb 1992) are consistent with the spin rates of the recycled rotation-powered pulsars (Ghosh & Lamb 1992) and the $\sim$250–350 Hz spin frequencies inferred from the difference between the frequencies of the two kilohertz QPOs seen in the Z sources (see § 1); and (3) only the fundamental and (sometimes) the first overtone of the HBO have ever been detected in the Z sources when they are on the horizontal branch, as one would expect if the HBO is the magnetospheric beat-frequency QPO (see van der Klis 1989). If the HBO *is* the magnetospheric beat-frequency oscillation in the Z sources, then *neither* of the two kilohertz QPOs can be the magnetospheric beat-frequency oscillation, because the HBO was always present when the kilohertz QPOs were detected (van der Klis et al. 1996e).

Steep increase of kilohertz QPO frequencies with increasing mass accretion rate.—In at least some sources, the frequencies of both kilohertz QPOs increase more steeply with inferred mass flux through the inner disk than is expected in the magnetospheric beat-frequency model, which predicts $\nu_{\rm K0} \propto \dot{M}_i^{0.4}$ for a GPD disk and $\nu_{\rm K0} \propto \dot{M}_i^{0.2}$ for an RPD disk (Ghosh & Lamb 1992; see Fig. 2). It is therefore difficult to explain why the frequencies of the kilohertz QPOs increase so steeply with $\dot{M}_i$ using this model.

The magnetospheric beat-frequency model *can* explain the steep increase of the HBO frequency with $\dot{M}_i$ observed in the Z sources, because these neutron stars are likely to have been spun up to frequencies comparable to the Keplerian frequency at the gas–magnetic field coupling radius, so the HBO frequency in a Z source is expected to be small compared to either the star's spin frequency or the Keplerian frequency at the gas coupling radius (see Lamb et al. 1985; Shibazaki & Lamb 1987). This expectation is consistent with the $\sim$250–350 Hz spin frequencies inferred from the differences between the frequencies of the QPOs in the kilohertz QPO pairs.

In contrast to the comparatively low frequency of the HBO, the frequency of the lower frequency QPO in the kilohertz QPO pairs (which is the beat frequency in the magnetospheric beat-frequency interpretation) is up to $\sim$0.7 times the frequency of the higher frequency QPO (which in this interpretation is the Keplerian frequency at which the gas in the disk couples to the magnetic field). It follows that in this interpretation the neutron star spin frequency is in some cases only $\sim$0.3 times the Keplerian frequency at the coupling radius. Hence the frequencies of both of the two kilohertz QPOs should increase as $\dot{M}_i$ increases in the same way that $\nu_{\rm K0}$ increases, which is much more slowly than observed as Figure 2 shows.

To summarize, whereas the inferred dependence of the HBO on the mass flux through the inner disk is explained naturally by the magnetospheric beat-frequency model of the HBOs, the inferred dependence of the kilohertz QPOs on this mass flux is difficult to explain using this model.

Observed range of kilohertz QPO frequencies.—The frequencies of the QPOs at what would be the Keplerian orbital frequency in the magnetospheric beat-frequency interpretation all range up to $\sim$1000–1200 Hz. This is understandable if these QPOs are generated within a few kilometers of the surface of the neutron star, as in the sonic-point model, whereas in the magnetospheric beat-frequency model the frequencies of these QPOs would be expected a priori to range from $\sim$50 Hz up to $\sim$1500 Hz for the wide range of neutron star magnetic field strengths and accretion rates inferred in the atoll and Z sources.

The expected range of orbital frequencies could be reduced if the mass accretion rate and the strength of the star's dipole magnetic field are tightly correlated in just the right way. However, the correlation that is indicated by spectral modeling (Psaltis et al. 1995; Psaltis & Lamb 1998a, 1998b, 1998c) gives magnetospheric beat frequencies in the range $\sim$20–200 Hz and orbital frequencies in the range $\sim$300–500 Hz, much smaller than the frequencies of the kilohertz QPOs.

Anticorrelation between kilohertz QPO amplitudes and inferred magnetic field strengths.—In the magnetospheric beat-frequency interpretation, the kilohertz QPOs should have higher amplitudes in systems with stronger neutron star magnetic fields. However, as discussed further in § 4.4, the rms amplitudes of the kilohertz QPOs in the atoll sources, which are thought to have the weakest neutron star magnetic fields, are considerably stronger than the rms amplitudes of the kilohertz QPOs in the Z sources, which are thought to have the strongest neutron star magnetic fields.

In the next section we describe a model that is consistent with both the physical picture of the atoll and Z sources developed over the past decade and with the properties of the kilohertz QPOs.

3. THE SONIC-POINT MODEL

We now analyze the physics of the sonic-point model of the kilohertz QPOs. In § 3.1 we describe the key elements of the sonic-point model and summarize the results of the general relativistic gas dynamical and radiation transport calculations that are described in more detail later in this section. In § 3.2 we investigate the motion of the gas in the inner disks of the Z and atoll sources and show that at a characteristic angular momentum loss radius $R_{\rm aml}$ that is typically several kilometers larger than the radius of the neutron star, radiation drag extracts angular momentum from the gas so quickly that the gas accelerates sharply inward. As a result, density fluctuations in the gas near the sonic point create brighter footprints that rotate around the stellar equator at the sonic point Keplerian frequency $\nu_{\rm Ks}$, producing a QPO at this frequency. We show further that a decrease in $R_{\rm aml}$ with accretion rate is to be expected.

In § 3.3 we show that the sonic-point Keplerian frequency is expected to be between $\sim$300 and $\sim$1200 Hz in all sources and should increase with increasing mass flux through the inner disk. The model therefore explains one of the most important features of the kilohertz QPOs. We also show that the sonic-point mechanism naturally produces a second QPO at the beat frequency between $\nu_{\rm Ks}$ and the stellar spin frequency $\nu_{\rm spin}$. In § 3.4 we show that this mechanism can produce QPOs with $\nu/\delta\nu \sim 100$, comparable to

the largest Q values observed. In § 3.5 we consider radiation transport in the footprints and surrounding hot central corona and show that the amplitude of the QPO at the sonic-point Keplerian frequency is expected to increase steeply with increasing photon energy. Also, to the extent that the effects of Comptonization dominate, the Keplerian-frequency oscillations at higher photon energies are expected to be delayed by $\sim 10\ \mu$s relative to the oscillations at lower energies. In § 3.6 we consider the effect of gas surrounding the neutron star and magnetosphere on the amplitudes of the kilohertz QPOs and demonstrate that QPO amplitudes as large as $\sim 20\%$ are understandable in the sonic-point model.

The light travel time across a neutron star is a fraction $\lesssim 10^{-15}$ of the time required for accretion to change the star's mass and spin rate, so the exterior spacetime is stationary to extremely high accuracy. The spacetime outside a steadily and uniformly rotating axisymmetric star with gravitational mass M and angular momentum J is unique to first order in the dimensionless angular momentum parameter $j \equiv J/M^2$ (Hartle & Thorne 1968) and is the same as the Kerr spacetime to this order (the spacetime outside a rotating star differs from the Kerr spacetime in second and higher orders; see, e.g., Cook, Shapiro, & Teukolsky 1994). All, or almost all, of the atoll and Z sources appear to have spin frequencies $\lesssim 350$ Hz (see §§ 2 and 4), in which case j is $\lesssim 0.3$ for these stars (see § 5.2). Hence the Kerr spacetime is a reasonably accurate approximation to the exterior spacetime. Therefore, in this work we use the familiar Boyer-Lindquist coordinates.

All analytical expressions given in this paper are accurate only to first order in j. These expressions would therefore be the same if written in terms of the circumferential radius. Calculation of physical quantities to higher order is straightforward, given a stellar model and interior and exterior metrics valid to the higher order, but no analytical expressions are known, so such calculations must be carried out numerically. For conciseness, in this section (only) we use units in which $c = G = k_B = 1$, where c is the speed of light, G is the gravitational constant, and k_B is Boltzmann's constant.

3.1. *Physical Picture and Summary of Calculations*

Before presenting our calculations of the most important elements of the sonic-point model, we first describe the model in more detail, summarizing the results of our calculations and indicating where these results are presented in the subsections that follow. We shall assume that the spin axes of the neutron stars in the kilohertz QPO sources are closely aligned with the rotation axes of their accretion disks. This is expected to be the case in these LMXBs, because mass transfer is expected to produce an accretion disk in which the gas circulates in the same sense as the orbital motion of the system. The torque on the neutron star created by such a disk will align the spin axis of the star with the axis of the accretion disk in a time short compared to the duration of the mass transfer phase in such systems (see Daumerie et al. 1996).

Accretion flow near the star.—As discussed in § 2.2, if the stellar magnetic field is of intermediate strength we expect a Keplerian disk flow to penetrate inside the magnetosphere. What happens to the flow there depends on the magnitude of the radiation drag force (Miller & Lamb 1993, 1996) and on whether the radius R of the neutron star is larger or smaller than the radius R_{ms} of the innermost stable circular orbit. There are four possibilities (see Table 2 for a summary).

Suppose first that $R < R_{ms}$. This will be the case if the equation of state of neutron-star matter is relatively soft and the star in question has an intermediate-to-high mass and is not spinning near its maximum rate. There are then two possibilities (§ 3.2).

Case 1a.—If the drag force exerted by radiation coming from near the neutron star's surface is strong enough to remove $\gtrsim 1\%$ of the angular momentum of the gas in the Keplerian disk flow just outside R_{ms}, gas in the inner disk drifts slowly inward in nearly circular orbits until it reaches the critical angular momentum loss radius R_{aml}, where it transfers so much angular momentum to the radiation so rapidly that centrifugal support fails and the radial velocity of the gas increases sharply. Inside R_{aml} the gas spirals inward in a disk flow in which the radial velocity is supersonic until the gas is channeled by the star's magnetic field or collides with the star's surface.

Case 1b.—If instead the radiation drag is so weak that it removes $\ll 1\%$ of the angular momentum of the gas in the Keplerian disk flow by the time the gas reaches R_{ms}, gas in the inner disk drifts slowly inward in nearly circular orbits until it approaches R_{ms}, where general relativistic corrections to Newtonian gravity cause the radial velocity of the flow to increase steeply (see, e.g., Muchotrzeb 1983; Muchotrzeb-Czerny 1986). Inside R_{ms}, the gas spirals inward in a disk flow in which the radial velocity is supersonic until the gas is channeled by the star's magnetic field or collides with the star's surface.

Whether case 1a or 1b applies depends primarily on the strength of the star's magnetic field and on the mass accretion rate.

Suppose now that $R > R_{ms}$. This will be the case if the equation of state of neutron-star matter is relatively stiff and the star in question has an intermediate-to-low mass or is spinning very rapidly. There are again two possibilities (§ 3.2).

Case 2a.—If the radiation drag force is at least moderately strong, gas in the inner disk drifts slowly inward until it reaches the critical radius R_{aml}, where it accelerates rapidly inward. Inside R_{aml} the gas spirals inward in a disk flow in which the radial velocity is supersonic until the gas is channeled by the star's magnetic field or collides with the star's surface.

Case 2b.—If instead the radiation drag is weak, gas in the inner disk drifts slowly inward in a disk flow in which the

TABLE 2

LOCATION OF THE SONIC POINT

Stellar Radius	Strong Radiation Drag Force	Weak Radiation Drag Force
$R < R_{ms}$	Sonic point at R_{aml} (Case 1a)	Sonic point at R_{ms} (Case 1b)
$R > R_{ms}$	Sonic point at R_{aml} (Case 2a)	No sonic point in Keplerian disk flow (Case 2b)

radial velocity is supersonic until the gas is channeled by the star's magnetic field or interacts directly with the star's surface.

Again, whether case 2a or 2b applies depends primarily on the strength of the star's magnetic field and on the mass accretion rate.

Regardless of whether the slow inward drift of the gas in the disk is terminated by loss of angular momentum to the radiation field or because the gas crosses the radius of the innermost stable circular orbit, the inward radial velocity of the gas increases abruptly at $R_{\rm aml}$ or $R_{\rm ms}$ and becomes supersonic within a very small radial distance. As mentioned in § 1 and earlier in this section and described in detail below, the radius where either radiation drag or general relativistic corrections to Newtonian gravity cause the radial velocity to increase sharply and become supersonic plays a key role in the model of the kilohertz QPOs proposed here. The radius of the sonic point is a useful indicator of the location of this transition.

Radiation drag can remove at most only a fraction of the specific angular momentum of the gas and therefore can create a radially supersonic inflow in the inner disk only within a few stellar radii (§ 3.2). The reason is that the specific angular momentum of gas in circular Keplerian orbits at radii much larger than the radius of the neutron star is much greater than in orbits just outside the stellar surface, so removal of a small fraction of the angular momentum of the gas at large radii cannot cause a large fraction of it to fall to the stellar surface. In contrast, the specific angular momentum of gas orbiting near the star is not much greater than the angular momentum of gas orbiting at the stellar surface, so radiation drag can cause gas in orbit near the star to plunge to its surface.

Radiation drag can cause gas to plunge inward from a radius larger than one would estimate using the Newtonian approximation, because (1) special and general relativistic effects on the gas dynamics and radiation transport significantly increase the fraction of the angular momentum of the accreting gas that can be removed by the radiation and (2) in general relativity the specific angular momentum of gas in circular Keplerian orbits with radii $r \lesssim 3R_{\rm ms}$ varies only slowly with r. For this reason, the sonic-point model predicts that if radiation drag produces a transition to rapid radial inflow, the transition will occur within ~ 36 km (for a 1.4 $M_\odot$ neutron star) and hence that the Keplerian frequency at the transition radius will be $\gtrsim 300$ Hz (§ 3.3).

Inside the sonic point, the vertical optical depth of the disk flow falls steeply with decreasing radius, usually to a value that is small compared to unity. The optical depth of the disk flow measured radially from the stellar surface to the sonic radius typically also becomes less than unity within a very small radial distance, unless the accretion rate is very high or the geometrical thickness of the disk in the vertical direction is very small. When the change from "optically thick" to "optically thin" disk flow is caused by the radiation drag force, the transition is somewhat analogous to the ionization front at the boundary of an H II region. In the disk-flow transition, the photon mean free path becomes longer because the radiation is removing angular momentum and the flow is accelerating inward, causing the density to fall sharply, whereas in an ionization front the radiation is removing bound electrons from atoms and molecules, causing the opacity to fall sharply.

Generation of the QPO at the sonic-point Keplerian frequency.—Suppose first that the magnetic field of the neutron star is dynamically negligible. An element of gas in the disk flow outside the sonic radius diffuses inward subsonically. When it reaches the sonic radius, it falls supersonically to the stellar surface along a spiral trajectory like that shown in Figure 3*a*. This trajectory was computed in full general relativity for a nonrotating, isotropically emitting star, using the numerical algorithm described in Miller & Lamb (1996). (The shape of the trajectory depends on the luminosity, spin, and other properties of the source; the example shown in Fig. 3*a* is only illustrative.) The surface density of the disk flow is much smaller inside the sonic radius than outside because of the sharp increase in the radial velocity at the sonic point. Gas falls inward from the sonic radius and impacts the star all around its equator, producing a bright equatorial ring of X-ray emission.

The flow in the inner part of the accretion disk is expected to have density fluctuations ("clumps") produced by a variety of mechanisms, such as thermal instability, Kelvin-Helmholtz instability, and magnetoturbulence (see Lamb et al. 1985; Shibazaki & Lamb 1987). There may be as many as several hundred such clumps at a given radius in the disk outside the sonic point. The velocity-independent radially outward component of the radiation force and the velocity-dependent radiation drag force both tend to cause gas in the shadow of a clump to overtake the clump in azimuth and radius, and hence the radiation force tends to increase clumping.

As discussed in § 3.4, a clump that forms outside the sonic radius is dissipated by gas pressure forces, turbulence, and the shear in the velocity field before the gas from it can reach the stellar surface, so such clumps do not produce

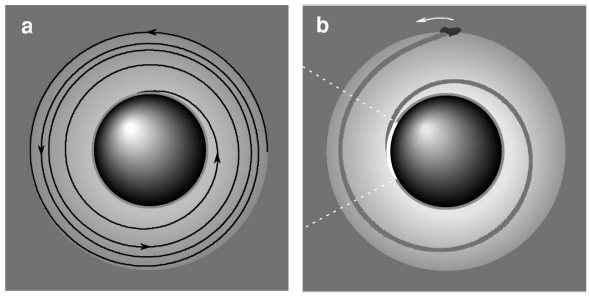

FIG. 3.—Neutron star with a dynamically negligible magnetic field, accreting via a Keplerian disk that penetrates close to the star. The star and disk are viewed along the rotation axis of the disk, which is rotating counterclockwise in this view. The panels show, in Boyer-Lindquist r, ϕ coordinates, (*a*) the spiral trajectory followed by a single element of gas as it falls supersonically from the sonic radius to the stellar surface and (*b*) the spiral pattern of higher gas density formed by gas streaming inward along spiral trajectories with the shape shown in panel (*a*) from a region of denser gas (a "clump") orbiting near the sonic radius. The gas trajectories and resulting density pattern were computed in full general relativity assuming that the gas is exposed to radiation from the star at a radius of $9M$ and that the star has a radius of $4M$, is nonrotating, radiates isotropically, and has a luminosity measured at infinity of $0.005L_{\rm E}$. The surface density of the disk flow is much smaller inside the sonic radius (*lighter shaded region*) than outside it (*darker shaded region*), because of the sharp increase in the inward radial velocity at the sonic radius. Gas falling inward from the sonic radius along spiral trajectories collides with the neutron star around its equator, producing an X-ray emitting equatorial ring, which is indicated by the grey ring around the star. The white arc at the stellar surface indicates the bright, arc-shaped "footprint" where the denser gas from the clump collides with the stellar surface and produces a beam of X-rays (*white dashed lines*) that rotates around the star at the sonic-point Keplerian frequency. The footprint generally moves with respect to the stellar surface.

significant inhomogeneities in the inflow from the sonic radius. In contrast, a clump that forms near the sonic radius can persist for up to ~ 100 times the infall time to the stellar surface, so such a clump generates a stream of denser infalling gas from the sonic point to the stellar surface that lasts as long as the clump survives.

The shape of the pattern formed by the denser gas falling inward from a clump depends on how the angular velocity of the infalling gas varies with radius. For example, if the angular velocity of the gas were independent of radius, the pattern of higher gas density would be a straight, radial line from the clump to the stellar surface. In general, the pattern formed by the denser gas from a clump is a fairly open curve. The shape of the pattern, like the trajectories that produce it, depends on the luminosity, spin, and other properties of the source. Figure 3*b* shows the pattern formed by inflow of gas along spiral trajectories with the shape shown in Figure 3*a*. In this example the pattern of denser gas is also a spiral. It is more open than the spiral trajectories of the individual elements of denser gas that produce it, because the source of the denser gas (the clump) orbits the star only slightly slower than the infalling gas.

We expect the time-averaged radiation field around the star to be nearly axisymmetric. Moreover, the gas from a given clump typically orbits the star ~ 5–10 times before colliding with the stellar surface, so the effects of any azimuthal variations in the radiation drag force are averaged out. Therefore, the spiral pattern of denser gas produced by the inflow from a given clump rotates nearly uniformly around the star with a rotation frequency equal to the orbital frequency of the clump that is producing it, which is the Keplerian frequency at a radius near the sonic point.

The time evolution that generates an X-ray oscillation at the sonic-point Keplerian frequency is illustrated by the four panels of Figure 4. In this figure a single clump is shown advancing in its orbit by 90° from one panel to the next. The pattern of higher density gas rotates uniformly around the star with a frequency equal to the orbital frequency of the clump, so it also advances by 90° from one panel to the next. Where the denser gas from a clump collides with the stellar surface, it produces an arc-shaped area of brighter X-ray emission. This arc-shaped brighter "footprint" moves around the star's equator with a frequency equal to the rotation frequency of the pattern, which is the orbital frequency of the clump and is therefore approximately equal to the Keplerian frequency $\nu_{\rm Ks}$ at the sonic point. In reality, many clumps are crossing the sonic radius at any given time, and hence there are many bright footprints moving around the star's equator. The radiation from these footprints carries the kinetic energy of infall that is released when the gas that has fallen inward from the clumps at the sonic radius collides with the stellar surface.

As seen by a distant observer whose line of sight is inclined with respect to the orbital axis of the disk, the aspect presented by a given bright footprint varies periodically and the footprint is eclipsed with a frequency equal to the rotation frequency of the pattern, which is approximately the Keplerian orbital frequency at the sonic point. Footprints come and go as clumps form near the sonic point and then dissipate. Also, the orbital frequencies of the clumps that are producing footprints at any given time differ slightly. As a result, a distant observer sees a strong, quasi-periodic oscillation of the X-ray flux and spectrum at the pattern rotation frequency, which is close to $\nu_{\rm Ks}$. *This is the sonic-point Keplerian-frequency QPO.*

The spin of the neutron star is not involved in generating the sonic-point Keplerian frequency QPO. The precise frequency of the sonic-point Keplerian QPO does depend weakly on the spin frequency of the neutron star, because the frame dragging caused by the star's spin has a small effect on the frequencies of Keplerian orbits near the neutron star. The sonic-point Keplerian frequency QPO mechanism described here, which generates a QPO with a frequency equal to the orbital frequency at the sonic point, differs fundamentally from the suggestion of Paczynski (1987), who speculated that when the sonic point is located at the radius of the marginally stable orbit, a QPO might be produced by unsteady flow through it with a low (~ 20–50 Hz) frequency that would have nothing directly to do with the orbital frequency of the marginally stable orbit.

Generation of the QPO at the sonic-point beat frequency.—Suppose now that the magnetic field of the neutron star is weak enough that a prograde Keplerian disk flow penetrates near the surface of the star but strong enough that close to the star some of the gas is channeled by the field. The channeled gas produces slightly brighter spots where it collides with the stellar surface. If these slightly brighter spots are offset from the star's spin axis, the enhanced radiation from them generates a beamed pattern of radiation that rotates with the star. This rotating radiation pattern

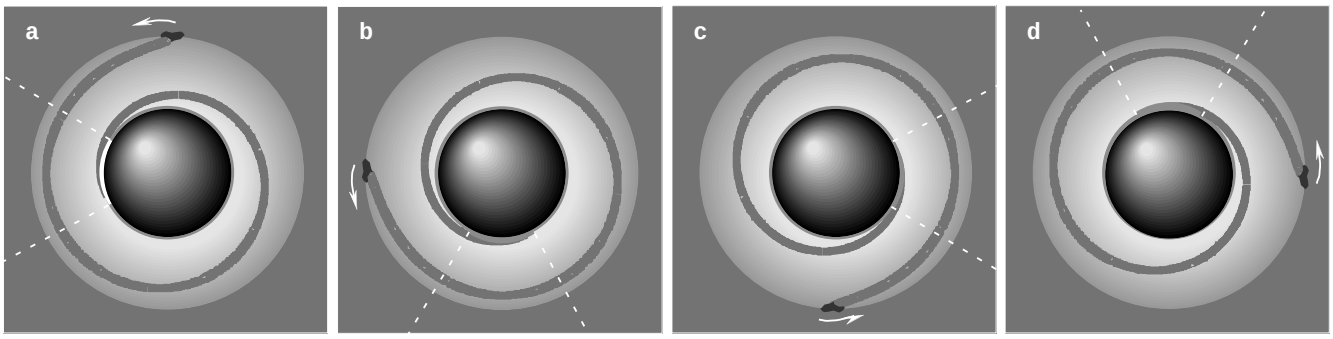

FIG. 4.—Time sequence of four snapshots of a neutron star with a dynamically negligible magnetic field accreting via a Keplerian disk that penetrates close to the star, showing schematically how the QPO at the sonic-point Keplerian frequency is produced. The viewpoint, gas trajectories, and density pattern are the same as in Fig. 3. The drop in the surface density of the disk flow at the sonic radius, the bright ring of emission around the stellar equator, the pattern of denser infalling gas inside the sonic radius, the bright footprint where the denser gas collides with the stellar surface, and the beam of radiation coming from the footprint are all indicated in the same way as in Fig. 3. The clump is shown advancing in its orbit by 90° from one panel to the next. The spiral pattern of higher density gas, its bright footprint, and the resulting beam of X-rays all rotate around the star with a frequency equal to the orbital frequency of the clump, so they are also shown advancing by 90° from one panel to the next. The footprint generally moves with respect to the stellar surface.

creates a periodic oscillation in the radiation force that is acting on the clumps of gas crossing the sonic radius. Hence, if conditions near the star are such that the nearly Keplerian motion of the gas in the clumps orbiting near the sonic radius is terminated by loss of angular momentum to the radiation, the inward flux of mass from the clumps near the sonic radius will increase once or twice each beat period, depending on the symmetry of the radiation pattern that rotates with the star.

As a specific example, suppose that the radiation drag force experienced by the gas in a given clump orbiting near the sonic radius peaks each time the beam of radiation that rotates with the star sweeps across the clump. This will occur with a frequency equal to 1 or 2 times the difference between the orbital frequency of the clump, which is the Keplerian orbital frequency near the sonic point, and the spin frequency $\nu_{\rm spin}$ of the neutron star, depending on the symmetry of the radiation pattern that rotates with the star. We call $\nu_{\rm Ks} - \nu_{\rm spin}$ the "sonic-point beat frequency" and denote it $\nu_{\rm Bs}$. If the transition to supersonic inflow is caused by radiation drag, the oscillation of the radiation drag force will cause the supersonic inflow of gas from the clumps orbiting near the sonic point to oscillate quasi-periodically with a frequency equal to 1 or 2 times the sonic-point beat frequency.

The time evolution that produces this oscillation is shown schematically in the six snapshots of Figure 5. For clarity, only a single clump is shown orbiting at the sonic radius and the six snapshots show the sequence of events as seen in a frame corotating with the star. In Figure 5*a* the clump is in the beam of radiation that rotates with the star and hence the inward flux of denser gas from the clump is greater than average. In Figure 5*b* the clump has moved out of the beam and hence the inward flux of gas from the clump is smaller than average; the pulse of gas that was dragged off the clump by the stronger radiation flux in Figure 5*a* is now falling inward from the clump. In Figure 5*c* the clump has moved ahead of the beam by 180°; the inward flux of gas from the clump remains smaller than average and the pulse of denser gas that began to fall inward in Figure 5*a* is further away from the clump. In Figure 5*d* the clump is now ahead of the beam by 270°; the

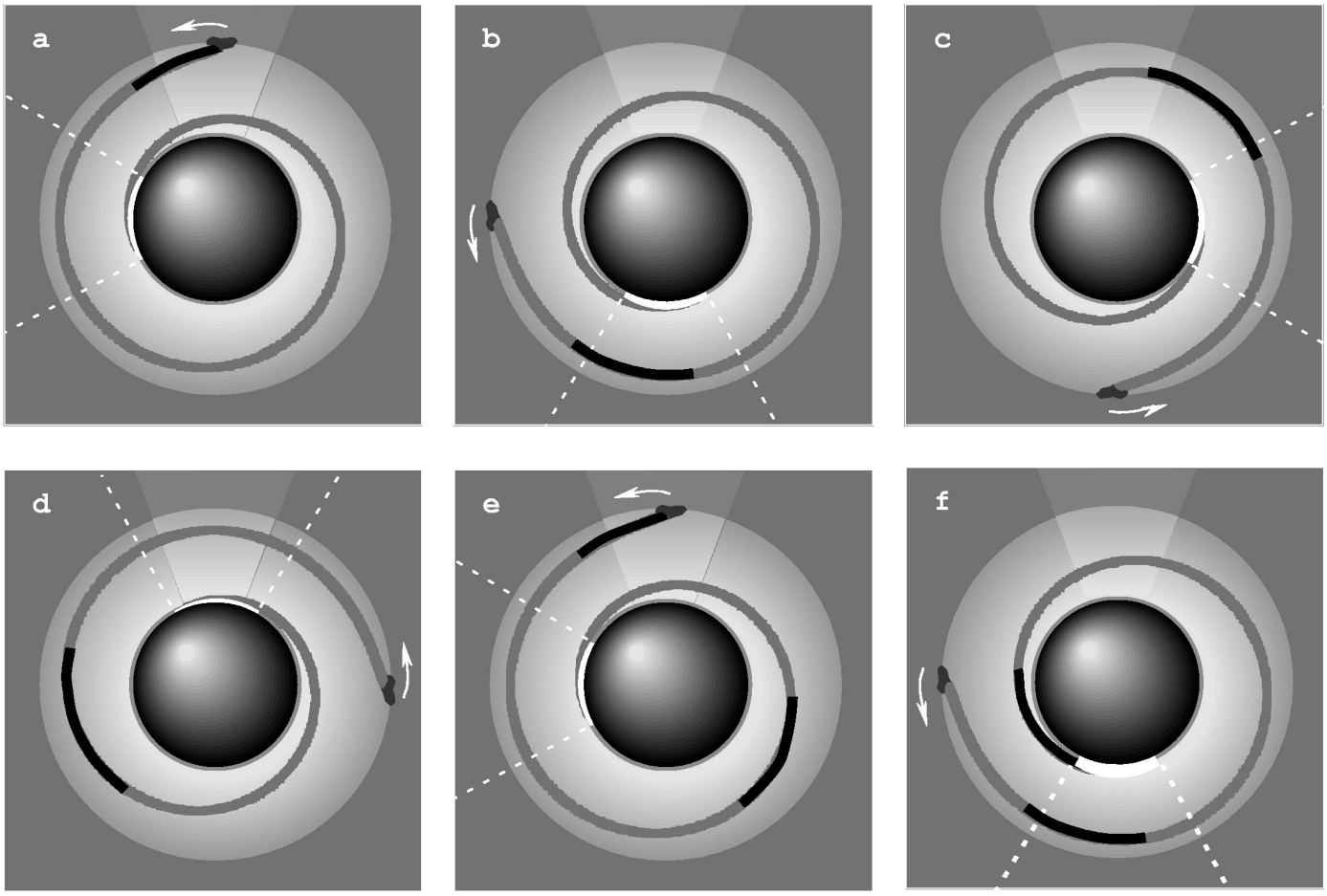

FIG. 5.—Time sequence of six snapshots of a spinning neutron star with a weak magnetic field accreting via a prograde Keplerian disk that penetrates close to the star, showing schematically how the QPO at the sonic-point beat frequency is produced. The disk and the star are viewed along their common rotation axes and are rotating counterclockwise in this view. The beam of radiation produced by the collision with the stellar surface of the gas channeled by the weak stellar magnetic field is indicated by the faint white beam emerging from behind the star; this beam rotates with the star. To make the sequence of events easier to visualize, the snapshots show the sequence of events as seen in a frame corotating with the star, so the beam of radiation that rotates with the star is always pointing in the same direction (here, the vertical direction). The angular velocity of the clump, which is orbiting near the sonic radius, is greater than the angular velocity of the star, so with time the clump advances counterclockwise relative to the beam of radiation that rotates with the star. In this sequence, the clump advances relative to the star by 90° from one snapshot to the next. The drop in the surface density of the disk flow at the sonic radius, the bright ring of emission around the stellar equator, the pattern of denser infalling gas inside the sonic radius, the bright footprint where the denser gas collides with the stellar surface, and the beam of radiation coming from the footprint are all indicated in the same way as in Fig. 3. The events occurring in each panel are described in the text.

inward flux of gas from the clump remains smaller than average and the pulse of denser gas that began to fall inward in Figure 5*a* is approaching the stellar surface. In Figure 5*e* the clump has now moved back into the beam of radiation and a new pulse of denser gas is leaving the clump; the pulse of denser gas that began to fall inward in Figure 5*a* is now very close to the stellar surface. In Figure 5*f* the clump has again moved ahead of the beam by 90° and the inward flux of gas from the clump is again smaller than average; the pulse of denser gas that began to fall inward in Figure 5*a* is now colliding with the stellar surface, producing a brighter beam of radiation from the footprint of the stream.

In reality, the radiation drag force, and hence the inward mass flux from a clump, may be greatest not when the clump is fully illuminated by the beam that rotates with the star, as assumed in this illustration, but at some other relative phase, because the radiation drag force depends in a complicated way on the various components of the radiation stress-energy tensor (see Miller & Lamb 1996). In any case, the inward mass flux from the orbiting clumps oscillates quasi-periodically with a frequency approximately equal to the sonic-point beat frequency $\nu_{\rm Bs}$, producing a quasi-periodic oscillation in the luminosity and spectrum of the X-ray emission from the stellar surface. *This is the sonic-point beat-frequency QPO.*

Properties of the sonic-point QPOs.—In § 3.3 we show that the sonic-point mechanism naturally generates Keplerian-frequency QPOs with frequencies $\sim$300–1200 Hz for a wide range of stellar magnetic fields and accretion rates and that it is natural for the frequencies of the sonic-point Keplerian and beat-frequency QPOs to increase steeply with increasing mass flux through the inner disk. The angular distribution of the emission from each emitting point within a footprint at the stellar surface is broad, so the power at $\nu_{\rm Ks}$ is likely to be much greater than the power at overtones of $\nu_{\rm Ks}$. The modulation of the inflow from clumps orbiting at the sonic radius is unlikely to be perfectly sinusoidal, so overtones of the sonic-point beat frequency $\nu_{\rm Bs}$ as well as $\nu_{\rm Bs}$ itself may be detectable.

In § 3.4 we argue that the sonic-point mechanism can produce QPOs with $\nu/\delta\nu$ ratios as large as $\sim$100, i.e., similar to those observed in the atoll and Z sources. The oscillation at the sonic-point beat frequency is generated by the beating of the stellar spin frequency, which is periodic, against the quasi-periodic sonic-point Keplerian frequency oscillation. It is therefore natural to expect the $\nu/\delta\nu$ values of the oscillations in a pair to be roughly similar, in the absence of other disturbing effects. In § 3.5 we show that the steep increase in QPO amplitude with photon energy observed in many kilohertz QPOs is understandable in the sonic-point model.

The visibilities of the various QPOs generated by the sonic-point mechanism depend on the mass flux in the Keplerian disk flow that penetrates to the sonic point, the number and distribution of clumps in the disk at the sonic point, the brightness of the footprints produced by the streams from the clumps relative to the brightness of the rest of the stellar surface, the geometry and optical depth of the scattering material around the star, and the inclination of the system.

If radiation forces are required to produce large clumps with substantial density contrasts, the amplitudes of the QPOs at the sonic-point Keplerian and beat frequencies are likely to become much smaller and may become undetectable once the angular momentum loss radius $R_{\rm aml}$ has retreated inward to the radius $R_{\rm ms}$ of the innermost stable circular orbit, because once this has happened, the gas in the disk near the sonic point is increasingly shielded from radiation coming from the stellar surface by gas in the disk closer to the star. However, if large clumps with substantial density contrasts are formed by other mechanisms, the sonic-point Keplerian frequency QPO may still be detectable if the sonic point is at $R_{\rm ms}$, even if the sonic-point beat frequency QPO—which can be generated only if radiation forces have a significant dynamical effect at the sonic radius—has disappeared.

In § 3.6 we show that scattering by the electrons in the central corona that surrounds the neutron stars in the Z and atoll sources strongly attenuates the already intrinsically weak beaming oscillation at the stellar spin frequency as well as the weak beaming oscillations at other frequencies, making all but the strongest beaming oscillation—the one at the sonic-point Keplerian frequency—difficult to detect with current instruments. In contrast, scattering only weakly attenuates luminosity oscillations, so the luminosity oscillations at the sonic-point beat frequency and its overtones are likely to be detectable. Taking into account both the generation of these various oscillations and their attenuation in the circumstellar environment, Keplerian-frequency and beat-frequency QPOs with rms amplitudes as large as 15% appear possible.

As discussed in § 2, the Z sources appear to have significantly stronger magnetic fields than the atoll sources. The magnetic fields of the Z sources are therefore likely to channel a larger fraction of the accreting gas out of the disk plane before it penetrates close to the stellar surface, so we expect the amplitudes of the kilohertz QPOs to be smaller in the Z sources than in the atoll sources. The magnetic field of the neutron star in some atoll sources may be so weak that the QPO at the sonic-point beat frequency is undetectable, even though a QPO at the sonic-point Keplerian frequency is visible. The sonic-point beat frequency may also be undetectable at some times if the scattering optical depth between the stellar surface and the sonic point is too large. In other sources or at other times, the luminosity oscillation at the sonic-point beat frequency may be detectable even though the beaming oscillation at the sonic-point Keplerian frequency has been suppressed by scattering in the corona surrounding the star.

3.2. *Transition to Rapid Radial Inflow*

In both the atoll and the Z sources, we expect radiation drag to cause gas in the Keplerian disk flow to make an abrupt transition from slow inward drift to rapid radial inflow several kilometers above the surface of the neutron star. This transition occurs at the radius where the drag exerted by radiation from the star removes enough angular momentum from the gas quickly enough that it falls to the surface of the star unimpeded by a significant centrifugal barrier. We first describe the consequences of the transfer of angular momentum from the gas in the inner disk to the radiation and then present a fully general relativistic calculation of the gas dynamics and radiation transport in the inner disk that shows the nature of this transition in the atoll sources, which have luminosities much less than the Eddington critical luminosity. We next give approximate analytical expressions for the location and width of this

transition, then discuss why the nature and location of the transition may be comparable in the Z and atoll sources even though the accretion rates and luminosities of the Z sources are much higher than the accretion rates and luminosities of the atoll sources, and finally summarize the implications for the sonic-point QPOs.

Transfer of angular momentum to the radiation field.—The azimuthal drag force exerted by radiation from the star can create a radially supersonic inflow in the inner disk. However, this is possible only within a few stellar radii if the luminosity of the star is produced by accretion and most of the accreting gas flows through the inner disk. The reason is that radiation drag can remove at most a fraction $\eta_{\rm rad}(\max) \approx 20\%$ of the specific angular momentum of the accreting gas (see Fortner et al. 1989; for more detailed discussions, see Miller & Lamb 1993, 1996). The specific angular momentum of gas in circular Keplerian orbits at radii large compared to the radius R of the neutron star is much larger than at R, so radiation drag cannot cause more than $\sim 20\%$–30% of the gas at such large radii to fall to the stellar surface. In contrast, the specific angular momentum of gas in circular Keplerian orbits very near the star is not much larger than the angular momentum of orbits at the stellar surface, so radiation drag can cause gas in Keplerian orbits near the star to plunge to the surface.

Radiation drag can create a radially supersonic inflow at a larger radius than one would estimate using the Newtonian approximation, because special and general relativistic effects significantly increase the fraction of the angular momentum of the accreting gas that is transferred to the radiation (Miller & Lamb 1993). Also, in general relativity the specific angular momentum of gas in circular Keplerian orbits with radii $r \lesssim 3R_{\rm ms}$ varies only slowly with radius. The latter point is illustrated by Figure 6, which shows the specific angular momentum of gas in circular Keplerian orbit around a nonrotating and a slowly rotating 1.4 $M_\odot$ neutron star, as a function of the radius of the orbit. The specific angular momentum varies fairly steeply at $r \gg R_{\rm ms}$, but only slowly with radius between $r = R_{\rm ms}$ and $r \sim 3R_{\rm ms}$. For example, the specific angular momentum of circular orbits changes by less than $\sim 10\%$ from $r = 12M$ (25 km) to $r = 6M$ (12 km). These curves are of course physically meaningful only at radii greater than the radius R of the neutron star. The relatively flat shape of the angular momentum curve for circular orbits near a neutron star means that if gas orbiting there loses even $\sim 20\%$ of its angular momentum, it will plunge to the stellar surface.

We can estimate the outer boundary of the region where radiation coming from near the stellar surface can remove sufficient angular momentum from the gas orbiting in the disk so that it falls supersonically to the stellar surface by comparing $\eta_{\rm rad}(\max)$, the largest fraction of angular momentum that can be removed by radiation coming from the surface of the neutron star, with $\eta_{\rm flow}$, the fraction of the specific angular momentum of gas in a circular Keplerian orbit at radius r that must be removed in order for the gas to fall from r to $R_{\rm ms}$ (if the radius of the star is less than $R_{\rm ms}$, gas that has reached $R_{\rm ms}$ can fall to the stellar surface without losing any more angular momentum). These two quantities are compared in Figure 7. Here $\eta_{\rm rad}(\max)$ was computed by assuming that the gravitational binding energy at the stellar surface is converted into radiation there, taking into account the relevant angular, special relativistic, and general relativistic factors (see Miller & Lamb

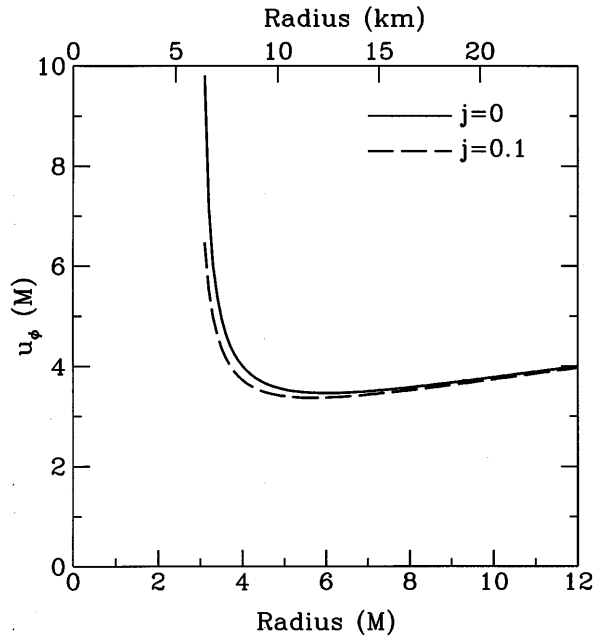

FIG. 6.—Angular momentum per unit mass u_ϕ (*solid curve*; as measured at infinity in units of the gravitational mass M of the star) of an element of gas in a circular Keplerian orbit around a nonrotating neutron star, as a function of the Boyer-Lindquist radial coordinate of the orbit (in units of M). The dashed curve shows u_ϕ for a rotating star with dimensionless angular momentum $j = 0.1$ which is close to the j-value given by the best modern neutron-star matter equations of state for a neutron star with $M = 1.4\ M_\odot$ and a spin frequency of 300 Hz as measured at infinity (see § 5.2). The top axis shows the radius in kilometers for $M = 1.4\ M_\odot$. The radius $R_{\rm ms}$ of the innermost stable circular orbit is the radius at which the specific angular momentum is a minimum; for $j = 0$, $R_{\rm ms} = 6M$, whereas for $j = 0.1$, $R_{\rm ms} = 5.7M$.

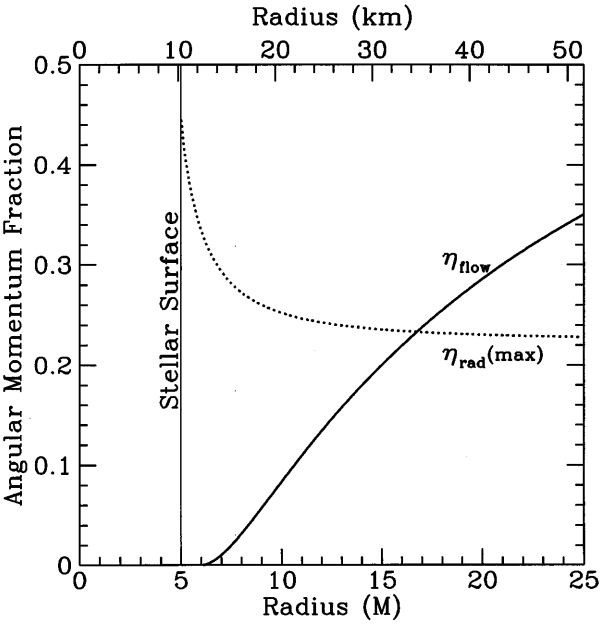

FIG. 7.—Fraction $\eta_{\rm flow}$ (*solid curve*) of the specific angular momentum of an element of gas in Keplerian circular orbit at Boyer-Lindquist radial coordinate r (measured in units of the stellar mass M) that must be removed in order for the gas to fall from r to the radius $R_{\rm ms}$ of the innermost stable circular orbit. The curve shown is for a static star ($j = 0$); the curves for slowly rotating stars would be little different. The dashed curve shows the estimate of the largest fraction $\eta_{\rm rad}(\max)$ of the specific angular momentum of an element of gas that can be removed by radiation coming from the surface of a nonrotating, isotropically radiating, spherical star of radius $5M$ (*dashed curve*; see text). The top axis shows the radius in kilometers for $M = 1.4\ M_\odot$.

1996), and assuming that all of the radiation emitted in the direction of the disk interacts with the disk flow ($f = 1$ in the notation of Miller & Lamb 1993). Figure 7 shows that $\eta_{\rm rad}$(max) exceeds $\eta_{\rm flow}$ only inside $\sim 17M$ (~ 36 km). This characteristic radius depends on the radius of the neutron star, because the luminosity is proportional to the gravitational binding energy at the stellar surface, but this dependence is relatively weak (the characteristic radius decreases from $21M$ to $13M$ as the stellar radius increases from $4M$ to $7M$). Hence, *the sonic-point model predicts that if radiation drag produces a transition to rapid radial inflow, the transition will occur within* $\sim 15M$ and hence that the Keplerian frequency at the transition radius will be $\gtrsim 300$ Hz (see § 3.3). Determining the actual radius of the transition requires gas dynamical and radiation transport calculations.

Model calculations.—The nature of the transition to supersonic radial inflow is illustrated by the following fully general relativistic calculations of the gas dynamics and radiation transport in the innermost part of the accretion disk flow. In these calculations, the azimuthal velocity of the gas in the disk is assumed to be nearly Keplerian far from the star. Internal shear stress is assumed to create a constant inward radial velocity $v^{\hat{r}}$ in the disk, as measured in the local static frame, of 10^{-5} (here and below we take $v^{\hat{r}}$ to be positive for radially inward flow). The half-height $h(r)$ of the disk flow at radius r is assumed to be ϵr at all radii, where ϵ is a constant and r is the radius, and the kinetic energy of the gas that collides with the surface of the star is assumed to be converted to radiation that emerges from a band around the star's equator with a half-height equal to ϵR. For simplicity, and to show the effects of radiation forces more clearly, any effect of the stellar magnetic field on the dynamics of the disk flow near the sonic transition is neglected in this model calculation.

The surface density $\Sigma_{\rm co} \equiv 2h\rho_{\rm co}$ of the disk flow as measured by a local observer comoving with the gas is related to the surface density $\Sigma_{\rm stat}$ of the disk flow as measured by a local static observer by a Lorentz boost, so

$$\Sigma_{\rm co} = \gamma^{-1}\Sigma_{\rm stat} , \tag{3}$$

where $\gamma \equiv [1 - (v^{\hat{r}})^2 - (v^{\hat{\phi}})^2]^{-1/2}$ and we have neglected $v^{\hat{z}}$. For stationary disk accretion, $\Sigma_{\rm stat}$ at radius r is given by (see eq. [5.6.3] of Novikov & Thorne 1973)

$$\Sigma_{\rm stat} = (\dot{M}_{\infty}/2\pi r v^{\hat{r}})(1 - 2M/r)^{-1/2} , \tag{4}$$

where $\dot{M}_{\infty}$ is the mass accretion rate through the disk, as measured at infinity.

Close to the star, the photon mean-free path is limited primarily by Thomson scattering and is therefore $1/n_e\sigma_{\rm T}$, where n_e is the electron number density in the disk flow as measured in the frame comoving with the flow and $\sigma_{\rm T} = 6.65 \times 10^{-25}$ cm^2 is the Thomson scattering cross section. Hence, for a steady flow, the radial optical depth from the stellar surface at radius R through the disk to radius r is

$$\tau_{\rm radial}(r) \equiv \sigma_{\rm T}\int_R^r n_e(r^p)dr^p = \left(\frac{\sigma_{\rm T}\dot{M}_{i,\infty}}{4\pi m_p}\right) \times \int_R^r \frac{[1 - v^{\hat{r}}(r')]^{-1}}{\gamma_r(r')\gamma(r')}\frac{(1 - 2M/r')^{-1}}{r'h(r')v^{\hat{r}}(r')}\,dr' , \tag{5}$$

where $\dot{M}_{i,\infty}$ is the mass accretion rate through the inner disk, as measured at infinity. The radial coordinate r^p in the first expression on the right-hand side is the proper radial distance in the frame comoving with the gas. In the second expression on the right-hand side we have estimated n_e in the disk flow between r and the stellar surface by assuming for simplicity that the gas in the disk is fully ionized hydrogen and using the continuity equation. Then $n_e = \Sigma_{\rm co}/2hm_p = \gamma^{-1}(\dot{M}_{i,\infty}/4\pi m_p v^{\hat{r}} rh)(1 - 2M/r)^{-1/2}$, where m_p is the proton mass and h is the half-thickness of the disk flow. The differential proper radial distance dr^p in the frame comoving with the gas is related to the differential radial distance in the local static frame by a Lorentz boost, so $dr^p = (1 - v^{\hat{r}})^{-1}\gamma_r^{-1}\,dr_{\rm stat}$, where $v^{\hat{r}}$ is the inward radial velocity and $\gamma_r \equiv [1 - (v^{\hat{r}})^2]^{-1/2}$. The differential radial distance in the local static frame is in turn related to the differential radial distance dr' in the global (Boyer-Lindquist) coordinate system by $dr_{\rm stat} = (1 - 2M/r')^{-1/2}\,dr'$, so $dr^p = (1 - v^{\hat{r}})^{-1}\gamma_r^{-1}(1 - 2M/r')^{-1/2}\,dr'$.

Once the drag force exerted by the radiation from the stellar surface begins to remove angular momentum from the gas in the Keplerian disk, centrifugal support is lost and the gas falls inward, accelerating rapidly. Radiation that comes from near the star and is scattered by the gas in the disk is generally scattered out of the disk plane and hence does not interact further with the gas in the disk. Moreover, second and successive scatterings do not contribute proportionately to the azimuthal radiation drag force on the gas because the radiation field is aberrated by the first scattering and afterward carries angular momentum (see Miller & Lamb 1993, 1996). We therefore treat the interaction of the radiation with the gas in the disk by assuming that the intensity of the radiation coming from the star is attenuated as it passes through the gas in the disk, diminishing as $\exp(-\tau_{\rm radial})$, where $\tau_{\rm radial}(r)$ is given by equation (5), and that scattered radiation does not contribute to removal of angular momentum from the gas. In calculating the radiation drag force, we assume for simplicity that the differential scattering cross section is isotropic in the frame comoving with the accreting gas (this gives results very close to those obtained using a Thomson differential cross section; see Lamb & Miller 1995). The radiation field and the motion of the gas are computed in full general relativity.

The optical depth of the disk flow near the star is generally much less than one would estimate by calculating it without taking into account the radiation forces. The reason is that the loss of centrifugal support caused by transfer of angular momentum to the radiation causes the inward radial velocity of the gas in the disk at radii less than the radius $R_{\rm aml}$ of the radiation-induced transition to supersonic inflow to be orders of magnitude higher, and the density of the gas to be orders of magnitude lower, than if radiation forces were neglected (see Miller & Lamb 1996). Hence the mean free path in the disk flow is much larger, and the optical depth from the stellar surface to a given radius in the flow is much smaller, than they would be in the absence of radiation drag. In this way the radiation increases the transparency of the disk flow, so its effects are felt much farther out in the flow than one would estimate from the properties of the undisturbed flow.

Figure 8 shows results obtained by solving self-consistently for the gas dynamics and the radiation field in this simple model, for a disk flow of semithickness $\epsilon \equiv h/r = 0.1$, a nonrotating neutron star with gravitational mass $M = 1.4\ M_{\odot}$ and radius $R = 5M$, and accretion rates through the inner disk of 0.02, 0.03, 0.04, and $0.05\dot{M}_{\rm E}$, where

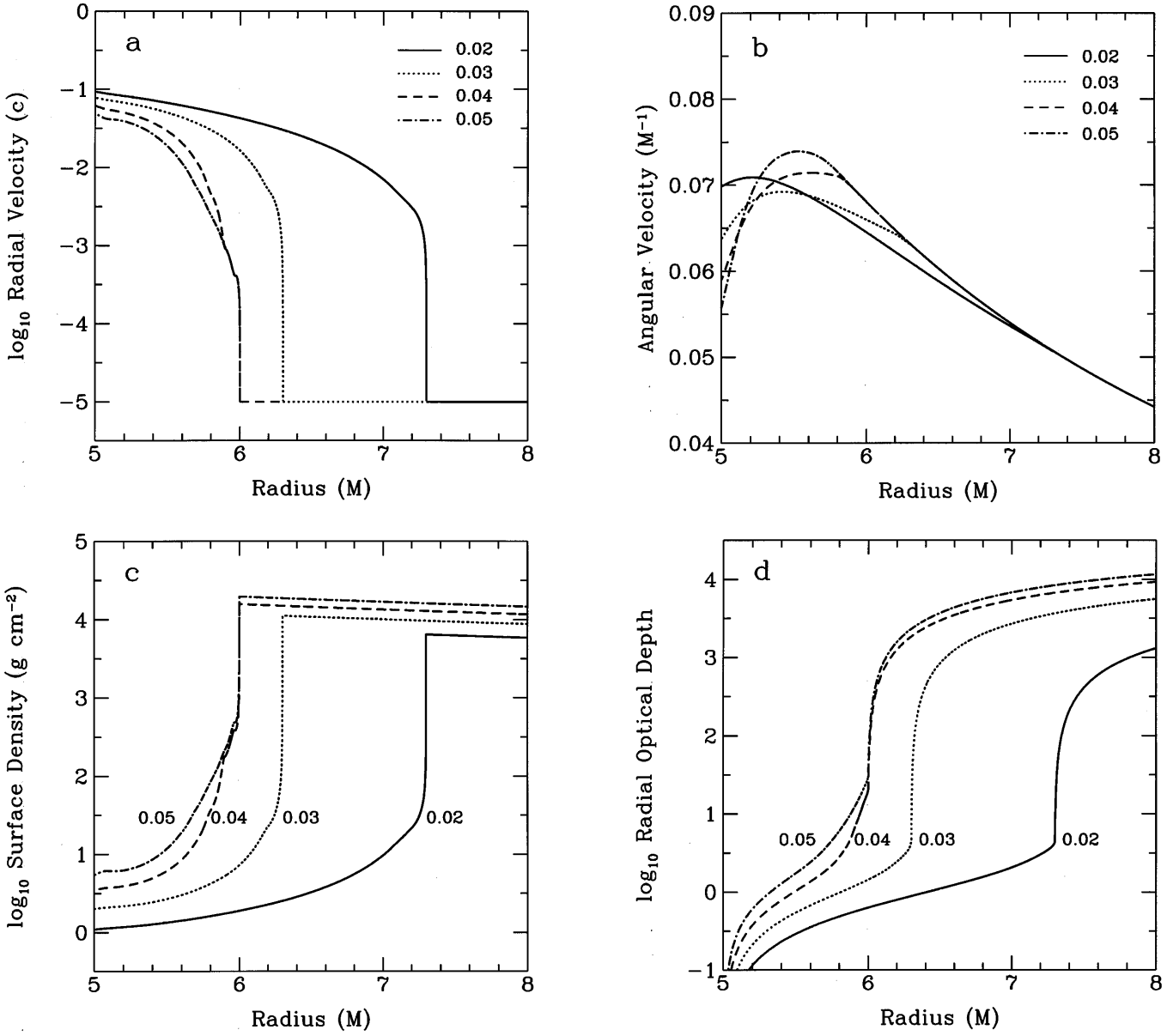

FIG. 8.—Numerical results for the structure of the accretion flow near the neutron star in the fully general relativistic model of gas dynamics and radiation transport in the inner disk described in the text. (*a*) The inward radial velocity v^r of the gas in the disk measured by a local static observer. (*b*) The angular velocity of the gas in the disk measured by an observer at infinity. (*c*) The surface density Σ_{co} of the disk flow measured by an observer comoving with the flow. (*d*) The radial optical depth τ_r from the stellar surface through the disk flow to the radius shown on the horizontal axis. The radial coordinate is the Boyer-Lindquist radius in units of the stellar mass M; the radius of the star is $5M$. The four curves in each panel are labeled with the assumed accretion rate $\dot{M}_i$ through the inner disk, measured in units of the accretion rate $\dot{M}_E$ that would produce an accretion luminosity at infinity equal to the Eddington critical luminosity.

$\dot{M}_E$ is the mass accretion rate that produces the Eddington critical luminosity at infinity (see Lamb & Miller 1995). These accretion rates are typical of the lower luminosity atoll sources. The calculations were carried out using the numerical algorithm described in Miller & Lamb (1996).

The results shown in Figure 8 demonstrate that radiation forces and general relativistic effects create a sharp transition to supersonic inflow several kilometers above the stellar surface and that the transition radius decreases with increasing mass flux when the transition is caused by radiation drag. These results are not intended to represent the inflow in any particular source. For $\dot{M}_i = 0.02\dot{M}_E$ and $0.03\dot{M}_E$, the transition to rapid radial inflow occurs at $7.3M$ and $6.3M$, respectively, and is caused by transfer of angular momentum from the gas to the radiation field. For $\dot{M}_i = 0.04\dot{M}_E$ and $0.05\dot{M}_E$, most of the radiation from the star does not penetrate as far out as the radius $R_{ms} = 6M$ of the innermost stable circular orbit, so the transition to rapid radial inflow occurs at R_{ms} and is caused by the absence at $r < R_{ms}$ of circular orbits with the specific angular momentum of the orbit at $r = R_{ms}$.

The radial velocity profiles plotted in Figure 8*a* show that at the sonic point the radial velocity typically increases by about 2 orders of magnitude in a very small radial distance ($\delta r \sim 0.001$–$0.01r$). The angular velocity profiles plotted in Figure 8*b* show that the effect of radiation forces on the angular velocity is smaller but is still very significant. For $\dot{M}_i = 0.04\dot{M}_E$ and $0.05\dot{M}_E$, the angular velocities outside

$6M$ are nearly Keplerian, because the gas there is shielded from the radiation by the gas further in. However, for $\dot{M}_i = 0.02\dot{M}_{\rm E}$ and $0.03\dot{M}_{\rm E}$, the angular velocity drops below the Keplerian value well outside $6M$. It is this departure from Keplerian orbital motion, and the associated loss of centrifugal support, that causes the flow to accelerate radially inward. All the angular velocity profiles turn downward near the stellar surface because of the strong azimuthal radiation drag force there. The decrease in the kinetic energy and angular momentum of the inflowing gas is exactly compensated by the increase in the energy and angular momentum carried outward by the escaping radiation (see Miller & Lamb 1993, 1996).

Figure 8*c* shows that the vertical column density of all four disk flows drops abruptly from $\sim 10^4$ g cm^{-2} outside the sonic radius to $\lesssim 10$ g cm^{-2} inside. The radial optical depth measured outward from the stellar surface is shown in Figure 8*d*; it decreases by about 2 orders of magnitude at the sonic radius, but not as sharply as the vertical optical depth. Even when the transition to rapid radial inflow occurs at $R_{\rm ms}$, the flow between $R_{\rm ms}$ and the stellar surface is generally strongly affected by radiation forces, as shown by the differences between the velocity and optical depth profiles for $\dot{M}_i = 0.04\dot{M}_{\rm E}$ and $0.05\dot{M}_{\rm E}$. We caution that these results are only illustrative. For example, X-rays may be emitted from a larger fraction of the stellar surface than we have assumed, in which case $R_{\rm aml}$ will be larger for a given accretion rate.

Radius of the transition.—In the model of gas dynamics and radiation transport just described, under conditions such that loss of angular momentum to radiation drag is important outside $R_{\rm ms}$, loss of centrifugal support and rapid radial inflow begins about 5 photon mean-free paths from the stellar surface, i.e., the transition occurs where $\tau_{\rm radial}(r) \approx 5$. In this model the inward radial velocity of the gas in the disk inside $R_{\rm aml}$ typically rises very sharply to $\sim 0.1c$ and then changes more slowly until the gas collides with the stellar surface (see also Miller & Lamb 1993, 1996). Hence we can estimate $R_{\rm aml}$ by setting $\tau_{\rm radial} = 5$ in equation (5), scaling $v^{\hat{r}}$ and h/r in units of 10^{-2} and $0.1c$, respectively, and solving for the radius. The result is

$$R_{\rm aml} \approx R + 5\left(\frac{\dot{M}_i}{0.01\dot{M}_{\rm E}}\right)^{-1}\left(\frac{R}{10\ {\rm km}}\right)\left(\frac{h/R}{0.1c}\right)\left(\frac{v^{\hat{r}}}{10^{-2}}\right)\ {\rm km}\ . \tag{6}$$

This estimate is in rough agreement with the transition radius found in our numerical calculations.

Width of the transition.—Under conditions such that the transition to rapid radial inflow is caused by radiation drag, the width δ of the radial velocity transition is determined by $\lambda_\gamma^{\rm K}$, the photon mean-free path in the Keplerian disk flow at $R_{\rm aml}$, because this is the characteristic distance over which the gas first becomes exposed to radiation from the star, and by the radial distance $\delta_{\rm aml}$ over which the gas in the disk loses its angular momentum once it is exposed to radiation from the star. From expressions similar to those used above to compute the radial optical depth in the Keplerian disk flow, we find

$$\frac{\lambda_\gamma^{\rm K}}{r} \sim 10^{-4}\left(\frac{\dot{M}_i}{0.01\dot{M}_{\rm E}}\right)^{-1}\left(\frac{h/R}{0.1}\right)\left(\frac{v^{\hat{r}}}{3\times 10^{-5}c}\right), \tag{7}$$

where we have scaled the quantities that enter this expression in terms of their approximate values in the transition region. This estimate is consistent with the results of our numerical calculations. From the expression for the radiation drag rate given by Miller & Lamb (1993, 1996), we find

$$\frac{\delta_{\rm aml}}{r} \sim 3c_s^{3/2}\left(\frac{\dot{M}}{\dot{M}_{\rm E}}\right)^{-1/2} \sim 10^{-3}\left(\frac{c_s}{10^{-3}}\right)^{3/2}\left(\frac{\dot{M}}{0.01\dot{M}_{\rm E}}\right)^{-1/2}, \tag{8}$$

where we have scaled c_s in terms of the typical value for a gas-pressure–dominated inner disk. These estimates show that the radial velocity is expected to increase over a very small radial distance $\delta \sim 10^{-3}r$ to $10^{-4}r$. This expectation is in accord with the results of our numerical calculations presented above. As noted in § 3.1, this transition is somewhat analogous to the transition at the boundary of a Strömgren sphere, except that here the radiation removes angular momentum from the gas rather than stripping electrons from atoms or molecules and causes a sharp increase in the inward radial velocity rather than in the degree of ionization.

If the neutron star radius is smaller than $R_{\rm ms}$ and conditions are such that the transition to rapid radial inflow is caused by general relativistic corrections to Newtonian gravity, the radial velocity increases rapidly near $R_{\rm ms}$ because gas inside $R_{\rm ms}$ can fall to the stellar surface without losing any angular momentum. The precise location of the sonic transition is slightly affected by pressure forces and, if the shear stress is large, by outward angular momentum transport within the disk flow (see Muchotrzeb 1983; Muchotrzeb-Czerny 1986). In the absence of shear stresses and pressure forces, the radial velocity $v^{\hat{r}}$ of an element of gas at radius $r = R_{\rm ms}(1-\xi)$, where $\xi \ll 1$, that has fallen inward from a circular orbit at $R_{\rm ms}$ is approximately $(\xi/2)^{3/2}$ (Miller & Lamb 1996). Hence, for $c_s \sim 10^{-3}$, the inflow becomes supersonic over a radial distance $\delta \sim \xi r \sim (c_s)^{2/3}r \sim 10^{-2}r$.

Summary and implications for kilohertz QPOs.—For sources in which the radius R of the neutron star is larger than the radius $R_{\rm ms}$ of the innermost stable circular orbit and accretion is under conditions such that angular momentum loss to the radiation field terminates the Keplerian flow at a radius is larger than R, our results show that the Keplerian disk flow near the star is terminated by angular momentum loss to radiation and that the radius of the transition to rapid radial inflow decreases steeply with increasing mass flux through the inner disk. Hence the orbital frequency at the sonic radius, and therefore the frequency of the associated QPO, increases steeply with increasing mass flux. If instead conditions are such that radiation forces do not terminate the Keplerian flow, the Keplerian flow is probably terminated by interaction with the stellar surface, in which case generation of a coherent QPO with a frequency equal to the orbital frequency at the stellar surface appears very unlikely.

For sources in which R is smaller than $R_{\rm ms}$ and accretion occurs under conditions such that radiation forces terminate the Keplerian flow outside $R_{\rm ms}$, our results show that the Keplerian flow is terminated by angular momentum loss to radiation and that the radius of the transition to rapid radial inflow decreases steeply with increasing mass flux. Hence the frequency of the QPO associated with the orbital frequency at the sonic radius again increases steeply with increasing mass flux. If instead conditions are such that

radiation forces do not terminate the Keplerian flow outside R_{ms}, the Keplerian flow is terminated by general relativistic corrections to Newtonian gravity and the radius of the transition to rapid radial inflow is approximately independent of the mass flux. Hence, under these conditions the frequency of any QPO with the orbital frequency at the sonic point will be approximately independent of the accretion rate.

Although the numerical results presented here are for accretion rates typical of the atoll sources, which have very weak magnetic fields and are accreting at rates much less than the Eddington critical rate, we expect the structure of the accretion flow and the behavior of the sonic-point Keplerian QPO frequency to be similar in the Z sources, even though they are thought to have stronger magnetic fields and are accreting at much higher rates. There are three reasons.

(1) The radius of the transition to rapid radial inflow that we are considering is necessarily close to the neutron star whatever the luminosity, because the fraction of the angular momentum in the Keplerian disk flow that can be removed by radiation drag is small and general relativistic corrections to Newtonian gravity are important only near the neutron star. (Although the luminosities of the Z sources are much higher, the angular momentum flux that must be removed to create a radial inflow is correspondingly higher. In sources with luminosities very close to the Eddington critical luminosity, radiation drag can significantly affect the motion of up to $\sim 20\%$ of the accreting gas further away but can affect the motion of most of the accreting gas only close to the star [see Fortner et al. 1989; Lamb 1989].)

(2) The inferred magnetic fields of the neutron stars in the Z sources are stronger than those of the neutron stars in the atoll sources, and hence a larger fraction of the disk flow is likely to be channeled out of the disk by the stellar magnetic field, causing the mass flux through the inner disks of the Z sources to be comparable to the mass fluxes through the inner disks of the atoll sources.

(3) The vertical thickness of the inner disk flow is likely to be larger in the Z sources than in the atoll sources.

All of these effects act in the direction of making the radius of angular momentum loss in the Z sources similar to its value in the atoll sources. We do expect significant departures from the behavior found in the present calculations when the luminosity equals or exceeds the Eddington critical luminosity. These points are discussed in more detail in § 4.

3.3. *Frequencies of the Sonic-Point QPOs*

We consider now the frequencies that are generated by the sonic-point mechanism. There are two fundamental QPO frequencies: (1) the Keplerian frequency at or near the sonic radius and (2) the sonic-point beat frequency, which is generated by interaction of radiation from the neutron star with the accretion flow near the sonic radius. QPOs may also be detectable at overtones of the Keplerian and beat frequencies. QPOs at sideband frequencies and oscillations at the spin frequency of the neutron star and its overtones are likely to be very weak.

In analyzing the frequencies generated by the sonic-point mechanism, we shall for definiteness use Boyer-Lindquist global coordinates, which are familiar because they are commonly used to describe the spacetime of rotating black holes. However, all of the expressions we give are accurate only to first order in j and hence would be unchanged if we used circumferential rather than Boyer-Lindquist coordinates.

In Boyer-Lindquist coordinates, the circular frequency of an element of matter on the surface of the rotating star or of an element of gas in orbit around it is

$$\nu \equiv (1/2\pi)(d\phi/dt) , \tag{9}$$

where ϕ and t are the azimuthal and time coordinates of the element of matter or gas. When measured in Boyer-Lindquist coordinates, any rotational frequency appears to be the same at every point in space and is equal to the frequency measured by a distant observer because of the symmetries of the spacetime outside a steadily rotating star[3] and the fact that the Boyer-Lindquist time coordinate is the proper time of an observer at radial infinity. We emphasize that the frequency in equation (9) is *not* the frequency that would be measured by a local observer (i.e., in a local orthonormal tetrad), unless the observer is at infinity.

Sonic-point Keplerian frequency.—As explained earlier in this section, the radiation drag force acting on the gas in a clump near the sonic radius generates a supersonic stream of denser gas that spirals inward toward the stellar surface. To the extent that the radiation field is axisymmetric, the inspiral trajectory of the gas from each such clump is identical and hence the azimuthal separation $\Delta\phi_{str}$ between any two such streams is the same at every radius inside the sonic point and equal to the azimuthal separation $\Delta\phi_{cl}$ of the two clumps at the sonic radius r_s that are producing the two streams. Therefore a collection of clumps distributed around the star at the sonic radius will generate a pattern of inspiral streams that rotates around the star at the orbital frequency $\nu_{Ks} \equiv \nu_K(r_s)$ of the gas at the sonic radius.

We can estimate ν_{Ks} by noting that, to first order in j, the spacetime outside a slowly and uniformly rotating star is the same as the Kerr spacetime (Hartle & Thorne 1968; the two spacetimes are not the same to higher orders in j). Hence, to first order in j the orbital frequency of an element of gas in a prograde Keplerian circular orbit at Boyer-Lindquist radius r_s in the rotation equator of a slowly rotating star is (see Bardeen, Press, & Teukolsky 1972)

$$\nu_{Ks} = \frac{1}{2\pi}\frac{d\phi_{Ks}(r)}{dt} = \frac{1}{2\pi}\left[1 - j\left(\frac{M}{r_s}\right)^{3/2}\right]\left(\frac{M}{r_s^3}\right)^{1/2}$$
$$\approx 1181\left(\frac{M}{1.4\ M_\odot}\right)^{1/2}\left(\frac{r_s}{15\ \mathrm{km}}\right)^{-3/2}\ \mathrm{Hz} . \tag{10}$$

The *pattern* of the gas streaming inward from the clumps at r_s rotates uniformly around the star with frequency ν_{Ks}. The pattern frequency is different from the orbital frequency $\nu_{orb}(r)$ of the gas inside the sonic radius, which varies with

[3] The spacetime outside a steadily rotating star has both timelike and spacelike Killing vector fields $\xi_{(t)}$ and $\xi_{(\varphi)}$, which reflect the stationarity and axial symmetry of the spacetime (see, e.g., Misner, Thorne, & Wheeler 1973, pp. 892–895). In any coordinate system in which the time and azimuthal coordinates are based on $\xi_{(t)}$ and $\xi_{(\varphi)}$, such as the Boyer-Lindquist coordinate system, the time interval required for one rotation of an element of the star or one orbit of an element of gas orbiting the star is the same everywhere, when measured in the global time coordinate. Stated more concretely, if an element of gas emits a pulse of X-rays each time its azimuthal coordinate ϕ increases by 2π, the time interval Δt between the arrival of successive pulses will be the same everywhere, when measured in the global time coordinate t.

radius. In particular, the pattern frequency is different from the orbital frequency of the gas just before it collides with the stellar surface.

The brightness pattern made by the collision of the inspiraling streams of denser gas with the stellar surface rotates around the star at frequency $\nu_{\rm Ks}$, as measured by an observer at infinity. This is therefore the frequency at which the radiation pattern produced by the bright footprints of the streams rotates around the star and hence also the centroid frequency of the resulting quasi-periodic oscillation in the X-ray flux and spectrum seen by a distant observer whose line of sight is inclined to the rotation axis of the disk. Therefore the radiation pattern produced by the bright footprints of the streams generally does *not* corotate with the star, but instead moves around the stellar surface.

Stellar spin frequency.—As explained in § 3.1, if the star's magnetic field is too weak to affect the accretion flow at the sonic point but is strong enough to partially channel the flow close to the stellar surface, it will create a weakly beamed pattern of radiation that rotates *with the star*. The surface magnetic fields of the neutron stars in the atoll and Z sources, which are thought to be several hundred million years old, may be nearly dipolar. If the magnetic field is dipolar but offset from the center of the star, the radiation pattern it produces will have two unequal maxima around the star, whereas if the field is a centered but tilted dipole field, the radiation pattern will have two nearly equal maxima around the star. We therefore expect that there will generally be a brightness oscillation with a frequency equal to 1 or 2 times the spin frequency $\nu_{\rm spin}$ of the star. However, as we discuss in detail in § 4.3, we expect the relatively weak magnetic fields of the atoll and Z sources to produce radiation patterns that are only weakly beamed, even near the star. When the substantial attenuation of this inherently weak beaming that is caused by scattering in the central corona is taken into account, the X-ray oscillation at $\nu_{\rm spin}$ or $2\nu_{\rm spin}$ seen by a distant observer may be very weak or even undetectable with current instruments.

Sonic-point beat frequency.—The weakly beamed pattern of radiation rotating with the star causes the radiation drag force acting on the gas in a given clump orbiting near the sonic radius to peak with a frequency equal to 1 or 2 times the difference (beat) frequency $\nu_{\rm Bs}$ between the Keplerian frequency at the sonic point and the spin frequency of the star, as explained in § 3.1. The peak in the drag force will cause a temporary increase in the flux of denser gas streaming supersonically inward from the clump with a frequency equal to the sonic-point beat frequency

$$\nu_{\rm peak} = k\nu_{\rm Bs} \equiv k(\nu_{\rm Ks} - \nu_{\rm spin}) , \qquad (11)$$

where $k = 1$ or 2, depending on the symmetry (see Lamb et al. 1985). The inflow time from the sonic point is typically $\sim$5–10 beat periods, so there are typically this many density enhancements in the stream of gas from a given clump to the stellar surface. These density enhancements do not lie along a single gas streamline, but instead along a sequence of streamlines. As they collide with the stellar surface, they produce a sequence of brighter impact arcs around the surface in the plane of the disk. As the quasi-periodic increase in the mass flux from a given clump arrives at the stellar surface, it produces a quasi-periodic modulation in the luminosity of the star with frequency $\nu_{\rm Bs}$. Because this beat frequency is the difference between an orbital and a spin frequency, the frequency of the resulting quasi-periodic modulation of the X-ray flux and spectrum seen by an observer at infinity is $\nu_{\rm peak}$.

Expected range of sonic-point QPO frequencies.—In § 3.2 we showed that either radiation forces or general relativistic corrections to Newtonian gravity cause an abrupt transition to rapid radial inflow and that the radius of this transition is bounded below by the radius of the marginally stable orbit, which is 12 km for a nonrotating 1.4 $M_\odot$ star, and above by the $\sim$20% upper bound on the fraction of the angular momentum of the accreting gas that can be transferred to the radiation field, which constrains the transition radius to be $\lesssim$30 km for a 1.4 $M_\odot$ star. As discussed in § 4.2, there are several effects that are likely to reduce further the allowed range of the transition radius, perhaps to $\sim$15–25 km. Inserting these radii in equation (10) gives an expected range for the sonic-point Keplerian frequency of $\sim$500–1200 Hz. For stars with spin frequencies $\sim$200–300 Hz, the expected range of beat frequencies is then $\sim$200–1000 Hz. These ranges are similar to the frequencies of the kilohertz QPOs detected so far.

Overtones and sidebands of the sonic-point QPO frequencies.—In addition to the beaming oscillations at $\nu_{\rm Ks}$ and $\nu_{\rm spin}$ and the luminosity oscillation at $\nu_{\rm Bs}$, we expect accretion onto weakly magnetic neutron stars to generate brightness oscillations at several other frequencies. For example, the X-ray brightness modulation produced by the motion of the brighter impact footprints around the star with frequency $\nu_{\rm Ks}$ is unlikely to be exactly sinusoidal, so there may be some power at overtones of $\nu_{\rm Ks}$. However, the angular distribution of the X-ray emission from the impact footprints is expected to be very broad (see § 3.1), so the power at overtones of $\nu_{\rm Ks}$ is likely to be much smaller than the power at $\nu_{\rm Ks}$. The radiation pattern that rotates with the star is also expected to be very broad by the time the radiation escapes from the central corona, so the power at overtones of $\nu_{\rm spin}$ is likely to be much smaller than the power at $\nu_{\rm spin}$, which is itself expected to be small for the reasons discussed above. However, the radiation pattern that rotates with the star is likely to be narrower at the sonic radius than outside the central corona, causing the modulation of the mass flux from the sonic point to be somewhat nonsinusoidal and giving rise to weak overtones of the sonic-point beat frequency. Luminosity oscillations are not as strongly attenuated by scattering in the central corona (see § 4.1), so it may be easier to detect overtones of $\nu_{\rm Bs}$.

The sonic-point mechanism causes a modulation of the inward mass flux and hence the stellar luminosity at the sonic-point beat frequency; from the point of view of a distant observer, this luminosity is then modulated at the sonic-point Keplerian frequency by the motion of the brighter footprints around the star. As result, QPOs are generated at some sideband frequencies. However, by far the strongest QPOs are generated at the sonic-point Keplerian and beat frequencies. To see this, consider as an example the X-ray flux waveform

$$f(t) = [1 + K_1 \cos(2\pi\nu_{\rm K} t + \phi_{\rm K1}) + K_2 \cos(4\pi\nu_{\rm K} t + \phi_{\rm K2})] \times [1 + B_1 \cos(2\pi\nu_{\rm B} t + \phi_{\rm B1}) + B_2 \cos(4\pi\nu_{\rm B} t + \phi_{\rm B2})] , \qquad (12)$$

which describes these modulations. In equation (12) we have included for the sake of illustration only the fundamental and first overtones of the Keplerian and beat frequencies; higher harmonics may of course also be present.

The frequencies that are generated are listed in Table 3. The only first-order QPOs are those at the sonic-point beat and Keplerian frequencies. There are also QPOs at the second harmonics of the beat and Keplerian frequencies. The lowest order QPOs generated by the modulation of the beat-frequency "carrier" by the motion of the footprints around the star are of second order and are at the stellar spin frequency $\nu_{\rm spin}$ and at the very high frequency $2\nu_{\rm Ks} - \nu_{\rm spin}$. The only QPO of intermediate frequency generated by this modulation is a QPO at $\nu_{\rm Ks} - 2\nu_{\rm spin}$, that is third-order and hence likely to be very weak. All the other QPOs generated are also third-order and in addition have very high frequencies. They are therefore likely to be intrinsically weak, strongly attenuated by scattering in the central corona, and difficult to detect.

As we discuss in § 4.3, only brightness oscillations that are fairly large near the neutron star and are not strongly attenuated by the gas surrounding the star will be detectable by a distant observer. In the sonic-point model, only the sonic-point beat frequency QPO and its overtones are luminosity oscillations; the other QPOs are beaming oscillations and are therefore more attenuated by scattering. For this reason, we expect strong QPOs only at $\nu_{\rm Bs}$ and $\nu_{\rm Ks}$. Nonetheless, QPOs at other frequencies, such as $\nu_{\rm spin}$, $2\nu_{\rm Bs}$, and $2\nu_{\rm Ks}$ may be detectable. Detection of oscillations at any of these frequencies would corroborate the sonic-point model.

3.4. *Coherence of Sonic-Point QPOs*

A key question any theory of the kilohertz QPO sources that relates a QPO frequency to orbital motion must address is why narrow peaks are seen in power spectra of the brightness variations of these sources, rather than a broad continuum corresponding to the range of orbital frequencies in the inner disk. Indeed, the remarkably high coherence ($\nu_{\rm QPO}/\delta\nu_{\rm QPO} \gtrsim 100$) of some of the kilohertz QPOs places very strong constraints on any model of these QPOs, because there are many physical effects that tend to decrease the coherence of oscillations at kilohertz frequencies. We discuss some of the most important effects, derive the resulting constraints on the accretion flow, and show that the sonic-point mechanism can produce narrow peaks consistent with the observed coherence of the kilohertz QPOs.

Gas in the inner disk orbits the neutron star with a wide range of frequencies, so at first glance one might think that fluctuations in the gas density throughout the inner disk would generate a broad spectrum of brightness variations. For the reasons discussed in § 2.3, it is very unlikely that such fluctuations can produce large amplitude brightness variations via direct emission or occultation. We have therefore focused our attention on the brightness variations that such density fluctuations produce indirectly, as gas from them falls inward and impacts the stellar surface. Here we show that the accretion flow in the vicinity of the sonic radius acts as a filter that selects brightness oscillations at the sonic-point orbital frequency while suppressing brightness oscillations at higher and lower frequencies. In order to see how this filtering occurs, we analyze the X-ray emission at the stellar surface produced by clumps that form at different radii in the inner accretion disk.

Effects of azimuthal shear.—Let us suppose for the sake of argument that the thickness of the inner disk is infinitesimal and that the flow there is laminar (we discuss the effects of turbulence shortly). We suppose further that a very small, roughly spherical density fluctuation (a clump) has formed well outside the sonic radius and consider what will happen to the gas in this clump and how it will affect X-ray emission from the star. When a small clump forms, the orbital phases of the elements of gas that comprise it are necessarily very similar, because of the small azimuthal extent of the clump. The elements of gas that comprise the clump also have very similar orbital frequencies, because the radial extent of the clump is small. As the clump drifts inward, elements of gas at different radii are sheared relative to one another in the azimuthal direction.

The frequency of the X-ray brightness oscillation that is generated by the inspiraling gas from a clump is approximately equal to the Keplerian frequency at the radius where the clump originally formed (see discussion in § 3.3).[4] A clump that forms very near the sonic radius will therefore produce an X-ray brightness oscillation at the sonic-point Keplerian frequency. If clumps can form inside the sonic radius, such clumps would produce X-ray brightness oscillations at the orbital frequencies where they formed.

This analysis shows that if the clumps were small and the flow laminar, differential rotation of the gas would not by itself pick out any particular orbital frequency. Consequently, if clumps were to form at a wide range of radii and nothing besides inward drift and azimuthal shear were to happen, gas inspiraling from the clumps and colliding with the stellar surface would produce brightness fluctuations with a wide range of frequencies up to the $\sim$1500–2000 Hz orbital frequency at the stellar surface (see, e.g., Kluzniak, Michelson, & Wagoner 1990).

Effects of clump destruction.—In reality, clumps that form outside the sonic radius are destroyed before they drift

TABLE 3

AMPLITUDES OF FREQUENCIES GENERATED BY ACCRETION FLOW

Frequency	First Order	Second Order	Third Order
$\nu_{\rm Bs}$	B_1	...	...
$\nu_{\rm Ks}$	K_1	...	...
$2\nu_{\rm Bs}$	...	B_2	...
$2\nu_{\rm Ks}$	...	K_2	...
$\nu_{\rm spin}$	...	$\frac{1}{2}K_1 B_1$	...
$2\nu_{\rm Ks} - \nu_{\rm spin}$	...	$\frac{1}{2}K_1 B_1$	...
$\nu_{\rm Ks} - 2\nu_{\rm spin}$	...	...	$\frac{1}{2}K_1 B_2$
$\nu_{\rm Ks} + \nu_{\rm spin}$	...	...	$\frac{1}{2}K_2 B_1$
$3\nu_{\rm Ks} - 2\nu_{\rm spin}$	...	...	$\frac{1}{2}K_1 B_2$
$3\nu_{\rm Ks} - \nu_{\rm spin}$	...	...	$\frac{1}{2}K_2 B_1$

[4] At first glance, one might think that if the inward radial drift time from a given radius r in the inner disk to the stellar surface is large, azimuthal shearing of a clump formed at r would by itself reduce the amplitude of the brightness variation produced by gas from the clump, but this is not so. The reason is that, to first order, the azimuthal velocity shear in a Keplerian flow conserves the volume of the clump, because the velocity field is divergence free to this order. Hence, the density of the gas in a clump relative to the density of the background gas is affected only weakly by the differential rotation. In fact, if the flow were incompressible as well as laminar, the angular width of the brighter impact arc on the stellar surface would also be unaffected, even if the total angular extent of the clump at all radii becomes large, because the angular extent of that part of the clump that is crossing the sonic radius at any given time is unchanged by azimuthal shear.

inward to the sonic point and gas in them can reach the stellar surface. Clumps (if any) that form inside the sonic radius orbit the star at a rapidly changing frequency and collide with the stellar surface before gas from them can produce a long wavetrain. Hence, only clumps that form very near the sonic radius can produce strong, relatively coherent brightness oscillations. In this way the disk flow filters out brightness oscillations at orbital frequencies other than the sonic-point Keplerian frequency.

In order to illustrate the effects of clump destruction in the Keplerian flow, we consider a simple model in which clumps form and are then destroyed by small-scale turbulence in the disk, such as that produced by the magnetoturbulence that is thought to be responsible for angular momentum transport within the disk flow (Balbus & Hawley 1991, 1992, 1998; Brandenburg et al. 1995, 1996; Hawley, Gammie, & Balbus 1995, 1996). In this simple model we assume that the forces that formed the clump in the first place no longer act to hold it together. If the clump has size ξ, turbulent motions on scales $\ell \gtrsim \xi$ will tend to advect the clump without destroying it; only turbulent motions on scales $\ell \ll \xi$ will disrupt the clump. We assume that the effect of these small-scale turbulent motions on the clump can be described by a diffusion coefficient $D \sim \beta\xi c_s$, where β is a dimensionless parameter that describes the strength of the small-scale turbulence and c_s is the thermal sound speed in the disk; for turbulent motions with scales $\ell \ll \xi$, β is small compared to unity. As a result of outward angular momentum transport by the magnetoturbulence, a clump of initial size ξ that forms at radius r will drift slowly inward with radial velocity $v^{\hat{r}} \sim \alpha(h/r)c_s$, where α is the usual viscosity parameter and h is the half-thickness of the disk. Such clumps will be dissipated by turbulent diffusion in a time $t_{\rm diss} \sim (\xi/\beta c_s) \sim (\xi/\beta h\Omega_{\rm K})$.

In this model, a clump that forms a radial distance δr outside the sonic radius r_s can reach the sonic radius and generate a supersonically inspiraling stream of gas before being destroyed only if $\delta r < v^{\hat{r}} t_{\rm diss}$, i.e., only if the clump forms within a radial distance

$$\delta r \lesssim (\alpha/\beta)(h/r_s)(\xi/r_s)r_s \lesssim 10^{-2} r_s \qquad (13)$$

of the sonic radius. Turbulence on small scales may be weak, and the effects that form the clumps in the first place—such as thermal instability, magnetic stresses, and radiation forces—may tend to continue to hold them together as they drift inward toward the sonic point, so that clumps can survive somewhat longer than $t_{\rm diss}$. Even so, it is clear that clumps that form even a small distance outside the sonic radius will be disrupted by turbulence before they reach the sonic point. This process suppresses brightness oscillations with frequencies less than the sonic-point Keplerian frequency.

It appears improbable that clumps will form in the hypersonic radial inflow between the sonic radius and the stellar surface, but even if clumps do form in this region, they will not produce appreciable brightness oscillations, for two reasons. First, a clump that forms inside the sonic radius will collide with the stellar surface after completing $\sim$1–10 orbits. A clump that lives only for a time $t_{\rm lifetime}$ will generate power over a range of frequencies $\delta\nu_{\rm lifetime} \sim (\pi t_{\rm lifetime})^{-1}$. Hence the power produced by a clump that forms inside the sonic radius will be spread over a frequency range $\delta\nu_{\rm lifetime} \gtrsim 0.03\nu$. Second, a clump that forms inside the sonic radius orbits the star at a frequency that rapidly increases from, for example, the $\sim$500 Hz orbital frequency at the sonic radius to the $\sim$1500 Hz orbital frequency at the stellar surface, as the clump spirals inward. For these reasons, even if clumps do form inside the sonic radius, any power they generate will be spread over a wide range of frequencies rather than concentrated in a narrow peak.

Coherence of the sonic-point Keplerian frequency QPO.—Clumps that form outside the sonic radius but close enough to it to reach it before being destroyed have initial orbital frequencies in the relatively narrow range

$$\delta\nu \sim \left(\frac{\delta r}{r_s}\right)\nu_{\rm Ks} \sim \left(\frac{\alpha}{\beta}\right)\left(\frac{h}{r_s}\right)\left(\frac{\xi}{r_s}\right)\nu_{\rm Ks} \leq 10^{-2}\nu_{\rm Ks}\,, \qquad (14)$$

which is consistent with the observed narrowness of the kilohertz QPO peaks. Clumps orbiting at different distances above or below the midplane of the disk will generally also have slightly different orbital frequencies. To estimate the resulting spread in frequencies, we assume that at each distance z above and below the disk plane the inward radial velocity increases sharply from subsonic to supersonic at some cylindrical radius R_s. We call the axisymmetric two-dimensional surface defined by $R_s(z)$ the sonic surface. If the sonic surface is cylindrical, the oscillation frequency generated by the clumps orbiting in the midplane of the disk is slightly greater than the oscillation frequency generated by the clumps orbiting above and below the midplane. The spread in oscillation frequencies depends on the precise shape of the sonic surface, but to lowest order in (h/r_s) the spread in frequencies caused by this effect is $\delta\nu \sim (h/r_s)^2\nu_{\rm Ks}$, which is consistent with the observed narrowness of the kilohertz QPO peaks if $h_s/r_s \lesssim 0.1$.

The persistence of a clump orbiting at the sonic radius is limited by its decay as gas inspirals from it to the stellar surface and by its disruption by small-scale turbulence, pressure forces, and other effects. In the simple model considered here, the clump decay timescale is $t_{\rm decay} \sim \xi/v^{\hat{r}} \sim (1/\alpha)(\xi/h_s)(r_s/h_s)(1/\Omega_{\rm K})$, which broadens the QPO peak by an amount $\delta\nu_{\rm decay} \sim \alpha(h_s/\xi)(h_s/r_s)\nu_{\rm Ks} \lesssim 10^{-2}\nu_{\rm Ks}$, which is consistent with the observed narrowness of the kilohertz QPO peaks. The dissipation of clumps by turbulent diffusion contributes a relative width $\delta\nu_{\rm diss} \sim \beta(h_s/\xi)\nu_{\rm Ks}$, which is consistent with the observed narrowness of the Keplerian frequency QPO peaks if $\beta \ll 1$ or the effects that form the clumps in the first place, such as thermal instability, magnetic stresses, and radiation forces, continue to hold them together as they orbit at the sonic point.

This simple model shows that if a clump is too small, it will persist for such a short time that the power it generates will be spread over a broad frequency range, whereas if a clump is too large it will persist for such a long time that its orbital frequency will change appreciably during its lifetime and the power it generates will again be spread over a broad frequency range. It is the clumps of intermediate size that generate relatively coherent oscillations.

In addition to frequency variation and lifetime broadening, other effects may increase the width of the Keplerian frequency QPO peak. For example, the radiation field inside the sonic radius is not perfectly axisymmetric, and hence the radiation forces acting on the inspiraling gas will vary slightly with azimuth. As a result, the radius of the sonic point and the density patterns produced by the inspiraling gas will be slightly different at different azimuths. A

quantitative treatment of these effects is well beyond what is possible with current accretion disk models.

The simple model we have discussed shows the crucial role played by the sharp transition to rapid radial inflow at the sonic radius that was found in § 3.2. In the absence of such a transition, density and magnetic field fluctuations in the inner disk would produce weak brightness variations over a wide range of frequencies rather than in the narrow range of frequencies needed to create a QPO peak. In the presence of such a transition, on the other hand, clumps orbiting in a narrow range of radii near the sonic radius produce strong X-ray brightness variations with a correspondingly narrow range of frequencies. Simple estimates of the broadening produced by the different orbital frequencies of these clumps and by their finite lifetimes appear consistent with the high observed coherence of the Keplerian frequency QPOs.

Coherence of related QPOs.—If there is a QPO at the beat frequency $\nu_{\rm Bs}$, we expect that its FWHM will in general be comparable to the FWHM of the QPO at $\nu_{\rm Ks}$. This is because the peak at $\nu_{\rm Bs}$ is at the beat frequency of the sonic-point Keplerian frequency with the stellar spin frequency, which is nearly coherent and therefore adds relatively little to the width of the QPO peak. However, we do not expect the widths of the QPO peaks at $\nu_{\rm Bs}$ and $\nu_{\rm Ks}$ to be identical, because scattering by the moving gas in the central corona affects the oscillations at $\nu_{\rm Bs}$ and $\nu_{\rm Ks}$ differently.

3.5. *Photon-Energy Dependence of the Sonic-Point QPOs and Time Lags*

The X-ray spectra of systems powered by accreting, weakly magnetic neutron stars, such as the kilohertz QPO sources, are formed primarily by Comptonization, as described in § 2.2. Cyclotron and bremsstrahlung photons with energies $\lesssim 1$ keV are produced near the neutron star surface and are then Comptonized by hot electrons in the region where the accretion flow interacts with the stellar surface and in the hot central corona that surrounds the star and its magnetosphere, yielding the observed X-ray spectra.

During a sonic-point Keplerian or beat-frequency oscillation, the rotation of the patterns of denser gas spiraling inward from clumps orbiting at the sonic radius causes the optical depth along the line of sight from the neutron star surface to the observer to vary quasi-periodically. The rate of production of soft photons and the physical properties of the Comptonizing gas may also oscillate, especially during the sonic-point beat-frequency oscillation, which is mainly a luminosity (accretion rate) oscillation. These oscillations cause the X-ray spectrum produced by the system to oscillate quasi-periodically with various frequencies. A small fractional variation in the optical depth causes a much larger fractional variation in the number of photons at high photon energies, because of the characteristic way in which the spectrum produced by Comptonization changes as the optical depth oscillates (see Miller & Lamb 1992). To the extent that the effects of Comptonization dominate, the oscillations at $\gtrsim 10$ keV will lag the oscillations at ~ 5 keV, because the photons above 10 keV have scattered more times in escaping from the source.

An accurate, quantitative treatment of the X-ray spectral oscillations produced by the inhomogeneous and time-dependent accretion flow in the kilohertz QPO sources would require a three-dimensional, time-dependent radiation hydrodynamic calculation in full general relativity. This is beyond present computational abilities. However, one can obtain a qualitative understanding of the dependence of QPO amplitudes on photon energy and the time lags to be expected using the following simplified model of the Comptonization process.

Assume that soft photons with a characteristic energy $E_{\rm in}$ that is much smaller than the electron temperature T_e are injected at the center of a static, uniform, spherical Comptonizing region of radius $R_{\rm C}$, electron density n_e, and scattering optical depth $\tau \equiv n_e \sigma_{\rm T} R_{\rm C}$, where $\sigma_{\rm T}$ is the Thomson scattering cross section. Assume further that $y \equiv 4T_e\tau^2/m_e \lesssim 1$, where m_e is the electron rest mass, and that the electrons have a negligible bulk velocity. These are good approximations for modeling formation of the time-averaged X-ray spectra of the atoll sources (see Psaltis & Lamb 1998b). The region of approximately radial inflow that develops when the mass accretion rate becomes comparable to $\dot{M}_{\rm E}$ (see Lamb 1989, 1991, and § 2) introduces additional effects on the spectra of the Z sources that cannot be treated in this way; we do not consider these effects here (but see Psaltis & Lamb 1998b). We treat the effects of oscillations in the rate of soft-photon production and in the properties of the Comptonizing region near the star by varying these quantities in the spherical model. In particular, we mimic the effects of the quasi-periodic variation of the optical depth along the line of sight by varying the optical depth of the model. We assume that the oscillation period is longer than the mean time for photons to escape from the Comptonizing region, an approximation that appears to be excellent for the kilohertz QPO sources.

Photon-energy dependence of the sonic-point Keplerian and beat-frequency oscillation amplitudes.—The X-ray number spectrum that emerges from the Comptonizing region at photon energies $E \gg E_{\rm in}$ can be approximated by (see, e.g., Rybicki & Lightman 1979, pp. 221–222)

$$f(E) \propto \begin{cases} \left(\dfrac{E}{E_a}\right)^{2+\alpha}, & E \ll E_b \\ \left(\dfrac{E_b}{E_a}\right)^{\alpha}\left(\dfrac{E}{E_a}\right)^{2} \exp\left[-\dfrac{(E-E_b)}{T_e}\right], & E \gg E_b\,, \end{cases} \tag{15}$$

where T_e is the electron temperature, E_a is a normalization constant that is typically a few keV, $E_b \sim (1\text{–}3)T_e$ is the cutoff energy, and

$$\alpha = -\frac{3}{2} - \sqrt{\frac{9}{4} + \frac{4}{y}}\,. \tag{16}$$

For small-amplitude oscillations in which the variation of the electron temperature in the Comptonizing region is negligible (see below), the relative amplitude $\gamma(E)$ of the oscillation is approximately (Miller & Lamb 1992)

$$\gamma(E) = \frac{\Delta\dot{N}_s}{\dot{N}_s} + \frac{d}{d\tau}\ln\left[f(E)\right]\Delta\tau\,. \tag{17}$$

Here $\Delta\dot{N}_s/\dot{N}_s$ is the relative change in the rate at which soft photons are injected into the Comptonizing region during an oscillation and $\Delta\tau$ is the change in the optical depth of the region. The relative amplitude $\gamma(E)$ is computed by considering a full oscillation period.

In general, the soft photon injection rate and the optical depth both vary during the oscillation. If so, equations (15),

(16), and (17) give

$$|\gamma(E)| \simeq \left| \frac{\Delta \dot{N}_s}{\dot{N}_s} + \gamma_\tau(E) \right| , \tag{18}$$

where

$$\gamma_\tau(E) \simeq -0.6 \left(\frac{T_e}{10 \text{ keV}} \right)^{-1/2} \left(\frac{3}{\tau} \right) \left(\frac{\Delta\tau/\tau}{0.05} \right) \times \left[\frac{\ln(E_b/E_a)}{2} \right] \begin{cases} \dfrac{\ln(E/E_a)}{\ln(E_b/E_a)} , & E \ll E_b \\ 1 , & E \gg E_b \end{cases} \tag{19}$$

in terms of the expected properties of the Comptonizing region and we have neglected the weak dependence of the normalization constant E_a on τ. Equations (18) and (19) show that in this case the relative amplitude of the QPO depends both on the relative change in the soft-photon injection rate, $\Delta \dot{N}_s/\dot{N}_s$, and on the relative change in the optical depth, $\Delta\tau/\tau$. In writing equation (17) we have assumed that the electron temperature in the Comptonizing cloud remains constant during the oscillation. If the electron temperature were allowed to vary, then the relative amplitude of the oscillation would not be constant at high photon energies, in disagreement with observations.

The quantity γ_τ is negative for the spectrum (15) and is small at low photon energies. If the oscillation in the injection rate of the soft photons is in phase with the oscillation in the optical depth, i.e., if $\Delta \dot{N}_s/\dot{N}_s$ and $\Delta\tau/\tau$ have the same sign, and if γ_τ is larger in magnitude than $\Delta \dot{N}_s/\dot{N}_s$ at high photon energies, then the relative amplitude of the oscillation in the photon number will not be a monotonic function of photon energy. For $\Delta \dot{N}_s/\dot{N}_s$ comparable in magnitude to $\Delta\tau/\tau$ and a Comptonizing region with the properties used in scaling equation (19), the relative amplitude of the oscillation has a minimum in the energy range $\sim$5–10 keV. The sonic-point beat frequency QPO is primarily a luminosity oscillation (see § 3.1), so the photon production rate is likely to vary significantly at the beat frequency. *The relative amplitude of the beat-frequency QPO may therefore have a minimum in the* 5–10 keV *energy range.*

If the relative change in the photon injection rate during an oscillation is very small, the first term on the right-hand side of equation (18) is likely to be negligible compared to the second term. In this case the relative amplitude of the oscillation will increase monotonically with increasing photon energy for energies less than $E_b \simeq$ 10–30 keV but will become independent of photon energy for energies greater than E_b. We expect this to be the case for the oscillation at the sonic-point Keplerian frequency, which is mainly a beaming oscillation (see § 3.1) and involves a relatively small variation in the photon production rate. *We therefore expect the relative amplitude of the Keplerian-frequency QPO to increase steeply in the* 5–10 keV *energy range and then flatten at high energies.*

When the photon injection rate and spectrum of injected soft photons do not change appreciably during a QPO cycle, the amplitude of the oscillation in luminosity caused by the oscillation in optical depth is comparable to the amplitude of the optical depth oscillation and is given by

$$\frac{\Delta L}{L} \sim \Delta y = 0.07 \left(\frac{T_e}{10 \text{ keV}} \right) \left(\frac{\tau}{3} \right)^2 \left(\frac{\Delta\tau/\tau}{0.05} \right) . \tag{20}$$

Equations (19) and (20) demonstrate that *a relatively weak oscillation in optical depth of only a few percent that is accompanied by a luminosity oscillation of moderate amplitude can produce naturally a much larger oscillation in the count rate at high photon energies.*

Equation (19) also shows that the relative amplitude of the oscillation at a given photon energy is different for different electron temperatures and optical depths, unless the relative amplitude of the oscillation in optical depth $\Delta\tau/\tau$ varies in such a way as to compensate for this effect. We therefore expect that as the mass accretion rate onto the neutron star changes (on timescales much longer than a beat-frequency period), the electron temperature and optical depth in the Comptonizing region will change, causing the photon-energy dependence of the beat-frequency and Keplerian-frequency oscillation amplitudes to change.

Photon-energy dependence of the sonic-point Keplerian and beat-frequency oscillation phases.—At photon energies $\lesssim$30 keV, the cross section and hence the electron scattering mean free path of the photons in the central corona is nearly independent of photon energy. Therefore, the average escape time of photons from the corona is also independent of their energy. However, the photons that stay in the corona longer experience more scatterings on average and therefore gain more energy by scattering off hot electrons and emerge from the medium with a larger energy. As a result, the oscillation at high photon energies is expected to lag the oscillation at low photon energies. If the injection rate of soft photons and the properties of the corona are constant in time, the magnitude of the time lag is determined mainly by the properties of the corona (see, e.g., Wijers, van Paradijs, & Lewin 1987; Bussard et al. 1988). If instead the source of soft photons or the properties of the corona are time dependent, then the time lag will depend on the details of this time dependence.

For the simplified model described earlier in this section, the average energy after u scatterings of a photon injected at energy $E_{\rm in}$ is

$$E(u) \sim \min \left[E_{\rm in} \exp \left(4T_e u/m_e \right), E_b \right] . \tag{21}$$

Therefore, for photons with energies smaller than $\sim E_b$, the ratio of the energies of two photons that have experienced a different number of scatterings is $E_2/E_1 \sim \exp(4T_e \Delta u/m_e)$, where Δu is the difference in the number of scatterings. The photon mean-free time is $\sim (n_e \sigma_{\rm T} c)^{-1}$, and hence the time lag introduced between the oscillations at the two photon energies is

$$\delta t \sim \frac{R}{c\tau} \frac{m_e}{4T_e} \ln \left(\frac{E_2}{E_1} \right) = \frac{400}{\tau} \left(\frac{R}{10^6 \text{ cm}} \right) \left(\frac{T_e}{10 \text{ keV}} \right) \ln \left(\frac{E_2}{E_1} \right) \mu s , \tag{22}$$

when both E_1 and E_2 are smaller than $\sim E_b$. Because of the diffusion in energy and the systematic downscattering of photons with energies $\gtrsim E_b$, equation (22) is not valid at energies $\gtrsim E_b$.

We emphasize that, for a variety of reasons, equation (22) gives only an upper bound to the expected time lag at photon energies $\lesssim E_b$. First, this equation assumes that all photons are injected at the center of a spherical medium. However, if most of the photons are produced near the surface of the neutron star and escape a few kilometers above it, the time lag can be significantly smaller. Second,

equation (22) was derived under the assumption that photons slowly diffuse outward. This is not a very good approximation for electron scattering optical depths $\tau \lesssim 3$; if a fraction of the photons escape directly from the corona without interacting with the electrons, the average escape time could be significantly smaller. Finally, equation (22) was derived under the assumption of a uniform electron density. If instead most of the optical depth is concentrated near the center of the corona, this will also reduce significantly the average escape time.

In summary, to the extent that the effects of Comptonization dominate, the sonic-point Keplerian- and beat-frequency oscillations at high photon energies should lag the corresponding oscillations at lower photon energies; the time lag between a few and ~ 15 keV *should be a fraction of a millisecond* for the densities and temperatures of the electrons expected around the neutron stars in the Z and atoll sources.

3.6. *Attenuation of Kilohertz QPOs*

In the sonic-point model, gas spirals inward from density inhomogeneities in the accretion flow at the sonic radius and collides with the stellar surface, producing a radiation pattern that rotates around the star with the Keplerian frequency at or near the sonic point $\nu_{\rm Ks}$. Because the rate of mass accretion over the whole neutron star surface remains approximately constant in time as the radiation pattern rotates, the total luminosity emerging from the system also remains approximately constant in time. For conciseness we call the oscillations produced by rotation of this radiation pattern a "beaming" oscillation, because it is caused by the angular variation of the radiation field, even though the radiation pattern is unlikely to be a narrow beam. In a pure beaming oscillation, the total luminosity emerging from the source is independent of time. As described earlier, the accretion flow is also expected to produce a weak beaming oscillation at the stellar spin frequency $\nu_{\rm spin}$.

If the magnetic field of the neutron star is strong enough to channel the accretion flow near the stellar surface, the sonic-point model predicts that the resulting radiation pattern, which rotates with the star, will modulate inflow from the inner disk at the beat frequency $\nu_{\rm Ks} - \nu_{\rm spin}$, producing a "luminosity" oscillation with this frequency. In a pure luminosity oscillation, the total luminosity of the system changes with time, but the angular pattern of the radiation field remains unchanged. In the sonic-point model, the only luminosity oscillation is the beat frequency oscillation.[5]

When the luminosity oscillation is present, it is necessarily modulated by the motion of the emission regions around the stellar surface, which generates second-order beaming oscillations at the stellar spin frequency $\nu_{\rm spin}$ and the difference frequency $2\nu_{\rm Ks} - \nu_{\rm spin}$ (see § 3.3 and Table 3). In general, higher order oscillations are also generated at other (mostly much higher) frequencies.

[5] To clarify further the difference between luminosity and beaming oscillations, consider an observer whose line of sight to the neutron star is along the rotation axes of the disk and the star. X-rays from beams rotating with the gas in the disk or with the star will appear time-independent to such an observer and therefore will not generate any X-ray flux or color oscillations. However, the luminosity oscillation at the beat frequency caused by the oscillation of the mass flux at this frequency will be visible. Such an observer will therefore see an oscillation at the beat frequency and its overtones, but not at any other frequency.

Scattering generally attenuates beaming oscillations much more than luminosity oscillations for the conditions relevant to LMXBs (Lamb 1988). The reason is that an anisotropic radiation pattern becomes approximately isotropic after only a few scatterings, whereas a luminosity oscillation is attenuated by scattering only if the time required for photons to escape from the scattering region is much larger than the period of the oscillation, which requires a large optical depth for the oscillation frequencies and coronal dimensions of interest to us.

The relative amplitude A_∞ of a luminosity oscillation with angular frequency $\omega = 2\pi\nu$ outside a spherical scattering cloud of radius $R_{\rm C}$ and optical depth τ is related to the relative amplitude A_0 at the center of the cloud by the expression (Kylafis & Phinney 1989)

$$A_{\infty,\rm lum} \approx (2^{3/2} x e^{-x} + e^{-\tau}) A_{0,\rm lum} , \qquad (23)$$

where $x \equiv [(3/2)\omega R_{\rm C}\tau/c]^{1/2}$. This expression is accurate to better than 6% for $x > 1.3$ (Kylafis & Phinney 1989). The first term in parenthesis on the right-hand side of equation (23) describes the amplitude attenuation caused by the spread of escape times from the cloud whereas the second term (which has been added in by hand) describes the amplitude of the oscillation produced by the photons that escape from the cloud without scattering.

For a beaming oscillation caused by rotation of a narrow pencil beam, the amplitude of the oscillation outside the cloud is (Brainerd & Lamb 1987; Kylafis & Phinney 1989)

$$A_{\infty,\rm beam} \simeq \left[\left(\frac{2}{1+\tau}\right) 2^{3/2} x e^{-x} + e^{-\tau}\right] A_{0,\rm beam} . \qquad (24)$$

The factor multiplying $A_{0,\ \rm beam}$ in equation (24) describes the tendency of scattering to isotropize the photon distribution. The amplitudes of oscillations produced by the broad radiation patterns or the radiation patterns with more than one lobe that we are concerned with here are reduced even more by scattering (Brainerd & Lamb 1987).

Of all the beaming oscillations that may be generated by the accretion flow, only the one at the sonic-point Keplerian frequency is likely to have a large enough amplitude at the neutron star to produce an oscillation that is strong enough, after attenuation by passage through the central corona, to be observed easily with current instruments. In contrast, the oscillation at the sonic-point beat frequency, which is the only luminosity oscillation produced by the flow, should be strong enough to be observed even if its amplitude at the neutron star surface is moderate. As a result, we expect that from the collection of possible frequencies of oscillations, the only oscillations that will appear strong far from the star will be those at the sonic-point Keplerian and beat frequencies.

4. COMPARISON WITH OBSERVATIONS

In this section we describe the observational implications of the sonic-point model and compare them with observations of the kilohertz QPOs. We first list the important properties of these QPOs that any model must explain. These properties are (see § 1): (1) high ($\sim$300–1200 Hz) frequencies, which can vary by several hundred Hertz in a few hundred seconds (see Wijnands et al. 1998; van der Klis 1995); (2) similar frequency ranges in stars with significantly different magnetic field strengths and accretion rates; (3) relatively high coherence ($Q \equiv \nu/\delta\nu$ up to $\sim$100); (4) 2–60

keV rms amplitudes $\lesssim 1\%$ in the Z sources but much higher (up to $\sim 15\%$) in the atoll sources; (5) the common occurrence of two (but never more than two) simultaneous kilohertz QPOs in a given source; (6) a frequency separation $\Delta\nu$ between the two kilohertz QPOs that is approximately constant in a given source; (7) approximate consistency of $\Delta\nu$ with the stellar spin frequency inferred from burst oscillations; (8) the similarity of most atoll and Z source spin frequencies; (9) the frequently similar FWHM of the two QPO peaks seen simultaneously; (10) the increase of the frequencies of the kilohertz QPOs with increasing inferred accretion rate that is observed in many sources; and (11) a steep increase in the amplitude of the higher frequency of the two kilohertz QPOs with increasing photon energy in the 2–15 keV energy band in many sources.

In § 4.1 we show that the stellar magnetic field strengths and electron scattering optical depths required for the sonic-point mechanism to operate are consistent with the stellar magnetic field strengths and optical depths of the compact central corona inferred from previous modeling of the X-ray spectra and $\lesssim 100$ Hz X-ray variability of the atoll and Z sources. In § 4.2 we compare the kilohertz QPO and neutron star spin frequencies expected in the sonic-point model with the kilohertz QPO and neutron star spin frequencies observed in the atoll and Z sources. We also discuss the expected and observed dependence of the QPO frequencies on accretion rate. In § 4.3 we describe the amplitude and coherence of the various QPOs expected in the sonic-point model, comparing them with the observed amplitudes and coherence of the kilohertz QPOs. In particular, we show that the sonic-point model explains naturally why at most two kilohertz QPOs have been detected in the power spectrum of each source. We also discuss the relative coherence of QPOs at different frequencies and the expected dependence of QPO amplitudes on accretion rate and photon energy. In § 4.4 we describe the inverse correlation between QPO amplitude and stellar magnetic field expected in the sonic-point model and show that there is already substantial evidence for such a correlation.

4.1. *Consistency with Previously Inferred Properties of the Atoll and Z Sources*

The operation of the sonic-point mechanism for producing strong, coherent kilohertz QPOs requires that a number of conditions be satisfied.

(1) In order to produce the higher frequency kilohertz QPOs with the large amplitudes observed in some sources, the neutron star magnetic fields in these sources must be relatively weak, so that a substantial fraction of the accreting gas penetrates close to the star in a Keplerian disk flow (§ 3.1).

(2) In order to produce the lower frequency kilohertz QPOs, the neutron star magnetic field, although relatively weak, must be strong enough to channel some of the accreting gas near the stellar surface to produce bright spots that rotate with the star and modulate the accretion rate at the sonic-point beat frequency (§ 3.1).

(3) In order to generate QPOs with the high coherence observed in most sources, the disk flow at the sonic point must be geometrically thin (§ 3.4).

(4) In order that only the QPOs at the sonic-point Keplerian and beat frequencies be detectable and that X-ray oscillations at the stellar spin frequency be very weak or undetectable at present sensitivities, electron scattering in the central corona must help to attenuate the weak beaming oscillations at other frequencies and at the stellar spin frequency. The central corona must therefore have an electron scattering optical depth $\gtrsim 3$ (§ 3.6).

As we now explain briefly, all of these conditions follow naturally from the unified model of weak-field accreting neutron stars described in § 2.2.

The magnetic field strengths in the 4U atoll sources are thought to be low enough ($\lesssim 10^9$ G) that at their inferred accretion rates (~ 0.01–$0.1 \dot{M}_{\rm E}$) the cylindrical radius ϖ_0 at which the Keplerian disk flow couples strongly to the stellar magnetic field is $\lesssim 2 \times 10^6$ cm. The magnetic field strengths of the neutron stars in the Z sources are thought to be a few times larger than in the 4U atoll sources, but the accretion rates are much larger as well, so ϖ_0 is comparable to its value in the atoll sources. Thus, in both the 4U atoll sources and the Z sources, the gas in the Keplerian disk penetrates close to the star before any of it couples strongly to the stellar magnetic field. We therefore expect that a significant fraction of the accreting gas will remain in a Keplerian disk flow down to the sonic point and will continue in a disk flow very close to the stellar surface, as required in the sonic-point model.

Evidence that the magnetic fields of neutron stars in LMXBs, while typically weak, are nevertheless strong enough in many sources to channel the flow near the star and hence to produce a QPO at the sonic-point beat frequency comes from power spectra constructed from *RXTE* observations of GX $5-1$ (van der Klis et al. 1996e), Sco X-1 (van der Klis et al. 1996a, 1996b, 1996d, 1997a), GX $17+2$ (Wijnands et al. 1997a), and Cyg X-2 (Wijnands et al. 1998). In addition to two simultaneous kilohertz QPOs, these power spectra show horizontal branch oscillations, which appear to be magnetospheric beat-frequency oscillations (see § 2; Psaltis et al. 1998).

These power spectra indicate that in the Z sources, some of the gas in the disk couples strongly to the weak stellar magnetic field at 2 or 3 stellar radii and is funneled into hot spots that could modulate the mass flux from the sonic point at the sonic-point beat frequency by periodically irradiating the clumps at the sonic radius (see § 2). It is natural to expect that the magnetic fields of many of the atoll sources are only a little weaker than those in the Z sources and are therefore still strong enough to produce a QPO at the sonic-point beat frequency. This expectation is supported by the spectral modeling described in § 2.2.

Accretion via a geometrically thin Keplerian disk flow, which is required to explain the high coherence of the kilohertz QPOs, is expected in the atoll sources, because at their low accretion rates the inner part of the accretion disk is likely to be gas-pressure–dominated. In the Z sources, which are thought to be accreting at close to the Eddington critical rate, gas in the Keplerian disk flow that is not channeled by the stellar magnetic field is likely to be pinched by the stellar field into a geometrically thin disk.

The final requirement listed above for the sonic-point model, namely that the optical depth of the hot central corona exceed ~ 3, follows directly from the spectral modeling discussed in § 2.2.

In summary, the physical picture of the atoll and Z sources that was developed prior to the discovery of the

kilohertz QPOs, based on their 2–20 keV X-ray spectra and 1–100 Hz X-ray variability, gives the magnetic field strengths, accretion flows, and electron scattering optical depths required by the sonic-point model.

4.2. *Kilohertz QPO and Neutron Star Spin Frequencies*

In the sonic-point model, the frequency of the higher frequency kilohertz QPO (when two are present) is the Keplerian orbital frequency $\nu_{\rm Ks}$ at the point in the disk flow where the inward radial velocity increases rapidly within a small radial distance, whereas the frequency of the lower frequency kilohertz QPO is approximately the difference between $\nu_{\rm Ks}$ and the stellar spin frequency $\nu_{\rm spin}$. In this section we describe the range of sonic-point Keplerian and neutron star spin frequencies and the variation of the sonic-point Keplerian and beat frequencies with accretion rate expected in the model and then compare these expectations with the observations. We discuss the expected amplitudes of oscillations at other frequencies in § 4.3.

Similarity of the sonic-point Keplerian QPO frequencies in different sources.—A key question is why the higher frequency kilohertz QPOs in different sources always have frequencies between ~ 500 and ~ 1200 Hz, even though the neutron stars in these sources have time-averaged mass accretion rates that differ by more than a factor of 100 and magnetic fields that are thought to differ by more than a factor of 10. In the sonic-point model, there are three main reasons why the Keplerian-frequency QPO is restricted to this frequency range.

(1) As discussed in § 3.2, there is an upper bound on the radius R_s of the sonic point, which is set by the maximum fraction of the angular momentum of the accreting gas that can be removed by radiation from the stellar surface and is $\sim 3R_{\rm ms}$, where $R_{\rm ms}$ is the radius of the marginally stable orbit. There is also a lower bound on R_s, which is $R_{\rm ms}$ if the radius R of the neutron star is smaller than $R_{\rm ms}$, or R otherwise. Hence, the Keplerian frequency at the sonic point is confined to a similar interval in the atoll and Z sources, regardless of their accretion rates and magnetic field strengths. As a result, if the neutron stars in the kilohertz QPO sources have typically accreted a few tenths of a solar mass and therefore have masses $\sim 1.7\,M_\odot$, these constraints on the sonic-point Keplerian frequency mean that the frequencies of their sonic-point Keplerian QPOs will fall between ~ 400 and ~ 1300 Hz.

(2) Modeling of the 2–20 keV X-ray spectra and 1–100 Hz power spectra of the atoll and Z sources indicates that the magnetic fields of these neutron stars are positively correlated with their time-averaged accretion rates, i.e., sources with higher accretion rates appear to have stronger magnetic fields (see § 2.2; Psaltis & Lamb 1998a, 1998b, 1998c). This has an important implication for the frequency range of the kilohertz QPOs, because the stronger the stellar magnetic field, the *larger* the fraction of the gas in the disk that is likely to couple to the magnetic field at 2 or 3 stellar radii and be channeled out of the disk flow there. As a result, the stronger the magnetic field, the *smaller* the mass flux $\dot{M}_{\rm sp}$ through the disk at the sonic point. Hence, $\dot{M}_{\rm sp}$ differs by a much smaller factor in the Z and atoll sources than does the total mass flux $\dot{M}$ onto the neutron star. The sonic-point Keplerian frequency $\nu_{\rm Ks}$ is governed more by $\dot{M}_{\rm sp}$ than by $\dot{M}$, so the positive correlation between magnetic field and accretion rate means that the frequency ranges of the sonic-point QPOs are likely to be more similar in a collection of neutron-star LMXBs than one would expect, based only on the different ranges of $\dot{M}$ in different systems.

(3) In addition, the inner disk is expected to be thicker if $\dot{M}_{\rm sp}$ is large. As a result, the radial optical depth through the disk at a given accretion rate is smaller, which allows radiation from the neutron star surface to penetrate further out into the disk than one would expect based only on the different values of $\dot{M}$ in the different systems. This tendency also acts to make the range of sonic-point radii, and hence the frequency ranges of the Keplerian-frequency QPOs, more similar in different systems than consideration of the accretion rates alone would suggest (see § 3.2).

Expected and inferred neutron star spin rates.—In the sonic-point model, the separation between the frequencies of the QPOs in a pair is approximately equal to the stellar spin frequency. The frequency separations observed in the kilohertz QPO sources so far (see Table 4) all indicate spin rates of a few hundred hertz, consistent with the spin rates

TABLE 4

INFERRED SPIN FREQUENCIES OF NEUTRON STARS WITH KILOHERTZ QPOs[a]

Kilohertz QPO Source	$\nu_{\rm spin}$ from $\Delta\nu$ (Hz)	$\nu_{\rm spin}$ from $\nu_{\rm burst}$ (Hz)	References
4U 0614+091	~330	...	Ford et al. 1997a, 1997b
4U 1608−52	230–290	...	Méndez et al. 1998
4U 1636−536	~290	~580	Zhang et al. 1996, 1997a
4U 1728−34	~360	~363	Strohmayer et al. 1996b, 1996c, 1996d
KS 1731−260	~260	~520	Smith et al. 1997; Wijnands & van der Klis 1997
4U 1735−444	...	...	...
4U 1820−30	~275	...	Smale et al. 1997
Aql X-1	...	~550	Zhang et al. 1998a
Cyg X-2.....	~345	...	Wijnands et al. 1998
GX 5−1	~325	...	van der Klis et al. 1996e
GX 17+2	~295	...	Wijnands et al. 1997a
GX 340+0	~325	...	Jonker et al. 1998
GX 349+2	~266	...	Zhang et al. 1998b
Sco X-1	~250–300	...	van der Klis et al. 1996a, 1996b, 1996d, 1997a
Unknown.....	...	~590	Strohmayer et al. 1997a

[a] Complete as of 1998 May 31. Here $\Delta\nu$ is the difference between the frequencies of the kilohertz QPOs seen simultaneously in the persistent X-ray emission of the source and $\nu_{\rm burst}$ is the frequency of the brightness oscillation seen during type I (thermonuclear) X-ray bursts from the source.

expected in the magnetospheric beat-frequency model of the HBO (see § 2; Lamb et al. 1985; Ghosh & Lamb 1992).

Oscillations have been observed during thermonuclear X-ray bursts from five kilohertz QPO sources so far (again, see Table 4). Only a single oscillation has been observed from each source during a given burst, the oscillations in the tails of bursts appear to be highly coherent (see, e.g., Smith et al. 1997), and the frequencies are always the same in a given source. Furthermore, comparison of burst oscillations from 4U 1728−34 over about a year shows that the timescale for any variation in the oscillation frequency is $\gtrsim 3000$ yr (see, e.g., Strohmayer 1997). The burst oscillations are thought to be caused by emission from one or two regions of brighter X-ray emission on the stellar surface (see Strohmayer et al. 1997b), producing oscillations at the stellar spin frequency or its first overtone, respectively.

The 363 Hz frequency of the burst oscillation observed in 4U 1728−34 is consistent with the separation frequency of its two simultaneous kilohertz QPOs. The 524 and 581 Hz frequencies of the burst oscillations seen in KS 1731−260 and 4U 1636−536 are probably twice the spin frequencies of these neutron stars (see Morgan & Smith 1996; Smith et al. 1997; Wijnands & van der Klis 1997; Zhang et al. 1996, 1997a). If so, the spin rates of these stars are 262 and 290 Hz, respectively. The frequencies of the fairly coherent oscillations seen at 549 Hz in Aql X-1 (Zhang et al. 1998a) and at 589 Hz in the so-far unidentified source near the Galactic center (Strohmayer et al. 1996a) may also be twice the spin frequencies of these neutron stars. These spin rates are all consistent with those expected in the sonic-point model.

Similarity of the neutron-star spin frequencies in different sources.—If the neutron stars in the kilohertz QPO sources have spin frequencies comparable to their equilibrium spin frequencies, then we expect their spin frequencies to be a few hundred hertz. This can be seen from equation (1) in § 2.2, which can be solved for the equilibrium spin frequencies at which continued accretion at the given rate leaves the spin frequency unchanged, with the result

$$\nu_{\rm eq} = \begin{cases} 1590\omega_{\rm c}(\mu_{0,27})^{-0.87}(\dot{M}_i/\dot{M}_{\rm E})^{0.39} \\ \quad \times (M/1.4\ M_\odot)^{0.85}\ {\rm Hz}\ , \quad \text{for GPD disks}\ ; \\ 430\omega_{\rm c}(\mu_{0,27})^{-0.77}(\dot{M}_i/\dot{M}_{\rm E})^{0.23} \\ \quad \times (M/1.4\ M_\odot)^{0.70}\ {\rm Hz}\ , \quad \text{for RPD disks}\ . \end{cases} \tag{25}$$

Here ω_c is the critical fastness (Ghosh & Lamb 1979b). Hence, for $\omega_{\rm c} \approx 1$, a 1.7 $M_\odot$ atoll source with $\mu_{0,27} = 0.5$ accreting from a GPD disk at a rate $\dot{M}_i = 0.001\dot{M}_{\rm E}$ has an equilibrium spin frequency of 230 Hz, which is similar to the 240 Hz equilibrium spin frequency of a 1.4 $M_\odot$ Z source with $\mu_{0,27} = 2$ accreting from an RPD disk at a rate $\dot{M}_i = 0.5\dot{M}_{\rm E}$.

A recent analysis (Psaltis et al. 1998) of the properties of the HBOs and kilohertz QPOs in a collection of five Z sources shows that they are consistent with many of the predictions of the magnetospheric beat-frequency model of the HBO and that the agreement is best if, as expected in this model, they are all in spin equilibrium (see also Ghosh & Lamb 1992). In particular, this analysis shows that *the narrow range of spin frequencies observed in the Z sources is to be expected if they are in spin equilibrium.*

Variation of kilohertz QPO frequencies with mass accretion rate.—In the sonic-point model, the frequencies of the kilohertz QPOs are expected to rise as the accretion rate increases, within the bounds set by the orbital frequencies at the angular momentum loss radius and at the radius of the marginally stable orbit (see above and § 3.2). In order to see why an increase is expected, suppose that the sonic radius is at R_{s1} for a given accretion rate. An increase in the accretion rate will cause the radial optical depth from the stellar surface to R_{s1} to increase, if all other physical quantities remain constant, and hence the sonic point will move inward to the smaller radius R_{s2} at which the optical depth from the stellar surface is approximately the same as before, causing an increase in the orbital frequency at the sonic radius. The X-ray luminosity between bursts is produced almost entirely by accretion and hence an increase in the accretion rate causes an increase in the luminosity. We therefore expect a strong, positive correlation between the frequencies of the sonic-point Keplerian- and beat-frequency QPOs and the persistent X-ray luminosity.

These basic ideas are illustrated by the general relativistic accretion flow calculations of § 3.2. As shown in Figure 9, the sonic-point Keplerian and beat frequencies given by these calculations increase steeply with increasing mass accretion rate until the sonic point reaches $R_{\rm ms}$, at which point their frequencies stop changing. This flattening of the two frequency versus accretion luminosity relations is one possible signature of the existence of a marginally stable orbit (see also § 5.4). Coherent Keplerian- and beat-frequency QPOs are unlikely to be produced if the sonic point moves inward, close to the stellar surface, because of the disruptive effect of the surface magnetic field and the strong viscous shear layer that is expected to develop if the Keplerian flow interacts directly with the neutron star surface.

We emphasize that these calculations are intended to be illustrative rather than to reproduce the QPO frequency behavior of any particular source. If the mass of the neutron star is 1.7 $M_\odot$, rather than 1.4 $M_\odot$ as assumed in these

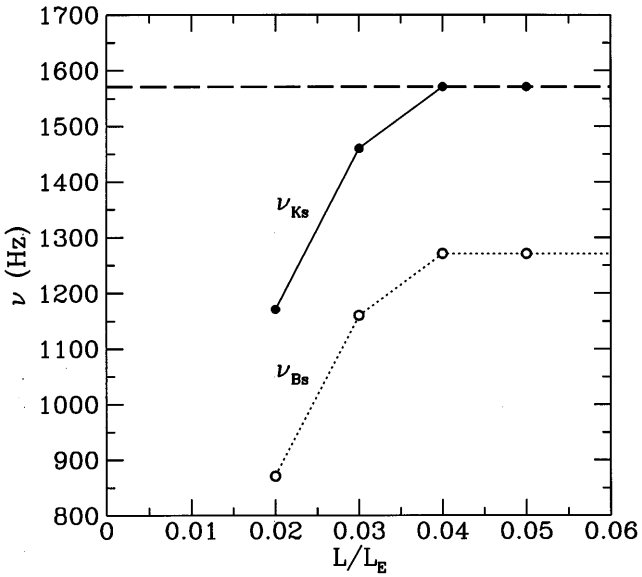

FIG. 9.—Sonic-point Keplerian and beat frequencies in Hertz as functions of the accretion luminosity in units of the Eddington critical luminosity, computed using the accretion flow model of § 3.2. The neutron star spin rate is assumed to be 300 Hz. The other assumptions are the same as in Fig. 8. The sonic-point Keplerian frequency $\nu_{\rm Ks}$ (*solid line*) increases steeply with increasing accretion luminosity until it reaches $\nu_{\rm K}(R_{\rm ms})$ (*dashed horizontal line*), the orbital frequency at the innermost stable circular orbit, at which point $\nu_{\rm Ks}$ stops increasing. The sonic-point beat frequency $\nu_{\rm Bs}$ (*dotted line*) increases steeply with increasing accretion luminosity until it reaches $\nu_{\rm K}(R_{\rm ms}) - \nu_{\rm spin}$, at which point it too stops increasing.

calculations, the limiting frequency would be 1.3 kHz rather than 1.6 kHz (see Miller, Lamb, & Psaltis 1998). Again, if the accretion disk is thicker near the star than is assumed in these calculations, more of the inner disk will be illuminated and hence the angular momentum loss radius $R_{\rm aml}$ will be larger, causing the sonic-point Keplerian frequency at a given accretion rate to be lower. If the disk thickness changes with accretion rate, then the variation of the sonic-point Keplerian frequency with accretion rate will be different from the variation found in the calculations reported here, which treat the disk thickness as constant. Despite these uncertainties, the calculations described here show that an increase in the mass accretion rate leads naturally to an increase in the sonic-point Keplerian frequency.

We stress that caution must be used in comparing the predicted variation of QPO frequencies with accretion with the count rate measured by a given X-ray detector, because count rates are known to be poor indicators of the mass accretion rate and the accretion luminosity, at least for some sources at some times. The most likely reason is that a particular instrument measures the photon number flux over only a restricted energy range and that a change in the mass accretion rate typically causes a change in the shape of the X-ray spectrum as well as its normalization. Hence the detector count rate typically is not proportional to the accretion rate.

In the Z sources, the mass accretion rate is known to be different when the *EXOSAT* count rate is the same but the source is on a different branch of the Z track (Hasinger & van der Klis 1989; Lamb 1989; Psaltis et al. 1995). Moreover, in the "Cyg-like" Z sources, the normal/flaring branch vertex, which is thought to correspond to a mass accretion rate approximately equal to $\dot{M}_{\rm E}$ (Lamb 1989), occurs at different count rates during different observations (Kuulkers 1995).

The observations of Ford et al. (1997a) show that the properties of the accretion flow are not uniquely related to the X-ray count rate in the atoll sources. In these observations, the dependence of the kilohertz QPO frequencies on count rate seen in data on 4U 0614+091 taken with *RXTE* in 1996 August differs, both in slope and in normalization, from the dependence of the QPO frequencies on count rate seen in data taken in 1996 April. In contrast, when the 4U 0614+091 QPO frequencies are plotted against the energy of the spectral peak, which may be a good indicator of the accretion rate (Psaltis & Lamb 1998c), the slope and normalization of the curves are the same for both observations (Ford et al. 1997b).

Clearly, bolometric and other corrections are typically important, so comparison of QPO frequency versus count rate data with the QPO frequency versus accretion rate predictions of theoretical models must be approached with caution. Despite this caveat, it is worth emphasizing that there is a strong, positive correlation between the frequencies of the kilohertz QPOs seen in 4U 1728−34, 4U 0614+091, 4U 1820−30, and KS 1731−260, and the count rate measured by *RXTE*, as expected in the sonic-point model if the count rate increases with increasing accretion rate.

It is interesting to speculate about the dependence of kilohertz QPO frequencies on luminosity that is to be expected if such QPOs are detected during a thermonuclear X-ray burst. In this case the mass accretion rate and the radial optical depth are no longer tied to the luminosity, and hence the expected dependence of $\nu_{\rm Ks}$ on luminosity is different from what is expected during the periods between type I X-ray bursts. When radiation forces are extremely strong, such as at the peak of a type I X-ray burst that causes photospheric radius expansion, the radiation controls the accretion flow out to large radii and we therefore do not expect any QPO at the sonic-point Keplerian frequency or at the sonic-point beat frequency. However, QPOs at these frequencies may reappear in the tail of the burst. While the burst luminosity is several times the persistent accretion luminosity, we expect the sonic point to be farther from the star than when the luminosity is lower. Thus, we expect that if sonic-point QPOs are detected in the tail of a thermonuclear burst, their frequencies will increase as the luminosity declines. Note, however, that during the decay phase of such a burst, the luminosity changes rapidly. If the frequencies of the QPOs track this change, the QPO peaks in power spectra will be smeared out, unless the spectra are constructed from short ($\lesssim$0.1 s) segments of data.

So far, no kilohertz QPOs have been observed near the maximum of type I X-ray bursts, which is consistent with what is expected in the sonic-point model. More sensitive searches will be required to determine if kilohertz QPOs are present during the decay phases of bursts.

4.3. *Kilohertz QPO Amplitudes and Coherence*

Amplitudes of oscillations at different frequencies.—A key question that any theory of the kilohertz QPOs must answer is why at most two strong QPOs have so far been seen simultaneously in the kilohertz QPO sources. In addressing this question, it is important to consider both the *generation* of oscillations near the neutron star and the effects of *propagation* of the radiation through the gas surrounding the neutron star. In order to be detectable far away, an oscillation must be strong at the source or have a small attenuation, or both.

The QPOs at the sonic-point Keplerian and beat frequencies are the only QPOs expected to have moderately high amplitudes far from the neutron star because the optical depth and luminosity oscillations that produce them generate relatively high amplitudes near the star, because these frequencies (and their overtones) are the *only* frequencies generated by the sonic-point mechanism in lowest order, and because scattering of photons by the gas surrounding the neutron star selectively suppresses the already weak higher frequency oscillations generated at higher orders.

As discussed in § 3.3, to lowest (first) order, the sonic-point mechanism generates oscillations only at the sonic-point Keplerian and beat frequencies (see Table 3). As explained there, only very weak overtones of the sonic-point Keplerian frequency are likely to be generated, because the angular distribution of the radiation from the bright impact footprints of the rotating density pattern produced by clumps is expected to be very broad.

The radiation pattern that rotates with the star is also expected to be broad, but at the sonic radius, where it interacts with the orbiting gas to generate the luminosity oscillation at the sonic-point beat frequency, it is not likely to be perfectly sinusoidal. Hence overtones of the sonic-point beat frequency $\nu_{\rm Bs}$ may be generated in the inward mass flux from the clumps at the sonic radius, producing overtones of $\nu_{\rm Bs}$ in the X-ray flux from the star. As radiation from the

stellar surface propagates outward through the part of the central corona that extends beyond the sonic radius, the radiation pattern that rotates with the star is likely to be broadened further (see below), reducing the amplitudes of oscillations at the stellar spin frequency and its overtones seen by a distant observer.

In addition to the QPOs at the sonic-point Keplerian and beat frequencies and their overtones, in second order the sonic-point mechanism also generates QPOs at $\nu_{\rm spin}$ and $2\nu_{\rm Ks} - \nu_{\rm spin}$ and, in the third order, $\nu_{\rm Ks} - 2\nu_{\rm spin}$, $\nu_{\rm Ks} + \nu_{\rm spin}$, $3\nu_{\rm Ks} - 2\nu_{\rm spin}$, and $3\nu_{\rm Ks} - \nu_{\rm spin}$ (again, see Table 3). These high-order oscillations are expected to be very weak, even near the neutron star.

The attenuation of an oscillation depends strongly on whether it is a beaming oscillation or a luminosity oscillation (see § 3.6). A beaming oscillation is an oscillation produced by rotation of an angular radiation pattern, like the beam of a lighthouse; in a pure beaming oscillation, the luminosity remains constant as the radiation pattern rotates. In contrast, a luminosity oscillation is one produced by an oscillation of the luminosity of the source; in a pure luminosity oscillation, the radiation pattern remains static as the luminosity oscillates. In the sonic-point model, the sonic-point Keplerian frequency is the only intrinsically strong beaming oscillation, and the sonic-point beat frequency is the only luminosity oscillation produced by the accretion flow.

In passing through a scattering region, luminosity oscillations are attenuated only by time-of-flight smearing whereas beaming oscillations are also attenuated by the isotropization of the radiation pattern by the scattering. Hence beaming oscillations are weakened more by propagation through a scattering corona. Figure 10 compares the attenuation of luminosity and beaming oscillations produced at the center of a uniform, spherical, scattering cloud of radius $R_{\rm C} = 3 \times 10^6$ cm, as a function of the optical depth of the cloud. The size of this cloud is comparable to the dimensions of the small scattering coronae with optical depths $\sim$3–5 that are thought to surround the neutron stars in the atoll and Z sources (Lamb 1989, 1991; see also § 2.2). The frequencies of the oscillations shown in Figure 10 have been chosen to represent a hypothetical accreting neutron star with $\nu_{\rm Ks} = 1100$ Hz and $\nu_{\rm spin} = 300$ Hz. The beat-frequency luminosity oscillation is therefore at 800 Hz. The attenuation factors have been calculated using equations (23) and (24). Figure 10 shows that the beaming oscillation at the sonic-point Keplerian frequency must have a relatively high intrinsic amplitude in order to produce a strong, observable QPO for a distant observer, whereas the luminosity oscillation at the sonic-point beat frequency needs only to have a moderate amplitude.

The amplitudes of the oscillations at the overtones of either luminosity or beaming oscillations seen by a distant observer are expected to be far smaller than the amplitudes seen at the fundamental frequencies, for several reasons. For example, beaming patterns with multiple lobes are much more easily isotropized by scattering than are beaming patterns with single lobes (see, e.g., Brainerd & Lamb 1987). Moreover, for either beaming or luminosity oscillations, overtones of an oscillation are at higher frequencies than the fundamental and are thus more susceptible to time-of-flight smearing.

As a specific example, we consider 4U 1728−34. As interpreted within the sonic-point model, the spin frequency of this neutron star is 363 Hz (see Table 3). During one observation, $\nu_{\rm Ks}$ was 1045 Hz. Assuming that this neutron star is surrounded by a central corona with a radius $R_{\rm C} = 3 \times 10^6$ cm and an optical depth $\tau = 5$, the amplitude of the luminosity oscillation at the beat frequency $\nu_{\rm Ks} - \nu_{\rm spin} = 682$ Hz seen by a distant observer is about 85% of the amplitude at the neutron star. For comparison, the beaming oscillation at $\nu_{\rm Ks} + \nu_{\rm spin} = 1408$ Hz, which is generated only in third order and is therefore likely to be very weak even near the neutron star, has an amplitude at infinity that is only about 20% of its amplitude at the star. The amplitudes of oscillations at the overtones of the sonic-point Keplerian frequency are all reduced by factors $\gtrsim$20. For these reasons, it is not surprising that the only strong QPOs seen are at the sonic-point Keplerian and beat frequencies.

Although oscillations at frequencies other than the sonic-point Keplerian and beat frequencies are likely to be very weak, their amplitudes are surely not zero. We therefore expect that, if neutron-star LMXBs are observed with sufficient sensitivity, oscillations at other frequencies will be detected. In particular, a careful search near the spin frequency, at the first overtone of the beat frequency, and near the sum of the Keplerian and spin frequencies in sources with pairs of high-frequency QPO peaks may reveal very weak QPOs at these frequencies.

The oscillation at the beat frequency is a luminosity oscillation, but in the sonic-point model it is created by interaction of the weakly beamed radiation pattern that is rotating at the stellar spin frequency with the clumps of gas that are orbiting at or near the sonic point. It is therefore important to emphasize why the beaming oscillation at the

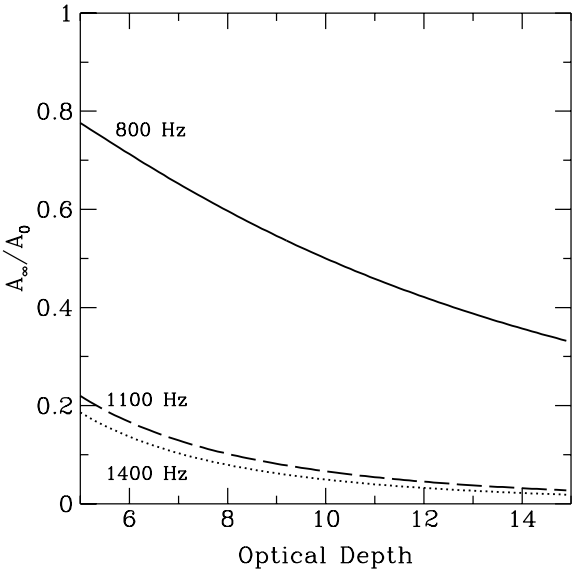

FIG. 10.—Sample attenuation factors A_∞/A_0 for the relative amplitudes of the X-ray brightness oscillations produced by a hypothetical accreting neutron star with a spin rate $\nu_{\rm spin} = 300$ Hz and a sonic-point Keplerian frequency $\nu_{\rm Ks} = 1100$ Hz, at the center of a uniform, spherical scattering cloud with a radius of 3×10^6 cm. The sonic-point beat frequency $\nu_{\rm Bs}$ is assumed to be $\nu_{\rm Ks} - \nu_{\rm spin}$ and is therefore 800 Hz. The attenuation factors for the oscillations at $\nu_{\rm Ks}$ (*dashed curve*) and at the upper sideband frequency $\nu_{\rm Ks} + \nu_{\rm spin} = 1400$ Hz (*dotted curve*), which are assumed for the sake of illustration to be pure beaming oscillations produced by a rotating pencil beam, are $\gtrsim$5 for scattering optical depths $\tau \gtrsim 5$. In contrast, the attenuation factor for the oscillation at $\nu_{\rm Bs}$ (*solid curve*), which is a pure luminosity oscillation, is much smaller.

stellar spin frequency is strong enough to modulate significantly the mass inflow rate from clumps at the sonic point yet too weak to produce a significant peak in power spectra constructed by a distant observer.

Previous modeling of the X-ray spectra (Lamb 1989, 1991; Psaltis et al. 1995; Psaltis & Lamb 1998a, 1998b, 1998c) and the 1–100 Hz X-ray variability of the atoll and Z sources (Lamb 1989, 1991; Miller & Lamb 1992) strongly indicates that a hot, central, Comptonizing corona surrounds the neutron star, extending several stellar radii from its surface (see § 2.2). The sonic radius is well inside this corona, so the scattering optical depth from the stellar surface to the sonic point is much less than the scattering optical depth from the stellar surface to infinity. The finite size of the neutron star also diminishes the effect of attenuation on the amplitude of X-ray brightness oscillations for gas orbiting close to the star. These factors make the brightness oscillation produced by the radiation pattern that rotates with the star much stronger at the sonic radius than it is far away.

Dependence of QPO amplitudes on accretion rate.—In the sonic-point model, the ratio of the amplitude of the QPO at the sonic-point Keplerian frequency to the amplitude of the QPO at the sonic-point beat frequency generally depends on the strength of the neutron star magnetic field. If the magnetic field is too weak to channel gas even near the stellar surface, the amplitude of the oscillation at the beat frequency will be too small to be detected (see § 3.1). However, the ratio of the amplitudes of the QPOs at different frequencies is also expected to depend on the mass accretion rate.

For example, as the mass accretion rate rises, the electron density and optical depth of the gas around the neutron star also rise. Hence, the amplitude at infinity of the beaming oscillation at the sonic-point Keplerian frequency will fall faster relative to the amplitude of the luminosity oscillation at the sonic-point beat frequency, all else being equal; indeed, the QPO at the Keplerian frequency may become undetectable while the QPO at the beat frequency remains strong. This expectation is consistent with the observed behavior of the kilohertz QPO pair in 4U 1728−34 (Strohmayer et al. 1996d), assuming that the increasing mass accretion rate causes an increase in the count rate (but see § 4.2). In this source, the amplitude of the higher frequency QPO decreases relative to the amplitude of the lower frequency QPO as the count rate increases.

Alternatively, if the sonic point moves far enough away from the stellar surface, as may happen at low accretion rates (and hence count rates), the optical depth through the flow from the stellar surface to the sonic radius may become large enough to reduce greatly the amplitude at the sonic point of the radiation pattern that rotates with the star, thereby suppressing the luminosity oscillation at $\nu_{\rm Bs}$. This is consistent with an observation of 4U 1728−34 in which the lower frequency QPO is not observed when the frequency of the higher frequency QPO is low (Strohmayer et al. 1996d).

This analysis shows that if only a single high-frequency QPO peak is observed, it could be either the sonic-point Keplerian-frequency QPO or the sonic-point beat-frequency QPO, depending on the magnetic field of the neutron star and the mass accretion rate at the time. In this case, a secure identification can be made only by considering other properties of the QPO and comparing them with the properties of the QPOs seen in other observations of the same source.

Dependence of QPO amplitudes on photon energy.—In the sonic-point model, the relative amplitudes of the Keplerian frequency and beat frequency QPOs are expected to increase steeply with photon energy over the ∼5–10 keV energy range (see § 3.5). This is because the optical depth is expected to oscillate at both frequencies: the optical depth along the line of sight from the stellar surface oscillates at the Keplerian frequency, while the total optical depth of the scattering region oscillates at the beat frequency as the density of the accreting gas falling on the stellar surface oscillates at this frequency. As shown in § 3.5, a modest oscillation in the optical depth produces a QPO with a large relative amplitude at high photon energies. This is consistent with the steep increase of QPO amplitude with increasing photon energy observed in the higher frequency of the two simultaneous QPOs in 4U 1636−536 (Zhang et al. 1996), 4U 0614+091 (Ford et al. 1997b), and KS 1731−260 (Wijnands & van der Klis 1997), in the lower frequency of the two simultaneous QPOs in 4U 1608−52 (Berger et al. 1996; Méndez et al. 1998) and 4U 1728−34 (Strohmayer et al. 1996d), and in the kilohertz QPOs in the Z sources GX 5−1 (van der Klis et al. 1996e), GX 17+2 (Wijnands et al. 1997a), and Cyg X-2 (Wijnands et al. 1998).

In § 3.5 we used a simple analytical model to derive an expression for the photon energy dependence of the rms amplitude of a QPO produced by oscillations in the optical depth and in the injection rate of soft photons. Figure 11 compares the results of a more detailed numerical calculation performed using the algorithm of Miller & Lamb

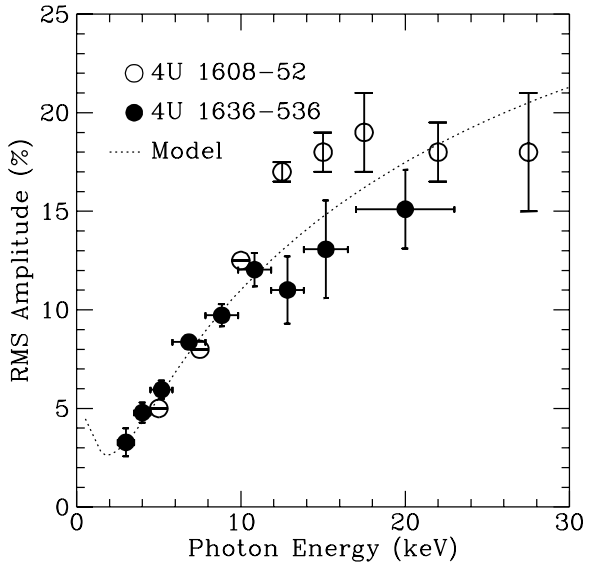

FIG. 11.—Measured amplitudes of the high-frequency QPOs seen in 4U 1608−52 (*open circles*) and 4U 1636−536 (*filled circles*) as a function of photon energy. Data for 4U 1636−536 were kindly provided by W. Zhang (1997, private communication) and reflect corrections made after the report by Zhang et al. (1996) was published. The dotted curve shows the variation of the rms amplitude with photon energy due to the optical depth variations expected in the sonic-point model (see text). This curve is not a fit; instead, for illustrative purposes we have assumed (consistent with the unified model of neutron star LMXBs) that the input spectrum is a blackbody of temperature $kT = 0.6$ keV and that the Comptonizing corona has a temperature $kT = 9$ keV and an optical depth that varies from $\tau = 3$ to $\tau = 3.3$.

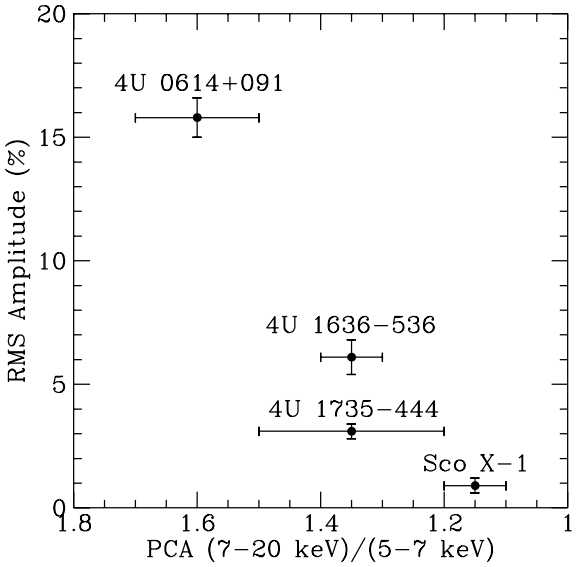

FIG. 12.—Measured rms amplitudes of the high-frequency QPOs seen in Sco X-1, 4U 1735−444, 4U 1636−536, and 4U 0614+091 plotted against the PCA X-ray hard colors (defined as the ratio of the counts in the 7–20 keV bin to the counts in the 5–7 keV bin) of these sources. The photon energy ranges used in computing these amplitudes were 2–20 keV for Sco X-1 (van der Klis et al. 1996b), 0.24–18.37 keV for 4U 1735−444 (Wijnands et al. 1996), 7–20 keV for 4U 1636−536 (van der Klis et al. 1996c), and 2–20 keV for 4U 0614+091 (van der Klis et al. 1996c). The observed steep increase of QPO amplitudes with photon energy (Fig. 11) means that a direct, quantitative comparison of QPO amplitudes in different sources can be made only if they are all computed using the same photon energy ranges. For example, the QPOs in GX 5−1 are not detected below 10 keV, but between 10 and 50 keV the QPO amplitude is as high as ∼7% (van der Klis et al. 1996e). It is not straightforward to compare this with the reported ∼1% amplitude for Sco X-1 in the 2–20 keV band. The range of hard colors for Sco X-1 is that near the soft vertex. The range of hard colors for 4U 1735−444 has been artificially extended to reflect possible systematic errors in the PCA response caused by gain changes. In neutron star LMXBs, the X-ray hard color is found to be greater for sources with weaker magnetic fields (Psaltis et al. 1995; Psaltis & Lamb 1998a, 1998b, 1998c), so the correlation evident in this figure is striking confirmation that the amplitudes of these QPOs are lower for sources with stronger magnetic fields. The PCA colors were kindly provided to us by Rudy Wijnands.

(1992) with amplitude data for the lower frequency kilohertz QPO observed in 4U 1608−52 and the higher frequency kilohertz QPO seen in 4U 1636−536. In performing this calculation, we made the same assumptions as in § 3.5 and assumed further that the injection rate of soft photons is constant in time, that the spectrum of the injected photons is a blackbody at temperature $kT = 0.6$ keV, that the electron temperature in the central corona is $kT_e = 9$ keV, and that the optical depth varies from $\tau = 3$ to $\tau = 3.3$ during an oscillation. The model matches the data well. The geometry of the actual upscattering region is undoubtedly much more complicated than assumed in this calculation, but the excellent correspondence with the data and the ubiquity of the steep increase of amplitude with photon energy over the 5–10 keV energy range suggest that the model has many elements in common with the true physical situation.

As a source moves in the X-ray color-color diagram and its spectrum changes (implying a change in the average optical depth and electron temperature of the Comptonizing region), we expect that the photon energy dependence of the rms amplitude of the oscillations will also change. Moreover, as discussed in § 3.5, we expect that, in general, the dependence of the beat-frequency QPO amplitude on photon energy will be different from the dependence of the Keplerian-frequency QPO amplitude. This is consistent with the observations of 4U 0614+091 (Ford et al. 1997b), in which the amplitude versus photon energy curve of the beat-frequency QPO has a minimum at ∼10 keV, whereas the amplitude versus photon energy curve of the Keplerian-frequency QPO increases monotonically from 2 to 20 keV. Because the QPO amplitude depends strongly on photon energy, to be meaningful, a comparison of QPO amplitudes measured for different sources or at different times for the same source must consider the same range of photon energies.

Coherence of the kilohertz QPOs.—In § 3.4 we showed that the high coherence of the Keplerian and beat-frequency QPOs in the sonic-point model is primarily a consequence of the extremely sharp increase in the inward radial velocity near the sonic point, which maps a small range of orbital frequencies onto the stellar surface. There we also considered the decoherence caused by destruction of clumps by turbulent dissipation within the disk flow, by advection to the stellar surface, and by decay as gas is stripped from them by the supersonic flow at the sonic point. We concluded that the QPO peaks can be as narrow as observed ($\nu/\delta\nu \sim 30$–200) for reasonable conditions in the accretion flow.

The FWHM $\delta\nu_{\rm BF}$ of the sonic-point beat frequency oscillation is expected to be comparable to the FWHM $\delta\nu_{\rm KF}$ of the sonic-point Keplerian frequency oscillation, because the beat-frequency QPO is produced by the beat of a nearly periodic signal at frequency $\nu_{\rm spin}$ against the Keplerian frequency (see § 3.4). We do not expect the FWHM of the two kilohertz QPO peaks to be identical, however, because there are processes that can affect the FWHM of one but not the other. For example, the FWHM of the beat-frequency peak depends in part on the range of radii over which radiation forces can affect the mass accretion rate significantly. This range can be either less than or greater than the range of radii over which the inward radial velocity increases rapidly, and hence $\delta\nu_{\rm BF}$ can be either less than or greater than $\delta\nu_{\rm KF}$. This effect can also displace the centroid of the beat-frequency peak relative to the centroid of the Keplerian frequency peak, so that the observed frequency difference $\nu_{\rm Ks} - \nu_{\rm Bs}$ is close to, but not exactly equal to, the stellar spin frequency.

4.4. *Amplitudes of QPOs Produced by Stars with Different Magnetic Field Strengths*

In the sonic-point model, the larger the magnetosphere, the smaller the fraction of the accreting gas that reaches the surface of the star without coupling to the magnetic field, and hence the smaller the amplitude of the kilohertz QPOs. Therefore, we expect the rms amplitudes of the kilohertz QPOs to be roughly anticorrelated with the strength of the stellar magnetic field, if all other physical quantities remain fixed. As discussed in § 2.2, the 4U atoll sources are thought to have the weakest magnetic fields, the GX atoll sources and the Sco-like Z sources are thought to have somewhat stronger fields, and the Cyg-like Z sources are thought to have the strongest fields (Psaltis & Lamb 1998a, 1998b, 1998c). Hence, we expect kilohertz QPOs to be common and strong in the 4U atoll sources, but weak or even undetectable with current instruments in the GX atoll sources

and the Z sources.[6] This is indeed the case, as is evident from Table 1. If, as indicated by the spectral modeling discussed in § 2, the magnetic field of Cir X-1 is weak, we expect it to exhibit sonic-point QPOs when it is in its low state. We also expect that kilohertz QPOs will be undetectable by current instruments in any sources that have strong magnetic fields and therefore produce strong, periodic oscillations at their spin frequencies.

The relation between kilohertz QPO amplitude and magnetic field strength may be made semiquantitative using the spectral calculations (see § 2.2) of Psaltis et al. (1995) and Psaltis & Lamb (1998a, 1998b, 1998c). These calculations indicate that LMXBs containing neutron stars with weaker magnetic fields generally have larger hard X-ray colors (e.g., the ratio of the 7–20 keV count rate to the 5–7 keV count rate). Based on this physical picture, we expect the rms amplitudes of the kilohertz QPOs produced by the sonic-point mechanism to be higher in sources with larger hard colors. This trend is evident in Figure 12, which shows the rms amplitudes versus the hard X-ray colors of four sources observed with the PCA detector aboard the *RXTE* satellite. If other sources with kilohertz QPOs follow this same trend, this will be strong support for the sonic-point model.

As discussed in § 2.3, the observed anticorrelation between kilohertz QPO amplitude and magnetic field strength is also strong evidence that the magnetospheric beat-frequency mechanism is *not* the correct explanation of these oscillations.

5. IMPLICATIONS FOR NEUTRON STARS AND DENSE MATTER

In the sonic-point model, the higher frequency QPO in a kilohertz QPO pair has a frequency equal to the orbital frequency of gas near the sonic point; the relatively high coherence of this QPO is a consequence of the fact that the gas clumps that generate it are in nearly circular orbits. In this section we show that the inferred existence of a nearly circular orbit around a neutron star with a frequency in the kilohertz range can be used to derive interesting new upper bounds on the mass and radius of the star and constraints on the equation of state of the dense matter in all neutron stars. For simplicity we discuss first the case of a nonrotating star around which the radial component of the radiation force is negligible. We then consider the changes in the mass and radius constraints caused by frame dragging when the star is spinning and by the radial component of the radiation force. We show that rotation at ~ 300 Hz typically increases the bound on the mass by $\sim 20\%$ and the bound on the radius by a few percent. In contrast, the radiation force *reduces* the upper bounds on the masses and radii by a few percent or less in the atoll sources but perhaps by much larger percentages in the Z sources.

Observations of kilohertz QPOs may be able to establish the existence of an innermost stable circular orbit around some neutron stars (see § 4.2). If this can be accomplished, it would be the first evidence concerning a prediction of general relativity in the strong-field regime. If furthermore the frequency of a particular kilohertz QPO can be securely established as the orbital frequency at the radius of the innermost stable circular orbit and if the spin frequency of the neutron star can be determined, then the frequency of the QPO can be used to fix the mass of the neutron star for each assumed equation of state, tightening the constraints on the properties of dense matter and possibly ruling out many currently viable equations of state. We discuss how this can be done and the evidence that would signal detection of a QPO with the orbital frequency of the marginally stable orbit.

5.1. *Nonrotating Star*

Suppose that the frequency of the higher frequency QPO in a kilohertz pair is $\nu_{\rm QPO2}$ and that, as in the sonic-point model, $\nu_{\rm QPO2}$ is the orbital frequency of gas in a nearly circular Keplerian orbit around the neutron star. Assume for now that the star is not rotating and is spherically symmetric. Then the exterior spacetime is the Schwarzschild spacetime. In this spacetime, the orbital frequency (measured at infinity) of gas in a circular orbit at Boyer-Lindquist radius r around a star of mass M is (see eq. [10])

$$\nu_{\rm K}^0(M, r) = (1/2\pi)(GM/r^3)^{1/2} . \tag{26}$$

Here and below, the superscript zero indicates that the relation is that for a nonrotating ($j = 0$) star. If the mass of the star is known, equation (26) may be solved for the orbital radius $R_{\rm orb}$ where the Keplerian frequency is $\nu_{\rm QPO2}$, with the result

$$R_{\rm orb}^0(M, \nu_{\rm QPO2}) = (GM/4\pi^2\nu_{\rm QPO2}^2)^{1/3} . \tag{27}$$

Conversely, if the orbital radius of the gas is known, equation (26) may be solved for the mass of the star that gives an orbital frequency equal to $\nu_{\rm QPO2}$, with the result

$$M^0(R_{\rm orb}, \nu_{\rm QPO2}) = (4\pi^2/G)R_{\rm orb}^3\,\nu_{\rm QPO2}^2 . \tag{28}$$

If, as is so far the case for the kilohertz QPO sources, neither M nor $R_{\rm orb}$ is known, equations (27) and (28) do not determine $R_{\rm orb}$ or M but do establish a relation between them. In the radius-mass plane, this relation is a curve that begins at the origin and rises up and to the right.

As a specific example, the dashed curve marked $M^0(R_{\rm orb})$ in Figure 13 shows the relation given by equation (28) for $\nu_{\rm QPO2} = 1220$ Hz, a value of $\nu_{\rm QPO2}$ observed in 4U 1636−536 (W. Zhang 1997, personal communication). Hence, if 4U 1636−536 were not rotating, the mass of the neutron star in this source and the orbital radius of the gas clumps producing the QPO during this observation would have to correspond to some point along this dashed curve.

Consider now the constraints on the neutron star mass and radius that follow from the *frequency* of the higher frequency QPO. Obviously, in order for gas to be in orbit, it must be outside the star. This means that for an orbit of given radius $R_{\rm orb}$, the mass M of the star must be greater than $M^0(R_{\rm orb}, \nu_{\rm QPO2})$; alternatively, for a star of given mass M, the radius R of the star must be less than $R_{\rm orb}^0(M, \nu_{\rm QPO2})$. Thus, the point that represents the mass and radius of the neutron star must lie above the curve $M^0(R_{\rm orb}, \nu_{\rm QPO2})$ in the radius-mass plane. The larger the value of $\nu_{\rm QPO2}$, the higher the curve, so the most stringent—and hence the relevant—constraint on the mass and radius of the neutron star in a particular source is given by the highest value of $\nu_{\rm QPO2}$ ever observed in that source, which we denote $\nu_{\rm QPO2}^*$. For example, 1220 Hz is the highest value of $\nu_{\rm QPO2}$ seen so far in 4U 1636−536, so this is the current value of $\nu_{\rm QPO2}^*$ for this

[6] After this specific prediction was made in the originally submitted and circulated version of the present paper, kilohertz QPOs with very low amplitudes were detected in all six of the originally identified Z sources; see Table 1. To date, kilohertz QPOs have not been detected in any of the GX atoll sources.

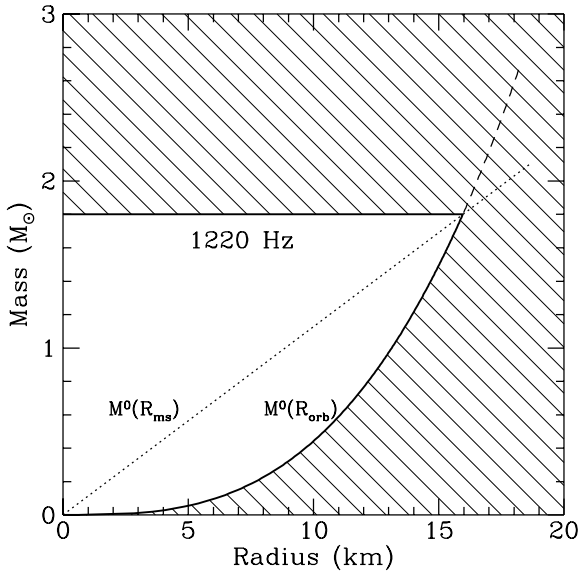

FIG. 13.—Radius-mass plane, showing how bounds on the mass and radius of a nonrotating neutron star in a QPO source with $\nu^*_{QPO2} = 1220$ Hz can be constructed. The dashed curve that begins at the origin and rises up and to the right is the relation $M = M^0(R_{orb}, \nu^*_{QPO2})$, for $\nu^*_{QPO2} = 1220$ Hz; this curve gives the mass for which the orbital frequency at the radius shown on the horizontal axis is 1220 Hz. The diagonal dotted line is the relation $M = M^0(R_{ms})$; this line gives the mass for which the radius R^0_{ms} of the innermost stable circular orbit is equal to the radius shown on the horizontal axis. The horizontal solid line is the mass M^0_{max} at which $M^0(R_{ms})$ is equal to $M^0(R_{orb}, \nu^*_{QPO2})$ and hence $R^0_{ms}(M)$ is equal to $R^0_{orb}(M, \nu^*_{QPO2})$, for $\nu^*_{QPO2} = 1220$ Hz. The hatched region shows the combinations of stellar mass and radius that are exluded. The region outlined by the heavy solid line shows the combinations allowed by the frequency and coherence of the QPO (see text). Only masses less than $M^0_{max} = 1.8\ M_\odot$ and radii less than $R^0_{max} = 16.0$ km are allowed. The allowed region collapses to the heavy solid horizontal line if the QPO frequency is identified as the orbital frequency of gas in the innermost stable circular orbit (see § 5.1). The steps in the construction are the same for a rotating star but the bounds are different (see § 5.2).

source (in fact, this is the highest value of ν_{QPO2} seen so far in any source). Consequently, if the neutron star in 4U 1636−536 were not rotating, the point in the radius-mass plane that represents its mass and radius would have to lie above the curve $M = M^0(R_{orb}, 1220\ \text{Hz})$, which is the dashed curve shown in Figure 13.

So far, the only information we have used to constrain the mass and radius of the star is the frequency of the higher frequency QPO in a kilohertz pair. However, we have the additional information that the *coherence* of the higher frequency QPO is high ($\nu_{QPO}/\delta\nu_{QPO} \sim 100$) in many sources. Let us assume that the higher frequency QPO in a pair is generated by the same mechanism in all sources that show such pairs. Then the high coherence of these higher frequency QPOs imposes additional constraints on the neutron star's mass and radius because, in order to produce a QPO with such high coherence, the gas that generates the QPO must be in a nearly circular orbit. Hence $R_{orb}(M, \nu^*_{QPO2})$ must be greater than the radius $R_{ms}(M)$ of the innermost stable circular orbit, because gas inside R_{ms} spirals quickly inward to the stellar surface.

For a nonrotating star, the radius of the innermost stable circular orbit is a function only of the mass of the star and is given by $R^0_{ms}(M) = 6GM/c^2$. Inverting this relation gives

$$M^0(R_{ms}) = (c^2/6G)R_{ms}\ . \tag{29}$$

In the radius-mass plane, equation (29) is a straight line of slope +1 through the origin and is the dotted line marked $M^0(R_{ms})$ in Figure 13. This line intersects $M^0(R_{orb}, \nu^*_{QPO2})$ at the mass and radius values

$$M^0_{max} \equiv c^3(\sqrt{864}G\pi\nu^*_{QPO2})^{-1} = 2.2(1000\ \text{Hz}/\nu^*_{QPO2})\ M_\odot\ , \tag{30}$$

and

$$R^0_{max} \equiv c(\sqrt{24}\pi\nu^*_{QPO2})^{-1} = 19.5(1000\ \text{Hz}/\nu^*_{QPO2})\ \text{km}\ . \tag{31}$$

If M were larger than M^0_{max}, the orbital radius $R^0_{orb}(M, \nu^*_{QPO2})$ of the gas generating the QPO would be less than $R^0_{ms}(M)$, so M^0_{max} is an upper bound on the mass of the star; M^0_{max} is inversely proportional to ν_{QPO2} but independent of the star's radius and the orbital radius of the gas clumps that are producing the higher frequency QPO. Similarly, R^0_{max} is an upper bound on the radius of the star; R^0_{max} is also inversely proportional to ν_{QPO2} but independent of the star's mass and the orbital radius of the gas clumps that are producing the higher frequency QPO.

The heavy horizontal line plotted in Figure 13 shows the upper bound on the mass of a nonrotating star for $\nu^*_{QPO2} = 1220$ Hz. This upper bound is 1.8 $M_\odot$, so the mass of the neutron star in 4U 1636−536 would have to be less than this if it were not rotating. For $\nu^*_{QPO2} = 1220$ Hz, R^0_{max} is 16.0 km, so the radius of the neutron star in 4U 1636−536 would have to be less than this if the star were not rotating.

Suppose now that the frequency ν^*_{QPO2} of a particular QPO is securely identified as the orbital frequency of gas in the innermost stable circular orbit around a particular neutron star. Then $R_{orb} = R_{ms}$ for this QPO, so the representative point of the orbit is at the intersection of the diagonal $M^0(R_{ms})$ line and the $M^0(R_{orb}, \nu^*_{QPO2})$ curve. The mass of the star is therefore M^0_{max}. Hence *identification of a QPO frequency with the frequency of the innermost stable circular orbit immediately determines the mass of the star.* The radius of the star is not determined by such an identification, but it must still be less than R^0_{max}.

As a specific example, suppose that the 1220 Hz QPO observed in 4U 1636−536 is securely identified as the orbital frequency of gas in the innermost stable circular orbit around this neutron star. Then the mass of this neutron star would be determined as 1.8 $M_\odot$, if it were not rotating.

These arguments apply to stars with arbitrary spin rates as well as to nonrotating stars, although the expressions for $R_{orb}(M, \nu^*_{QPO2})$ and $R_{ms}(M)$ are different for a rotating star and depend on the star's spin rate as well as its mass. They may be summarized as follows.

1. Stellar radii $R > R_{orb}(M, \nu^*_{QPO2})$ are excluded, because there is no Keplerian orbit with frequency ν^*_{QPO2} outside a star with such a large radius; the value of $R_{ms}(M)$ is irrelevant.

2. If $R < R_{orb}(M, \nu^*_{QPO2})$ but $R_{ms}(M) > R_{orb}(M, \nu^*_{QPO2})$, there is a Keplerian orbit with frequency ν^*_{QPO2} outside the star but any oscillation produced by gas in this orbit would have a coherence much lower than that observed.

3. If $R < R_{orb}(M, \nu^*_{QPO2})$ and $R_{ms}(M) < R_{orb}(M, \nu^*_{QPO2})$, there is a Keplerian orbit with frequency ν^*_{QPO2} outside the star and the oscillation produced by gas in this orbit can have the required high coherence.

4. If the frequency $\nu^*_{\rm QPO2}$ of a particular QPO is securely identified as the orbital frequency of gas in the innermost stable circular orbit around a particular neutron star, the mass of the star is $M^0_{\rm max}$; its radius must be less than $R^0_{\rm max}$.

For a nonrotating star with $\nu^*_{\rm QPO2} = 1220$ Hz, the combinations of stellar mass and radius allowed by condition (3) are the points in the radius-mass plane above the curve $M = M^0(R_{\rm orb}, 1220\ {\rm Hz})$ but below $M = M^0_{\rm max}$. This region is outlined in Figure 13 by the heavy solid line. The point representing the mass and radius of the neutron star in 4U 1636−536 would have to lie in this region if the star were not rotating. The allowed region collapses to the heavy solid horizontal line if the QPO frequency is identified as the orbital frequency of gas in the innermost stable circular orbit so that condition (4) applies.

Figure 14 compares the mass-radius relations for nonrotating neutron stars given by five equations of state for neutron-star matter ranging from soft to hard with the regions of the radius-mass plane allowed if $\nu^*_{\rm QPO2}$ is a Keplerian orbital frequency, for nonrotating stars and three values of $\nu^*_{\rm QPO2}$. In order to make possible comparisons with previous studies of neutron star properties (see, e.g., Pethick & Ravenhall 1995), we show the mass-radius curve given by the early Friedman-Pandharipande-Skyrme (FPS) realistic equation of state (Friedman & Pandharipande 1981; Lorenz, Ravenhall, & Pethick 1993). The FPS equation of state uses a different approach but is similar to the softest equations of state permitted by modern realistic models of the nucleon-nucleon interaction (Pandharipande, Akmal, & Ravenhall 1998). These equations of state all give maximum gravitational masses of about 1.8 $M_\odot$ for nonrotating stars.

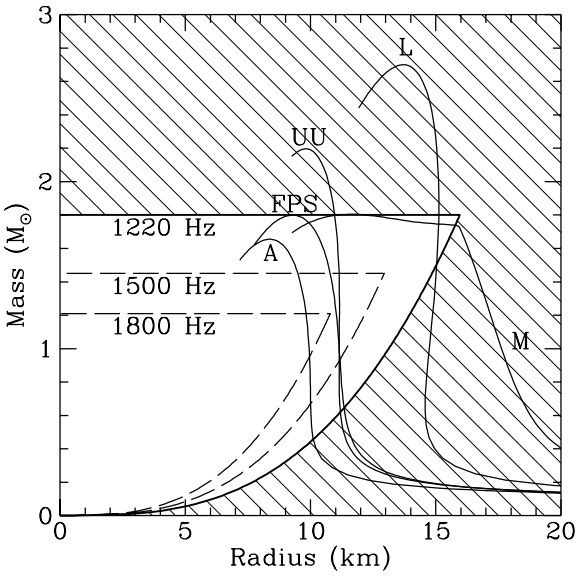

FIG. 14.—Comparison of the mass-radius relations for nonrotating neutron stars given by five representative equations of state for neutron-star matter with the regions of the mass-radius plane allowed for nonrotating stars (see Fig. 13 and text) in sources with three values of $\nu^*_{\rm QPO2}$, the highest observed frequency of the higher frequency QPO in a pair. The light solid curves show the mass-radius relations given by equations of state A (Pandharipande 1971), FPS (Lorenz et al. 1993), UU (Wiringa et al. 1988), L (Pandharipande & Smith 1975b), and M (Pandharipande & Smith 1975a). Each allowed region is labeled by the value of $\nu^*_{\rm QPO2}$ assumed in constructing it. As in Fig. 13, the hatched region shows the combinations of stellar mass and radius that are excluded for $\nu_{\rm QPO2} = 1220$ Hz. The region bounded by the heavy line is the region that would be allowed for the neutron star in 4U 1636−536 if it were not rotating (see text). The star's probable spin rate affects the mass-radius relations hardly at all but enlarges the allowed region by ~20% (see § 5.2 and Fig. 15).

As an example of the mass-radius curves given by later realistic equations of state, we show the mass-radius curve predicted by the UU equation of state (Wiringa, Fiks, & Fabrocini 1988). Although it is based on older scattering data, the UU equation of state is similar to the recent A18 + UIX′ + $\delta v_{\rm b}$ equation of state (Akmal, Pandharipande, & Ravenhall 1998), which is based on the most modern scattering data. Like the A18 + UIX′ + $\delta v_{\rm b}$ equation of state, the UU equation of state gives a maximum mass of about 2.2 $M_\odot$ for a nonrotating neutron star.

As an example of the mass-radius curves predicted by the relatively stiff equations of state typically given by mean field theories, we include the mass-radius curve for the mean-field equation of state of Pandharipande & Smith (1975b; "L" in the Arnett & Bowers 1977 survey). The maximum mass of a nonrotating star constructed using equation of state L is 2.7 $M_\odot$. We also show the mass-radius curve given by the very early tensor interaction (TI) equation of state of Pandharipande & Smith (1975a; "M" in the Arnett & Bowers 1977 survey) and the Reid soft-core equation of state of Pandharipande (1971; "A" in the Arnett & Bowers 1977 survey). The maximum masses of nonrotating stars constructed using equations of state M and A are 1.8 $M_\odot$ and 1.65 $M_\odot$, respectively. Equations of state A, L, and M are no longer of interest to nuclear physicists and are included here primarily to facilitate comparison with previous work on mass-radius constraints.

For a particular source, QPO frequency, and equation of state, the allowed portion of the mass-radius relation is the segment within the pie-slice shaped region analogous to the region in Figure 13 outlined by the heavy line or, if the QPO frequency is identified as the frequency of the innermost stable circular orbit, simply the horizontal heavy line. If the mass-radius relation given by a particular equation of state intersects the allowed region defined by the highest QPO frequency seen in a given source, that particular equation of state is viable. If that equation of state is furthermore the correct equation of state, the mass and radius of the neutron star in the source must correspond to one of the points along the segment of the mass-radius relation that lies within the pie-slice shaped region, so the mass and radius of the star are bounded from above *and* from below; for most equations of state, only a narrow range of radii is allowed.

For example, the highest frequency QPO so far seen in any source is the 1220 Hz QPO observed in 4U 1636−536 (W. Zhang 1997, personal communication). Hence, if equation of state M is the correct equation of state, then the mass and radius of the neutron star in 4U 1636−536 would have to satisfy $1.7\ M_\odot < M < 1.8\ M_\odot$ and 11.6 km $< R <$ 16.0 km if it were nonrotating. If equation of state M is the correct equation of state and 1220 Hz is identified as the frequency of the innermost stable circular orbit, then the mass and radius of the neutron star in 4U 1636−536 would be determined as about 1.8 $M_\odot$ and between 11 and 12 km if the star were not rotating.

An equation of state that gives a mass-radius relation that does not intersect the region allowed for a given source is ruled out for that source. We stress that *because the equation of state of the matter in neutron stars is expected to be essentially the same in all such stars, an equation of state that is inconsistent with the properties of any neutron star is*

excluded for all neutron stars. For example, observation of a 1500 Hz Keplerian orbital frequency in any source would rule out equations of state L and M.

So far our discussion of constraints on the neutron stars in the kilohertz QPO sources has assumed that they are not rotating. As we discuss in the next subsection, the changes in these constraints caused by the spin of the star are likely to be small in most sources.

5.2. *Effects of Stellar Rotation*

Rotation affects the structure of the star for a given mass and equation of state and the spacetime exterior to the star. Hence the mass-radius relation, the orbital frequency at a given radius, and the radius $R_{\rm ms}$ of the innermost stable circular orbit are all affected. As a result, the bounds on the mass and radius of the star and the constraints on the equation of state implied by observation of a kilohertz QPO of a given frequency are affected. Obviously, the size of these effects depends on the spin rate of the star. Treating these effects accurately will be particularly important if the frequency of a kilohertz QPO is ever securely identified as the Keplerian frequency at the marginally stable orbit around a neutron star (see § 5.4), because the ability to rule out some equations of state may depend on it.

The parameter that characterizes the importance of rotational effects is the dimensionless quantity $j \equiv cJ/GM^2$, where J and M are the angular momentum and gravitational mass of the star. The value of j that corresponds to a given observed spin frequency depends on the neutron star mass and equation of state and is typically higher for lower masses and stiffer equations of state. For example, at the 363 Hz spin frequency inferred for 4U 1728−34 (Strohmayer et al. 1996d), a 1.4 $M_\odot$ neutron star with the softer equation of state A has $j \approx 0.1$, whereas a 1.4 $M_\odot$ neutron star with the very stiff equation of state L has $j \approx 0.3$ (see Table 5).

As discussed in § 5.1, if the frequency of the higher frequency QPO in a kilohertz QPO pair is an orbital frequency, then the region of the radius-mass plane allowed for the neutron star in that source is bounded below by the curve $R_{\rm orb}(M)$, which gives the orbital radius at which the Keplerian frequency is equal to the highest observed frequency $\nu^*_{\rm QPO2}$ of the higher frequency QPO. Given j, it is straightforward to compute the orbital radius for any given orbital frequency as a function of M. However, it is not j but instead the star's spin frequency $\nu_{\rm spin}$ that is determined by the observations. Hence, *to obtain the relevant* $R_{\rm orb}(M)$ *curve one must vary* j *in such a way that* $\nu_{\rm spin}$ *is kept constant as* M *is varied*. Moreover, j depends not only on $\nu_{\rm spin}$ and M but also on the equation of state. Thus the relevant $R_{\rm orb}(M)$ curve depends not only on the star's spin rate, but also on the equation of state assumed. Therefore, for rotating stars (unlike static stars), one cannot present a single $R_{\rm orb}(M)$ curve that constrains all equations of state, even for a star with a given spin frequency.

TABLE 5

DIMENSIONLESS ANGULAR MOMENTA FOR $\nu_{\rm spin} = 363$ Hz

Equation of State	Mass ($M_\odot$)	$j \equiv cJ/GM^2$
A	1.40	0.13
	1.66	0.10
FPS	1.40	0.16
	1.80	0.11
L	1.40	0.28
	2.70	0.17
M	1.40	0.31
	1.80	0.13

As also discussed in § 5.1, the region of the radius-mass plane allowed for the neutron star in a given source is bounded above by the horizontal line $M = M_{\rm max}$, which is the mass at which the curve $R_{\rm orb}(M)$ intersects the curve $R_{\rm ms}(M)$; the radius R of the star is bounded above by $R_{\rm orb}(M_{\rm max})$. The two curves $R_{\rm ms}(M)$ and $R_{\rm orb}(M)$ are both affected by rotation of the star, so $M_{\rm max}$ depends on the stellar spin rate.

Determining the mass at which $R_{\rm orb}(M) = R_{\rm ms}(M)$ is equivalent to determining the mass at which $\nu_{\rm K}(R_{\rm ms})$ is equal to $\nu^*_{\rm QPO2}$. Here we focus on the latter condition. The allowed mass of a rotating star is bounded above if, as M is increased at constant $\nu_{\rm spin}$, the orbital frequency $\nu_{\rm K}(R_{\rm ms})$ crosses the QPO frequency $\nu^*_{\rm QPO2}$ from above once and only once. As we show below, this is the case for slowly rotating stars. However, this may not be the case for some neutron star equations of state and spin rates. [For a Kerr black hole with fixed spin frequency, $\nu_{\rm K}(R_{\rm ms})$ first decreases and then increases with increasing mass.]

Fortunately, most of the neutron stars that exhibit kilohertz QPOs appear to have spin frequencies in the range 250–350 Hz (see § 4.2), which is low enough that a first-order treatment of rotational effects is adequate. To see this, note that neutron stars with masses $\sim$1.5–2 $M_\odot$ have moments of inertia $I \sim (1\text{–}3) \times 10^{45}$ g cm^{-2}, so stars with spin frequencies $\lesssim$350 Hz have j-values $\lesssim$0.3 (see Table 5). The lowest order changes in the structure of a rotating star are $\mathcal{O}(j^2)$ so, to first order in j, the mass-radius relation and moment of inertia of a rotating star are the same as for a nonrotating star of the same mass (Hartle & Thorne 1968). Thus the error made by neglecting higher order terms is $\lesssim$10% for spin frequencies $\lesssim$350 Hz.

We now compute the mass and radius constraints imposed on a slowly rotating neutron star by observation of a kilohertz orbital frequency. The calculation is simplified by the fact that, to first order in j, the spacetime outside a uniformly and steadily rotating relativistic star is the same as the Kerr spacetime for the same M and j (Hartle & Thorne 1968).

Consider first the effect of stellar rotation on the motion of gas orbiting the star. To first order in j, the orbital frequency (measured at infinity) of gas in a prograde Keplerian orbit at a given Boyer-Lindquist radius r is

$$\nu_{\rm K}(r, M, j) \approx [1 - j(GM/rc^2)^{3/2}]\nu^0_{\rm K}(r, M) , \qquad (32)$$

and the radius of the marginally stable orbit is

$$R_{\rm ms}(M, j) \approx [1 - j(2/3)^{3/2}]R^0_{\rm ms}(M) , \qquad (33)$$

where $\nu^0_{\rm K}$ and $R^0_{\rm ms}$ are the Keplerian frequency and radius of the marginally stable orbit for a nonrotating star. Equations (32) and (33) are first-order expansions of the exact expressions for these quantities given by Bardeen et al. (1972) for the Kerr spacetime. Hence, to first order in j, the frequency of the prograde orbit at $R_{\rm ms}$ around a star of given mass M and dimensionless angular momentum j is (cf. Kluźniak, Michelson, & Wagoner 1990)

$$\nu_{\rm K,ms} \approx [1 - j(1/6)^{3/2}][1 + j(2/3)^{1/2}]\nu^0_{\rm K,ms}$$
$$\approx 2210(1 + 0.75j)(M_\odot/M)\ {\rm Hz} , \qquad (34)$$

where $\nu^0_{\rm K,ms}$ is the Keplerian orbital frequency at the radius of the innermost stable circular orbit for a nonrotating star. *Therefore, the net effect of the star's rotation is to increase the frequency of the prograde orbit at* $R_{\rm ms}$.

As explained above, the region of the radius-mass plane allowed for a given star is not the region allowed for constant j but is instead the region allowed for constant $\nu_{\rm spin}$. To demonstrate that the mass and radius of the star are bounded from above, it is sufficient to show that $\nu_{\rm K}(R_{\rm ms})$ decreases with increasing M at fixed $\nu_{\rm spin}$, or equivalently, that $(d\nu_{\rm K,ms}/dM)_{\nu_{\rm spin}} < 0$ for all M for the equation of state under consideration. Now to first order in j,

$$\left[\frac{d\nu_{\rm K,ms}(M,j)}{dM}\right]_{\nu_{\rm spin}} = \left\{\left[\frac{\partial \nu_{\rm K,ms}}{\partial M}(M,0)\right]_j + \left[\frac{\partial \nu_{\rm K,ms}}{\partial j}(M,0)\right]_M \left(\frac{dj}{dM}\right)\right\}_{\nu_{\rm spin}} \quad (35)$$

$$\approx -\frac{\nu^0_{\rm K,ms}(M)}{M}\left[1 + 0.75j\left(2 - \frac{d\ln I}{d\ln M}\right)\right]_{\nu_{\rm spin}} . \quad (36)$$

Note that the derivatives on the right-hand side of equation (35) are to be evaluated at $j = 0$. In order to show that $(d\nu_{\rm K,ms}/dM)_{\nu_{\rm spin}}$ is negative for slowly rotating stars, it is sufficient (but not necessary) to show that $(d\ln I/d\ln M)_{\nu_{\rm spin}}$ is always less than 2. This is the case for all the equations of state tabulated by Cook et al. (1994) and is the case even for incompressible matter, which is unphysically stiff. (For a star made of incompressible matter, $I \propto MR^2 \propto M^{5/3}$, so $(d\ln I/d\ln M) = 5/3 < 2$.) Thus, *for slowly rotating stars* $\nu_{\rm K}(R_{\rm ms})$ decreases with increasing mass for constant $\nu_{\rm spin}$, so the masses and radii of such stars are bounded above.

Computation of the mass and radius constraints is straightforward but depends on the stellar spin rate and equation of state. The upper bounds on the mass and radius are given implicitly by

$$M_{\rm max} \approx [1 + 0.75j(\nu_{\rm spin})]M^0_{\rm max} \quad (37)$$

and

$$R_{\rm max} \approx [1 + 0.20j(\nu_{\rm spin})]R^0_{\rm max} , \quad (38)$$

where $j(\nu_{\rm spin})$ is the value of j for the observed stellar spin rate at the maximum allowed mass for the equation of state being considered and $M^0_{\rm max}$ and $R^0_{\rm max}$ are the maximum allowed mass and radius for a nonrotating star (see eqs. [30] and [31]). Equations (37) and (38) show that *the bounds are always greater for a slowly rotating star than for a nonrotating star, regardless of the equation of state assumed.*

Figure 15 illustrates the effects of stellar rotation on the region of the radius-mass plane allowed for a given star for spin rates $\sim$300 Hz, like those inferred for the kilohertz QPO sources, and $\nu^*_{\rm QPO2} = 1220$ Hz, the frequency of the highest frequency QPO so far observed in 4U 1636−536, which is also the highest frequency QPO so far observed in any source. *Our calculations show that the mass of the neutron star in 4U 1636−536 must be less than* $\sim 2.2\ M_\odot$ *and its radius must be less than* $\sim$17 km. As explained above, the precise upper bounds depend on the equation of state assumed.

For rapidly rotating stars, j is not small compared to unity and the structure of the star depends appreciably on its rotation rate. Derivation of bounds on the mass and radius of a given star for an assumed equation of state therefore requires construction of a sequence of stellar models and spacetimes for different masses using the assumed equation of state, with $\nu_{\rm spin}$ as measured at infinity held fixed. The maximum and minimum possible masses and radii allowed by the observed QPO frequency can then be determined.

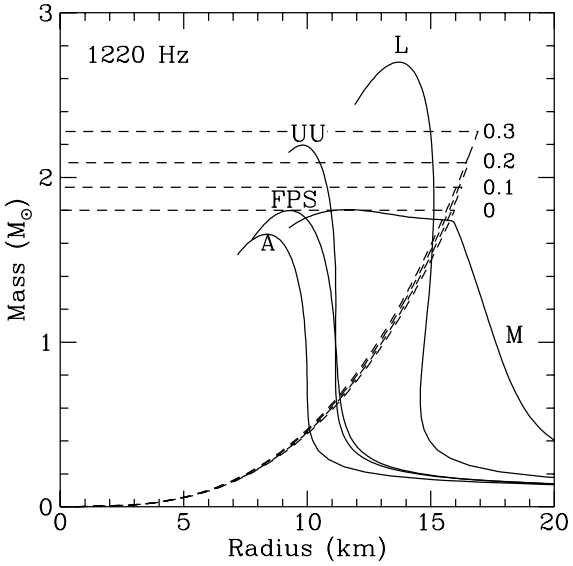

FIG. 15.—Approximate constraints imposed on the mass, radius, and equation of state of neutron stars by the 1220 Hz QPO frequency observed in 4U 1636−536, when first-order effects of the stellar spin are included. The QPO frequency is assumed to be the Keplerian frequency of gas in a prograde orbit. The light solid lines are the mass-radius relations for the same equations of state as in Fig. 14. Allowed combinations of mass and radius for the indicated values of the dimensionless angular momentum j are those within the corresponding pie-shaped regions bounded by the heavy dashed lines. For a rotating star, accurate determination of the allowed region requires computation of the bounding curves with $\nu_{\rm spin}$ held equal to the observed value rather than with j held constant and therefore depends on the equation of state assumed as well as the QPO frequency and the mass of the star (see text).

5.3. *Effects of the Radial Radiation Force*

The luminosities of the Z sources are typically $\sim$0.5–1 $L_{\rm E}$, where $L_{\rm E}$ is the Eddington luminosity (see § 2). Hence, in the Z sources the outward acceleration caused by the radial component of the radiation force can be a substantial fraction of the inward acceleration caused by gravity. Therefore, in these sources the radial component of the radiation force must be included in computing the Keplerian orbital frequency near the neutron star and taken into account when constraints on the mass and radius of the star are derived using the procedures discussed in §§ 5.1 and 5.2.

The radially outward component of the radiation force reduces the orbital frequency at a given radius. For example, if the star is spherical and nonrotating and emits radiation uniformly and isotropically from its entire surface, the orbital frequency (measured at infinity) of a test particle at Boyer-Lindquist radius r is

$$\nu_{\rm K}(L) = \nu_{\rm K}(0)\left[1 - \frac{(1 - 3GM/rc^2)^{1/2}}{(1 - 2GM/rc^2)}\frac{L}{L_{\rm E}}\right]^{1/2} , \quad (39)$$

where L is the luminosity of the star measured at infinity and $\nu_{\rm K}(0)$ is the Keplerian frequency in the absence of radiation forces. Thus, the Boyer-Lindquist radius of a circular orbit with a given frequency is smaller in the presence of the radial radiation force and the constraints on the mass and radius of the star are therefore tightened.

For the atoll sources, which have luminosities $L \lesssim 0.1 L_E$, the change in the Keplerian frequency is at most $\sim 5\%$. For the Z sources, on the other hand, which have luminosities $L \approx L_E$, the change may be much larger, although the change in the sonic-point Keplerian frequency may be smaller than would be suggested by a naive application of equation (39), if a substantial fraction of the radiation produced near the star is scattered out of the disk plane before it reaches the sonic point. A more detailed analysis of the effect of the radial radiation force on the constraints on the mass and radius of the star will be reported elsewhere.

5.4. *Signatures of the Innermost Stable Circular Orbit*

As explained in § 4.2, observations of kilohertz QPO sources may be able to demonstrate the existence of an innermost stable circular orbit around some of the neutron stars in these sources. If so, this would be the first confirmation of a strong-field prediction of general relativity and an important step forward in our understanding of strong-field gravity.

If the frequency of a kilohertz QPO produced by an LMXB can be securely established as the orbital frequency at the radius of the innermost stable circular orbit and the spin frequency of the star can be determined, the mass of the neutron star in that source can be determined for each assumed equation of state. Depending on the range of allowed equations of state and masses, this could have profound consequences for our understanding of the equation of state of neutron stars.[7] For example, establishing a mass of $2.0\ M_\odot$ for a slowly rotating neutron star would rule out eight of the 12 currently viable equations of state considered by Cook et al. (1994).

Given the profound consequences that would follow from identifying the frequency of a kilohertz QPO with the orbital frequency of the innermost stable orbit in any source, it is very important to establish what would constitute strong, rather than merely suggestive, evidence of such a detection. Observations that would signal detection of the innermost stable orbit include the following.

QPO frequency signature.—The strongest evidence that a QPO with the orbital frequency of the innermost stable orbit has been detected would be reproducible observation of a fairly coherent kilohertz QPO with a frequency that first increases steeply with the accretion rate but then, at a high frequency, becomes nearly constant as the accretion rate continues to increase (see §§ 3.3 and 4.2 and Fig. 9).

The QPO frequency will approach a constant because the sonic point in the flow cannot retreat closer to the star than the radius of the marginally stable orbit and coherent QPOs are not expected from the rapidly inspiraling gas inside the sonic point. Although the count rate above which the frequency becomes constant may vary, the constant frequency itself should not vary, because the orbital frequency of the marginally stable orbit depends only on the mass and rotation rate of the neutron star, which remain almost constant over many years.

In the sonic-point model, the frequency of the lower frequency QPO in a kilohertz QPO pair is the beat frequency and therefore should also increase steeply with the accretion rate at first but then become approximately constant at the same accretion rate at which the frequency of the higher frequency QPO becomes constant.

QPO amplitude signature.—A second signature that the marginally stable orbit has been detected would be reproducible observation of a decrease in the amplitude of the lower frequency QPO in a kilohertz QPO pair or a simultaneous decrease in the amplitudes of both QPOs in a pair, at a QPO frequency that is always the same in a given source.

The amplitude of the QPO at the beat frequency is expected to decrease once the sonic point has moved inward to the marginally stable orbit because in the sonic-point model, the QPO at the beat frequency is generated by the drag force exerted by the radiation coming from the stellar surface that reaches the sonic point. Therefore, a strong QPO is expected at the sonic-point beat frequency only if the drag force exerted by the radiation is dynamically important at the sonic point. If, however, the sonic point has moved inward to the innermost stable orbit and remains there as the accretion rate continues to increase, the optical depth from the stellar surface to the sonic point will continue to rise and radiation drag will become less and less important there, causing modulation of the inflow from the sonic point by the radiation force to weaken. Thus, a decrease in the amplitude of the QPO at the sonic-point beat frequency with increasing accretion rate would signal the approach of the sonic-point to the radius of the innermost stable orbit (see § 3.1).

If radiation forces play an important role in creating or amplifying the clumps that produce the QPOs (see § 3.1), the amplitude of the Keplerian-frequency QPO may also decrease with increasing accretion rate, once the radius of the sonic point has reached the radius of the innermost stable orbit (see § 3.2).

Possible QPO coherence signature.—A possible signature that the orbit of the gas that is generating the QPO has receded inside the radius of the marginally stable orbit would be a steep drop in the coherence of both QPOs in a kilohertz QPO pair (or in the coherence of the Keplerian-frequency QPO, if the beat-frequency QPO is not visible), at a certain critical frequency, as the frequencies of the QPOs increase steadily with accretion rate. This would occur if radiation forces are able to generate clumping in the flow at a radius inside the sonic point. If this occurs at all, clumps are likely to be produced at a range of radii and to last only a short time, so any oscillations that may be generated are likely to have low coherence (see § 3.4). The critical frequency would be the orbital frequency at the marginally stable orbit and hence should always be the same in a given source.

Approach of the sonic radius to the radius of the innermost stable orbit can be distinguished from approach of the sonic radius to the radius of the star because coherent Keplerian- and beat-frequency QPOs may continue in the first case but are very unlikely in the second. Kilohertz QPOs are unlikely to be generated if the sonic point moves close to the stellar surface because of the disruptive effect of the stellar magnetic field and the viscous shear layer that is expected to develop if the Keplerian flow interacts directly with the stellar surface (see § 4.2).

6. SUMMARY AND CONCLUSION

The sonic-point model explains naturally the most important features of the kilohertz QPOs observed in the

[7] Following submission and circulation of the original version of the present paper, Kaaret, Ford, & Chen (1997) and Zhang, Strohmayer, & Swank (1997b) considered the implications if the frequencies of some of the kilohertz QPOs that have already been observed are the orbital frequencies of innermost stable circular orbits.

atoll and Z sources, including their frequencies, large amplitudes, and high coherence. It also explains the frequent occurrence of two simultaneous QPOs, the observed steep increase of kilohertz QPO amplitudes with increasing photon energy in the $\sim$5–10 keV energy range, and the anticorrelation of kilohertz QPO amplitudes with the strength of the stellar magnetic field inferred from spectral models. An attractive feature of the sonic-point model is that the magnetic fields, accretion rates, and scattering optical depths that it requires are completely consistent with those inferred previously from observations and modeling of the X-ray spectra and lower frequency X-ray variability of the kilohertz QPO sources.

The sonic-point model leads to several general expectations about the kilohertz QPOs.

(1) Kilohertz QPOs with the properties seen in the atoll and Z sources should not be observed in black-hole LMXBs, because collision of the accretion flow with the stellar surface plays an essential role in the sonic-point model.

(2) The rms amplitudes of the kilohertz QPOs should be anticorrelated with the strength of the neutron star's magnetic field. From this it follows that kilohertz QPOs should be very weak or undetectable with current instruments in the GX group of atoll sources and in the Cyg-like Z sources (which include Cyg X-2, GX 5$-$1, and GX 340$+$0), and undetectable with current instruments in any sources that have strong magnetic fields and therefore produce strong, periodic oscillations at their spin frequencies. (After this specific prediction was made in the original version of this paper, kilohertz QPOs with very low amplitudes were detected in all six of the originally identified Z sources; see § 4.4.) Another consequence of expectation (2) is that the positive correlation of rms amplitude with hard color shown by the four sources plotted in Figure 12 should be found to be general among sources showing kilohertz QPOs.

(3) If kilohertz QPOs are detected in the tails of X-ray bursts, their frequencies will tend to be lower when the accretion rate is higher.

(4) Weak oscillations should eventually be detected at overtones of the sonic-point beat and Keplerian frequencies and perhaps at the stellar spin frequency, but oscillations at other frequencies, such as $\nu_{\rm Ks} + \nu_{\rm spin}$, should be extremely weak.

At a lower level of certainty, the sonic-point model suggests that (1) the dependence of QPO amplitude on photon energy will change as the X-ray spectrum of the source changes, (2) the amplitude of the higher frequency QPO in a kilohertz QPO pair will drop relative to the amplitude of the lower frequency QPO at high luminosities, and (3) either the lower frequency QPO or the higher frequency QPO in a pair may be undetectable even when the other QPO is detectable.

In closing, we emphasize that measurement of Keplerian frequencies in the kilohertz range provides interesting new upper bounds on the masses and radii of the neutron stars in the kilohertz QPO sources and important new constraints on the equation of state of the matter in all neutron stars, as we have shown in § 5. As we demonstrated there, if the neutron star in the atoll source 4U 1636$-$536 has a spin frequency of $\sim$290 Hz, as indicated by the difference between the spin frequencies of its two high-frequency QPOs, the 1220 Hz QPO observed in this source constrains its mass to be less than about 2.2 $M_\odot$ and its radius to be less than about 17 km; the precise bounds depend on the equation of state assumed.

If at some future time we are able to demonstrate the existence of an innermost stable circular orbit around one or more neutron stars using observations of kilohertz QPOs, this would be the first confirmation of a prediction of general relativity in the strong-field regime and a major advance in our understanding of strong-field gravity. If the frequency of a kilohertz QPO is securely established as the orbital frequency at the radius of the innermost stable circular orbit in a particular system by, for example, observing the signatures discussed in § 5, and if, in addition, the spin frequency of the neutron star can be determined, then the frequency of the QPO will fix the mass of the neutron star for each assumed equation of state, providing a better understanding of the properties of dense matter and possibly ruling out many currently viable equations of state.

It is a pleasure to thank Phil Kaaret, Vicky Kalogera, Ed Morgan, Michiel van der Klis, Tod Strohmayer, Tom Baumgarte, Stu Shapiro, and Tomek Bulik for useful discussions. We especially thank Rudy Wijnands for providing the PCA response matrix and the X-ray spectral data used to compute the X-ray colors plotted in Figures 11 and 12, Greg Cook for providing the mass-radius relations for the equations of state plotted in Figure 14, and Ron Taam for discussions about black hole disk solutions.

This work was supported in part by NSF grants AST 93-15133 and AST 96-18524, NASA grant NAG 5-2925, and NASA *RXTE* grants at the University of Illinois, NASA grant NAG 5-2868 at the University of Chicago, and through the *Compton Gamma-Ray Observatory* Fellowship Program, by NASA grant NAS 5-2687.

REFERENCES

Akmal, A., Pandharipande, V. R., & Ravenhall, D. G. 1998, preprint (nucl-th 9804027)
Alpar, A., & Shaham, J. 1985, Nature, 316, 239
Angelini, L., Stella, L., & Parmar, A. N. 1989, ApJ, 346, 906
Arnett, W. D., & Bowers, R. L. 1977, ApJS, 33, 415
Balbus, S. A., & Hawley, J. F. 1991, ApJ, 376, 214
———. 1992, ApJ, 400, 610
———. 1998, Rev. Mod. Phys., in press
Bardeen, J. M., Press, W. H., & Teukolsky, S. A. 1972, ApJ, 178, 347
Berger, M., et al. 1996, ApJ, 469, L13
Bradt, H., Shirey, R., & Levine, A. 1998, in The Active X-Ray Sky: Results from *BeppoSAX* and *Rossi-XTE*, Nuclear Phys. B Proceedings Supplements, ed. L. Scarsi, H. Bradt, P. Giommi, & F. Fiore (Amsterdam: North Holland), in press
Brainerd, J., & Lamb, F.K. 1987, ApJ, 317, L33
Brandenburg, A., Nordlund, Å., Stein, R. F., & Torkelsson, U. 1995, ApJ 446, 741
———. 1996, ApJ, 458, L45
Bussard, R. W., Weisskopf, M. C., Elsner, R. F., & Shibazaki, N. 1988, ApJ, 327, 284
Cook, G. B., Shapiro, S. L., & Teukolsky, S. A. 1994, ApJ, 424, 823
Daumerie, P., Kalogera, V., Lamb, F. K., & Psaltis, D. 1996, Nature, 382, 141
Dieters, S., & van der Klis, M. 1998, MNRAS, in press
Finger, M. H., Wilson, R. B., & Harmon, B. A. 1996, ApJ, 459, 288
Ford, E., Kaaret, P., Tavani, M., Harmon, B. A., Zhang, S. N., Barret, D., Bloser, P., & Grindlay, J. 1996, IAU Circ. 6426
Ford, E., et al. 1997a, ApJ, 475, L123
———. 1997b, ApJ, 486, L47
Fortner, B. I. 1992, Ph.D. thesis, Univ. Illinois Urbana-Champaign

Fortner, B. I., Lamb, F. K., & Miller, G. S. 1989, Nature, 342, 775
Friedman, B., & Pandharipande, V. R. 1981, Nucl. Phys. A, 361, 501
Ghosh, P. 1996, ApJ, 459, 244
Ghosh, P., & Lamb, F. K. 1979a, ApJ, 232, 259
———. 1979b, ApJ, 234, 296
———. 1991, in Neutron Stars: Theory and Observation, ed. J. Ventura & D. Pines (Dordrecht: Kluwer), 363
———. 1992, in X-Ray Binaries and Recycled Pulsars, ed. E. P. J. van den Heuvel & S. A. Rappaport (Dordrecht: Kluwer), 487
Hartle, J. B., & Thorne, K. S. 1968, ApJ, 153, 807
Hasinger, G., & van der Klis, M. 1989, A& A 225, 79
Hawley, J. F., Gammie, C. F., & Balbus, S. A. 1995, ApJ, 440, 742
———. 1996, ApJ, 464, 690
Jonker, P. G., Wijnands, R., van der Klis, M., Psaltis, D., Kuulkers, E., & Lamb, F. K. 1998, ApJ, 499, L191
Kaaret, P., Ford, E. C., & Chen, K. 1997, ApJ, 480, L27
Kluźniak, W., Michelson, P., & Wagoner, R. V. 1990, ApJ, 358, 538
Kuulkers, E. 1995, Ph.D. thesis, Univ. Amsterdam
Kuulkers, E., van der Klis, M., Oosterbroek, T., Asai, K., Dotani, T., van Paradijs, J., & Lewin, W. H. G. 1995, A& A, 289, 795
Kuulkers, E., van der Klis, M., & Vaughan, B. A. 1996, A& A, 311, 197
Kylafis, N., & Phinney, E. S. 1989, in Timing Neutron Stars, ed. H. Ögelman & E. P. J. van den Heuvel (Dordrecht: Kluwer), 731
Lamb, F. K. 1984, in AIP Conf. Proc. 115, High Energy Transients in Astrophysics, ed. S. E. Woosley (New York: AIP), 179
———. 1988, Adv. Space Res., 8, 421
———. 1989, in Proc. 23rd ESLAB Symp. on X-ray Astronomy, ed. N. E. White, ESA SP-296 (Noordwijk: ESA), 215
———. 1991, in Neutron Stars: Theory and Observation, ed. J. Ventura & D. Pines (Dordrecht: Kluwer), 445
Lamb, F. K., & Miller, M. C. 1995, ApJ, 439, 828
Lamb, F. K., Shibazaki, N., Alpar, A., & Shaham, J. 1985, Nature, 317, 681
Lorenz, C. P., Ravenhall, D. G., & Pethick, C. J. 1993, Phys. Rev. Lett., 70, 379
Méndez, M., van der Klis, M., van Paradijs, J., Lewin, W. H. G., Lamb, F. K., Vaughan, B., & Kuulkers, E. 1997, ApJ, 485, L37
Méndez, M., et al. 1998, ApJ, 494, L65
Middleditch, J., & Priedhorsky, W. 1986, ApJ, 306, 230
Miller, G. S., & Lamb, F. K. 1992, ApJ, 388, 541
Miller, M. C., & Lamb, F. K. 1993, ApJ, 413, L43
———. 1996, ApJ, 470, 1033
Miller, M. C., Lamb, F. K., & Psaltis, D. 1998, in preparation
Misner, C. W., Thorne, K. S., & Wheeler, J. A. 1973, Gravitation (New York: Freeman)
Morgan, E. H., & Smith, D. A. 1996, IAU Circ. 6437
Muchotrzeb, B. 1983, Acta. Astron., 33, 79
Muchotrzeb-Czerny, B. 1986, Acta. Astron., 36, 1
Novikov, I. D., & Thorne, K. S. 1973, in Black Holes, ed. C. DeWitt & B. DeWitt (New York: Gordon & Breach), 343
Oosterbroek, T., van der Klis, M., Kuulkers, E., van Paradijs, J., & Lewin, W. H. G. 1995, A& A, 297, 141
Paczynski, B. 1987, Nature, 327, 303
Pandharipande, V. R. 1971, Nucl. Phys. A, 174, 641
Pandharipande, V. R., Akmal, A., & Ravenhall, D. G. 1998, in Nuclear Astrophysics, Proc. International Workshop XXVI on Gross Properties of Nuclei and Nuclear Excitations, ed. M. Buballa, N. Nörenberg, J. Wambach, & A. Wirzba (Darmstadt: GSI), 11
Pandharipande, V. R., & Smith, R. A. 1975a, Nucl. Phys. A, 237, 507
———. 1975b, Phys. Lett., 59B, 15
Pethick, C. J., & Ravenhall, D. G. 1995, Annu. Rev. Nucl. Part. Sci., 45, 429
Psaltis, D., & Lamb, F. K. 1998a, Astron. Astrophys. Trans., in press
———. 1998b, in Neutron Stars and Pulsars, ed. N. Shibazaki, N. Kawai, S. Shibata, & T. Kifune (Tokyo: Universal Academy), 179
———. 1998c, in preparation
Psaltis, D., Lamb, F. K., & Miller, G. S. 1995, ApJ, 454, L137
Psaltis, D., et al. 1998, ApJ, submitted
Rybicki, G. B., & Lightman, A. P. 1979, Radiative Processes in Astrophysics (New York: Wiley)
Scharlemann, E. T. 1978, ApJ, 219, 617
Shibazaki, N. 1989, in Proc. 23rd ESLAB Symp. on Two Topics in X-Ray Astronomy, ed. N. E. White (Noordwijk: ESA), 237
Shibazaki, N., & Lamb, F. K. 1987, ApJ, 318, 767
Shinoda, K., Kii, T., Mitsuda, K., Nagase, F., Tanaka, Y., Makishima, K., & Shibazaki, N. 1990, PASJ, 42, L27
Shirey, R. E., Bradt, H. V., Levine, A. M., & Morgan, E. H. 1996, ApJ, 469, L21
Smale, A. P., Zhang, W., & White, N. E. 1996, IAU Circ. 6507
———. 1997, ApJ, 483, L119
Smith, D. A., Morgan, E. H., & Bradt, H. 1997, ApJ, 479, L137
Spruit, H. C., & Taam, R. E. 1990, A& A, 229, 475
Strohmayer, T. 1997, talk presented at the 1997 meeting of the High Energy Astrophysics Division of the American Astronomical Society in Estes Park, Colorado (unpublished)
Strohmayer, T., Jahoda, K., Giles, A. B., & Lee, U. 1997a, 486, 355
Strohmayer, T., Lee, U., & Jahoda, K. 1996a, IAU Circ. 6484
Strohmayer, T., Zhang, W., Smale, A., Day, C., Swank, J. H., Titarchuk, L., & Lee, U. 1996b, IAU Circ. 6387
Strohmayer, T., Zhang, W., & Swank, J. H. 1996c, IAU Circ. 6320
———. 1997b, ApJ, 487, L77
Strohmayer, T., Zhang, W., Swank, J. H., Smale, A., Titarchuk, L., & Day, C. 1996d, ApJ, 469, L9
van der Klis, M. 1989, ARA& A, 27, 517
———. 1995, in X-Ray Binaries, ed. W. H. G. Lewin, J. van Paradijs, & E. P. J. van den Heuvel (Cambridge: Cambridge Univ. Press), 252
van der Klis, M., Jansen, F., van Paradijs, J., Lewin, W. H. G., van den Heuvel, E. P. J., Trümper, J., & Sztajno, M. 1985, Nature, 316, 225
van der Klis, M., Swank, J., Zhang, W., Jahoda, K., Morgan, E., Lewin, W. H. G., Vaughan, B., & van Paradijs, J. 1996a, IAU Circ. 6319
———. 1996b, ApJ, 469, L1
van der Klis, M., van Paradijs, J., Lewin, W. H. G., Lamb, F. K., Vaughan, B., Kuulkers, E., & Augusteijn, T. 1996c, IAU Circ. 6428
van der Klis, M., Wijnands, R., Horne, K., & Chen, W. 1997a, ApJ, 481, L97
van der Klis, M., et al. 1996d, IAU Circ. 6424
———. 1996e, IAU Circ. 6511
———. 1997b, IAU Circ. 6565
Vaughan, B. A., et al. 1994, ApJ, 435, 362
Wijers, R. A. M. J., van Paradijs, J., & Lewin, W. H. G. 1987, MNRAS, 228, P17
Wijnands, R., et al. 1997a, ApJ, 490, L157
———. 1998, ApJ, 493, L87
Wijnands, R. A. D., & van der Klis, M. 1997, ApJ, 482, L65
Wijnands, R. A. D., van der Klis, M., Kuulkers, E., Asai, K., & Hasinger, G. 1997b, A& A, 323, 399
Wijnands, R. A. D., van der Klis, M., van Paradijs, J., Lewin, W. H. G., Lamb, F. K., Vaughan, B., & Kuulkers, E. 1997c, ApJ, 479, L141
Wijnands, R. A. D., van der Klis, M., van Paradijs, J., Lewin, W. H. G., Lamb, F. K., Vaughan, B., Kuulkers, E., & Augusteijn, T. 1996, IAU Circ. 6447
Wiringa, R. B., Fiks, V., & Fabrocini, A. 1988, Phys. Rev. C, 38, 1010
Yu, W., et al. 1997, ApJ, 490, L153
Zhang, W., Jahoda, K., Kelley, R. L., Strohmayer, T. E., Swank, J. H., & Zhang, S. N. 1998a, ApJ, 495, L9
Zhang, W., Lapidus, I., Swank, J. H., White, N. E., & Titarchuk, L. 1997a, IAU Circ. 6541
Zhang, W., Lapidus, I., White, N. E., & Titarchuk, L. 1996, ApJ, 469, L17
Zhang, W., Strohmayer, T., & Swank, J. H. 1997b, ApJ, 482, L167
———. 1998b, ApJ, 500, L167